LANDAU SINGULARITIES AND POSITIVE GEOMETRIES

by

Stefan Stanojevic

May 2020

A dissertation submitted to the

Faculty of Physics at the Graduate School of Brown University

in partial fulfilment of the requirements for the

degree of

Doctor of Philosophy

Acknowledgments

It has been a privilege to have Marcus Spradlin as my advisor on this journey, and a pleasure to work alongside Igor Prlina and Giulio Salvatori.

I am grateful to Antal Jevicki and Stephon Alexander for being on my thesis commitee.

I would like to thank Nima Arkani-Hamed for stimulating discussions and Isidore Gitler for useful correspondence and results that made our work possible.

I would like to thank Anastasia Volovich, James Stankowicz and Tristan Dennen for collaboration during different phases of my PhD.

Table of Contents

List of Tables

List of Figures

Abstract

This work studies the analytical structure of scattering amplitudes in a class of toy models, from the perspective of novel geometrical structures underlying scattering amplitudes, and utilizing discrete mathematics. We find the set of all-loop n - point Landau singularities of the first type arising in any massless planar theory using graph operations inspired by the theory of electrical circuits. We also describe how to find the set of possible branch points of amplitudes at any fixed loop order and all particle multiplicities in planar $\mathcal{N} = 4$ SYM theory, using the information contained in the boundaries of the amplituhedra. Along the way, we devise a method for classifying the boundaries of amplituhedra for any loop order L and helicity k. We determine the branch points of all two-loop NMHV amplitudes by solving the Landau equations for the relevant configurations and are led thereby to a conjecture for the symbol alphabets of all such amplitudes. The study of amplituhedra is then pushed beyond the realm of $\mathcal{N} = 4$ SYM theory. We provide an efficient recursive formula to compute the canonical forms of arbitrary d-dimensional *simple* polytopes, and illustrate our method via an application to Stokes polytopes, related to ϕ^4 theory.

Chapter 1

Introduction

It has been a long-standing goal to determine scattering amplitudes in quantum field theory from knowledge of their analytic structure coupled with other basic physical and mathematical input. In planar $\mathcal{N} = 4$ super-Yang–Mills theory (which we refer to as SYM theory), the current state of the art for carrying out explicit computations of multi-loop amplitudes is a bootstrap program that relies fundamentally on assumptions about the location of branch points of certain amplitudes.

The aim of the bulk of the work in this thesis, building on the research program initiated in [4, 5] for MHV amplitudes and generalized to non-MHV amplitudes in [6], is to provide an *a priori* derivation of the set of branch points for any given amplitude. For sufficiently simple amplitudes in SYM theory[1] this information can go a long way by leading to natural guesses for the *symbol alphabets* [65] of various amplitudes. The possibility to do so exists because of the simple fact pointed out in [74] that the locus in the space of external data $\mathrm{Conf}_n(\mathbb{P}^3)$ where the symbol letters of a given amplitude vanish should be the same as the locus where the corresponding Landau equations [9, 59] admit solutions.

In the context of SYM theory, a geometrical picture of tree level amplitudes and loop integrands arising from the geometry of amplituhedron [25] has recently emerged. This beautiful geometrical picture is the first mathematical ingredient in our story - by focusing our attention on the boundaries

[1] General amplitudes lie outside the class of generalized polylogarithm functions that have well-defined symbols, see for example [24, 23, 78] for a discussion of this in the context of SYM theory.

of the amplituhdedron we can distinguish the physical branch points from the spurious ones.

The other ingredient comes from an apparently very different and unexpected place - from the study of the equivalence moves between graphs interpreted as electrical circuits. The theorem by Isidoro Gitler [48] presents a monumental advance in our understanding of the analytical structure of scattering amplitudes by allowing us to analyze the problem at *all loops*. In our opinion, the full implications of this theorem have yet to be understood and could lead to even more unexpected outcomes.

The author of this thesis had a pleasure of working with Igor Prlina through the majority of his graduate studies. It therefore comes at no surprise that this thesis will have significant overlap with [104]; the Chapter 2 detailing our proudest accomplishment is contained in both of our thesis, and Chapter 3 has overlap as well.

The outline of the thesis is as follows. In Chapter 2, we describe how to find the set of the Landau singularities of the first type in an massless planar theory, via an application of graph operations inspired by the theory of electrical circuits. In Chapter 3, we present our method of finding the set of possible branch points appearing in NMHV scattering amplitudes in the SYM theory, at two loops, using the amplituhedron as a tool. Chapter 4 extends the study of amplituhedra to a broader set of theories and derives recursive relations for a class of amplituhedra corresponding to simple polytopes.

Chapter 2

All loop singularities in massless planar theories

For over half a century much has been learned from the study of scattering amplitudes in quantum field theory, an important class of which are encoded in the Landau equations [9]. Our work here combines two simple statements to arrive at a general result about such singularities. The first is based on the analogy between Feynman diagrams and electrical circuits, which also has been long appreciated and exploited; see for example [44, 45, 46] and chapter 18 of [47]. Here we use the fact that in *massless* field theories, the sets of solutions to the Landau equations are invariant under the elementary graph operations familiar from circuit theory, including in particular the Y-Δ transformation which replaces a triangle subgraph with a tri-valent vertex, or vice versa. The second is a theorem of Gitler [48], who proved that any *planar* graph (of the type relevant to the analysis of Landau equations, specified below) can be Y-Δ reduced to a class we call *ziggurats* (see Fig. 2.2).

We conclude that the n-particle $\lfloor (n-2)^2/4 \rfloor$-loop ziggurat graph encodes all possible first-type Landau singularities of any n-particle amplitude at any finite loop order in any massless planar theory. Although this result applies much more generally, our original motivation arose from related work [4, 5, 6, 2] on planar $\mathcal{N} = 4$ supersymmetric Yang-Mills (SYM) theory, for which our result has several interesting implications which we discuss in Sec. 2.6.

2.1 Landau Graphs and Singularities

We begin by reviewing the Landau equations, which encode the constraint of locality on the singularity structure of scattering amplitudes in perturbation theory via Landau graphs. We aim to connect the standard vocabulary used in relativistic field theory to that of network theory in order to streamline the rest of our discussion.

In *planar* quantum field theories, which will be the exclusive focus of this paper, we can restrict our attention to plane Landau graphs. An *L-loop m-point plane Landau graph* is a plane graph with $L{+}1$ faces and m distinguished vertices called *terminals* that must lie on a common face called the *unbounded face*. Henceforth we use the word "vertex" only for those that are not terminals, and the word "face" only for the L faces that are not the unbounded face.

Each edge j is assigned an arbitrary orientation and a four-component (or, more generally, a D-component) (energy-)momentum vector q_j, the analog of electric current. Reversing the orientation of an edge changes the sign of the associated q_j. At each vertex the vector sum of incoming momenta must equal the vector sum of outgoing momenta (current conservation). This constraint is not applied at terminals, which are the locations where a circuit can be probed by connecting external sources or sinks of current. In field theory these correspond to the momenta carried by incoming or outgoing particles. If we label the terminals by $a = 1, \ldots, m$ (in cyclic order around the unbounded face) and let P_a denote the D-momentum flowing into the graph at terminal a, then energy-momentum conservation requires that $\sum_a P_a = 0$ and implies that precisely L of the q_j's are linearly independent.

Scattering amplitudes are (in general multivalued) functions of the P_a's which can be expressed as a sum over all Landau graphs, followed by a DL-dimensional integral over all components of the linearly independent q_j's. Amplitudes in different quantum field theories differ in how the various graphs are weighed (by P_a- and q_j-dependent factors) in that linear combination. These differences are indicated graphically by decorating each Landau graph (usually in many possible ways) with various embellishments, in which case they are called *Feynman diagrams*. We return to this important point later, but for now we keep our discussion as general as possible.

Our interest lies in understanding the loci in P_a-space on which amplitudes may have singularities, which are highly constrained by general physical principles. A Landau graph is said to have *Landau singularities of the first type* at values of P_a for which the *Landau equations* [9]

$$\alpha_j q_j^2 = 0 \text{ for each edge } j, \text{ and} \tag{2.1}$$

$$\sum_{\text{edges } j \in \mathcal{F}} \alpha_j q_j = 0 \text{ for each face } \mathcal{F} \tag{2.2}$$

admit nontrivial solutions for the *Feynman parameters* α_j (that means, omitting the trivial solution where all $\alpha_j = 0$). In the first line we have indicated our exclusive focus on *massless* field theories by omitting a term proportional to m_j^2 which would normally be present.

The Landau equations generally admit several branches of solutions. The *leading* Landau singularities of a graph $\mathcal{G}$ are those associated to branches having $q_j^2 = 0$ for all j (regardless of whether any of the α_j's are zero). This differs slightly from the more conventional usage of the term "leading", which requires all of the α_j's to be nonzero. However, we feel that our usage is more natural in massless theories, where it is typical to have branches of solutions on which q_j^2 and α_j are *both* zero for certain edges j. Landau singularities associated to branches on which one or more of the q_j^2 are not zero (in which case the corresponding α_j's must necessarily vanish) can be interpreted as leading singularities of a *relaxed* Landau graph obtained from $\mathcal{G}$ by contracting the edges associated to the vanishing α_j's.

A graph is called *c-connected* if it remains connected after removal of any $c-1$ vertices. It is easy to see that the set of Landau singularities for a 1-connected graph (sometimes called a "kissing graph" in field theory) is the union of Landau singularities associated to each 2-connected component since the Landau equations completely decouple. Therefore, without loss of generality we can confine our attention to 2-connected Landau graphs.

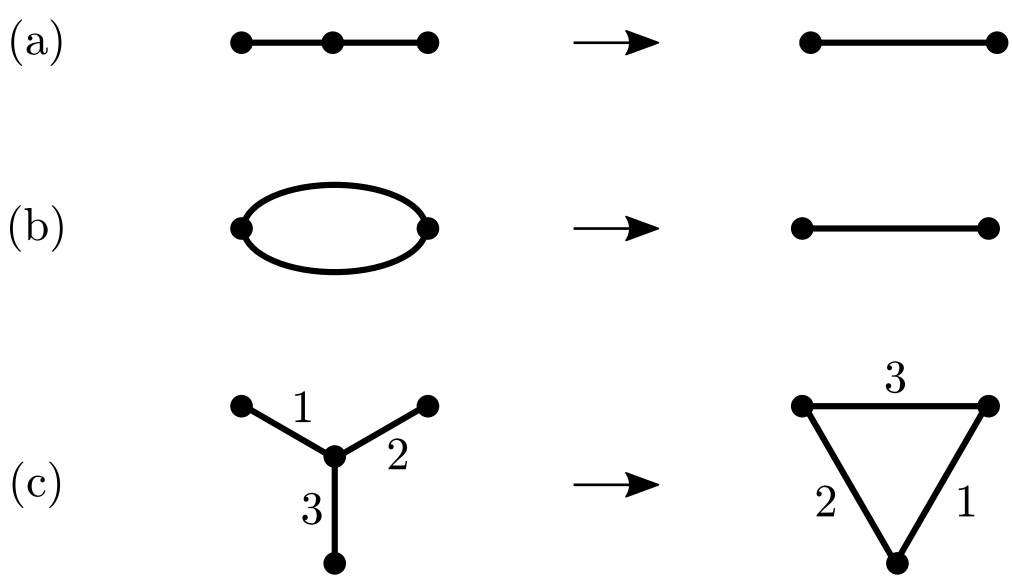

Figure 2.1: Elementary circuit moves that preserve solution sets of the massless Landau equations: (a) series reduction, (b) parallel reduction, and (c) Y-Δ reduction.

2.2 Elementary Circuit Operations

We refer to Eq. (2.2) as the *Kirchhoff conditions* in recognition of their circuit analog where the α_j's play the role of resistances. The analog of the *on-shell conditions* (2.1) on the other hand is rather mysterious, but a very remarkable feature of massless theories is that:

The graph moves familiar from elementary electrical circuit theory preserve the solution sets of Eqs. (2.1) and (2.2), and hence, the sets of first-type Landau singularities in any massless field theory.

Let us now demonstrate this feature, beginning with the three elementary circuit moves shown in Fig. 2.1.

Series reduction (Fig. 2.1(a)) allows one to remove any vertex of degree two. Since $q_2 = q_1$ by momentum conservation, the structure of the Landau equations is trivially preserved if the two edges with Feynman parameters α_1, α_2 are replaced by a single edge carrying momentum $q' = q_1 = q_2$ and Feynman parameter $\alpha' = \alpha_1 + \alpha_2$.

Parallel reduction (Fig. 2.1(b)) allows one to collapse any bubble subgraph. It is easy to verify (see for example Appendix A.1 of [5]) that the structure of the Landau equations is preserved if

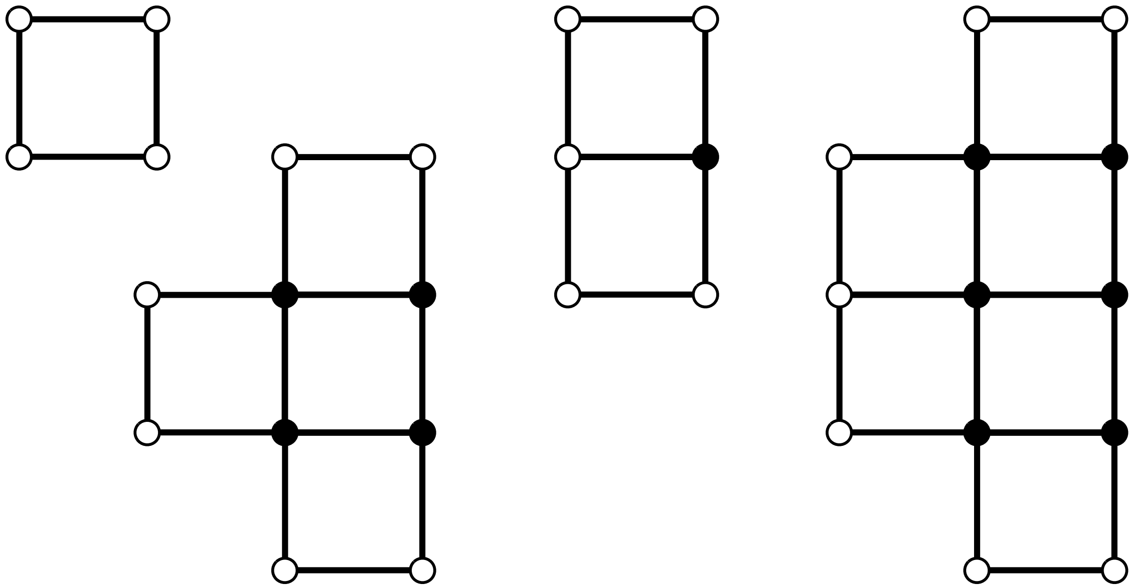

Figure 2.2: The four-, six-, five- and seven-terminal ziggurat graphs. The open circles are terminals and the filled circles are vertices. The pattern continues in the obvious way, but note an essential difference between ziggurat graphs with an even or odd number of terminals in that only the latter have a terminal of degree three.

the two edges of the bubble are replaced by a single edge carrying momentum $q' = q_1 + q_2$ and Feynman parameter $\alpha' = \alpha_1\alpha_2/(\alpha_1 + \alpha_2)$.

The Y-Δ reduction (Fig. 2.1(c)) replaces a vertex of degree three (a "Y") with a triangle subgraph (a "Δ"), or vice versa. Generically the Feynman parameters α_i of the Δ are related to those of the Y, which we call β_i, by

$$\beta_1 = \frac{\alpha_2\alpha_3}{\alpha_1 + \alpha_2 + \alpha_3}\,, \quad \text{and cyclic.} \tag{2.3}$$

On branches where one or more of the parameters vanish, this relation must be suitably modified. For example, if a branch of solutions for a graph containing a Y has $\beta_1 = \beta_2 = 0$ but β_3 nonzero, then the corresponding branch for the reduced graph has $\alpha_3 = 0$ but α_1, α_2 nonzero.

The invariance of the Kirchhoff conditions (2.2) under Y-Δ reduction follows straightforwardly from these Feynman parameter assignments. The invariance of the on-shell conditions (2.1) is nontrivial, and follows from the analysis in Appendix A.2 of [5] by checking that the on-shell conditions before and after the reduction are equivalent for each branch of solutions to the Landau

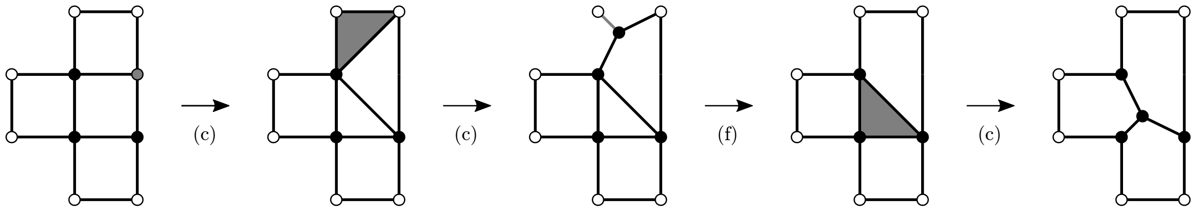

Figure 2.3: The six-terminal ziggurat graph can be reduced to a three loop graph by a sequence of three Y-Δ reductions and one FP assignment. In each case the vertex, edge, or face to be transformed is highlighted in gray.

equations. Actually [5] mentions only seven of the eight different types of branches. The eighth branch has $\alpha_1 = \alpha_2 = \alpha_3 = 0$, corresponding to $\beta_1 = \beta_2 = \beta_3 = 0$, but in this relatively trivial case both the Y and the Δ can effectively be collapsed to a single vertex.

The proof of the crucial theorem of [48] that we employ in the next section relies on three additional relatively simple moves that either have no analog in field theory or trivially preserve the essential content of the Landau equations. These are (d) the deletion of a "tadpole" (edges that connect a vertex or terminal to itself), (e) the deletion of a "hanging propagator" (a vertex of degree one and the edge connected to it), and (f) the contraction of an edge connected to a terminal of degree one (called "FP assignment" [49]). The last of these is strictly speaking not completely trivial at the level of the Landau equations; it just removes an otherwise uninteresting bubble singularity.

2.3 Reduction of Planar Graphs

The reduction of general graphs under the operations reviewed in the previous section is a well-studied problem in the mathematical literature. When it is declared that a certain subset of vertices are to be considered terminals (which may not be removed by series or Y-Δ reduction) the corresponding problem is called *terminal Y-Δ reducibility*. Aspects of terminal Y-Δ reducibility have been studied in [50, 51, 52, 53, 49, 54], including an application to Feynman diagrams in [55]. For our purpose the key result comes from the Ph.D. thesis of I. Gitler [48], who proved that any planar 2-connected graph with m terminals lying on the same face can be reduced to a graph of the kind shown in Fig. 2.2, which we call *ziggurat* graphs, or to a minor thereof. We denote the m-terminal ziggurat graph by $\mathcal{T}_m$, and note that a *minor* of a graph $\mathcal{G}$ is any graph that can be obtained from $\mathcal{G}$ by any sequence of edge contractions and/or edge deletions.

At the level of Landau equations an edge contraction corresponds, as discussed above, to a relaxation (setting the associated α_j to zero), while an edge deletion corresponds to setting the associated q_j to zero. It is clear that the Landau singularities associated to any minor of a graph $\mathcal{G}$ are a subset of those associated to $\mathcal{G}$. Consequently we don't need to worry about explicitly enumerating all minors of $\mathcal{T}_m$; their Landau singularities are already contained in the set of singularities of $\mathcal{T}_m$ itself.

It is conventional to discuss scattering amplitudes for a fixed number n of external particles, each of which carries some momentum p_i that in massless theories satisfies $p_i^2 = 0$. The total momentum flowing into each terminal is not arbitrary, but must be a sum of one or more null vectors. The momenta carried by these individual particles are denoted graphically by attaching a total of n *external edges* to the terminals, with at least one per terminal. In this way it is clear that any Landau graph with $m \leq n$ terminals is potentially relevant to finding the Landau singularities of an n-particle amplitude. However, it is also clear that if $m < n$ then $\mathcal{T}_m$ is a minor of $\mathcal{T}_n$, so again the Landau singularities of the former are a subset of those of the latter. Therefore, to find the Landau singularities of an n-particle amplitude it suffices to find those of the n-terminal ziggurat graph $\mathcal{T}_n$ with precisely one external edge attached to each terminal. We call this the *n-particle ziggurat graph* and finally summarize:

The first-type Landau singularities of an n-particle scattering amplitude in any massless planar field theory are a subset of those of the n-particle ziggurat graph.

While the Landau singularities of the ziggurat graph exhaust the set of singularities that may appear in any massless planar theory, we cannot rule out the possibility that in certain special theories the actual set of singularities may be smaller because of nontrivial cancellation between the contributions of different Landau graphs to a given amplitude. We return to this important point in Sec. 2.6.

Let us also emphasize that Y-Δ reduction certainly changes the number of faces of a graph, so the above statement does not hold at fixed loop order L; rather it is an all-order relation about the full set of Landau singularities of n-particle amplitudes at any finite order in perturbation theory. Since the n-particle ziggurat graph has $L = \lfloor (n-2)^2/4 \rfloor$ faces, we can however predict that a single computation at only $\lfloor (n-2)^2/4 \rfloor$-loop order suffices to expose all possible Landau singularities of any n-particle amplitude.

In fact this bound is unnecessarily high. Gitler's theorem does not imply that ziggurat graphs cannot be further reduced to graphs of lower loop order, and it is easy to see that in general this is possible. For example, as shown in Fig. 2.3, the six-terminal graph can be reduced by a sequence of Y-Δ reductions and one FP assignment to a particularly beautiful three-loop wheel graph whose 6-particle avatar we display in Fig. 2.4. Ziggurat graphs with more than six terminals can also be further reduced, but we have not been able to prove a lower bound on the loop order that can be obtained for general n.

2.4 Landau Analysis of the Wheel

In this section we analyze the Landau equations for the graph shown in Fig. 2.4. The six external edges carry momenta $p_1, \ldots, p_6$ into the graph, subject to $\sum_i p_i = 0$ and $p_i^2 = 0$ for each i. Using momentum conservation at each vertex, the momentum q_j carried by each of the twelve edges can be expressed in terms of the six p_i and three other linearly independent momenta, which we can take to be l_r, for $r = 1, 2, 3$, assigned as shown in the figure. Initially we consider the leading

Landau singularities, for which we impose the twelve on-shell conditions

$$
\begin{aligned}
(l_1 - p_1)^2 = l_1^2 = (l_1 + p_2)^2 = 0\,, \\
(l_2 - p_3)^2 = l_2^2 = (l_2 + p_4)^2 = 0\,, \\
(l_3 - p_5)^2 = l_3^2 = (l_3 + p_6)^2 = 0\,, \\
(l_1 + p_2 - l_2 + p_3)^2 = 0\,, \\
(l_2 + p_4 - l_3 + p_5)^2 = 0\,, \\
(l_3 + p_6 - l_1 + p_1)^2 = 0\,.
\end{aligned}
\tag{2.4}
$$

So far we have not needed to commit to any particular spacetime dimension. We now fix $D = 4$, which simplifies the analysis because for generic p_i there are precisely 16 discrete solutions for the l_r's, which we denote by $l_r^*(p_i)$. To enumerate and explicitly exhibit these solutions it is technically helpful to parameterize the momenta in terms of momentum twistor variables [56], in which case the solutions can be associated with on-shell diagrams as described in [87]. Although so far the analysis is still applicable to general massless planar theories, we note that in the special context of SYM theory, two cut solutions have MHV support, twelve NMHV, and two NNMHV.

With these solutions in hand, we next turn our attention to the Kirchhoff conditions

$$
\begin{aligned}
0 =& \alpha_1(l_1 - p_1) + \alpha_2 l_1 + \alpha_3(l_1 + p_2) + \\
& \alpha_{10}(l_3 + p_6 - l_1 + p_1) + \alpha_{11}(l_1 + p_2 - l_2 + p_3)\,, \\
0 =& \alpha_4(l_2 - p_3) + \alpha_5 l_2 + \alpha_6(l_2 + p_4) + \\
& \alpha_{11}(l_1 + p_2 - l_2 + p_3) + \alpha_{12}(l_2 + p_4 - l_3 + p_5)\,, \\
0 =& \alpha_7(l_3 - p_5) + \alpha_8 l_3 + \alpha_9(l_3 + p_6) + \\
& \alpha_{12}(l_2 + p_4 - l_3 + p_5) + \alpha_{10}(l_3 + p_6 - l_1 + p_1)\,.
\end{aligned}
\tag{2.5}
$$

Nontrivial solutions to this 12×12 linear system exist only if the associated *Kirchhoff determinant* $K(p_i, l_r)$ vanishes. By evaluating this determinant on each of the solutions $l_r = l_r^*(p_i)$ the condition for the existence of a non-trivial solution to the Landau equations can be expressed entirely in terms

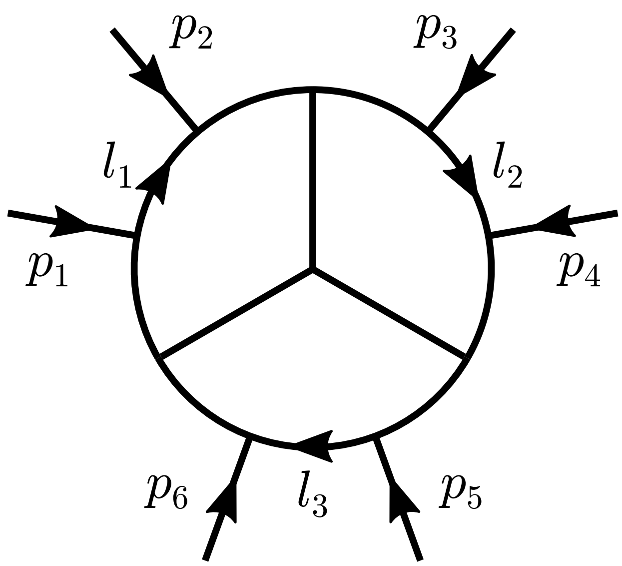

Figure 2.4: The three-loop six-particle wheel graph. The leading first-type Landau singularities of this graph exhaust all possible first-type Landau singularities of six-particle amplitudes in any massless planar field theory, to any finite loop order.

of the external momenta p_i. Using variables u, v, w, y_u, y_v, y_w that are very familiar in the literature on six-particle amplitudes (their definition in terms of the p_i's can be found for example in [57]), we find that $K(p_i, l_r^*(p_i)) = 0$ can only be satisfied if an element of the set

$$S_6 = \{u\,, v\,, w\,, 1{-}u\,, 1{-}v\,, 1{-}w\,, \frac{1}{u}\,, \frac{1}{v}\,, \frac{1}{w}\} \tag{2.6}$$

vanishes. We conclude that the three-loop $n = 6$ wheel graph has first-type Landau singularities on the locus

$$\mathcal{S}_6 \equiv \bigcup_{s \in S_6} \{s = 0\}\,. \tag{2.7}$$

It is straightforward, if somewhat tedious, to analyze all *subleading* Landau singularities corresponding to relaxations, as defined above. We refer the reader to [4, 5, 2] where this type of analysis has been carried out in detail in several examples. We find no additional first-type singularities beyond those that appear at leading order. Let us emphasize that this unusual feature does not occur for any of the examples in [4, 5, 2], which typically have many additional subleading singularities.

To summarize, we conclude that any six-particle amplitude in any four-dimensional massless planar field theory, at any finite loop order, can have first-type Landau singularities only on the locus $\mathcal{S}_6$ given by Eqs. (2.6) and (2.7), or a proper subset thereof.

2.5 Second-Type Singularities

The first-type Landau singularities that we have classified, which by definition are those encapsulated in the Landau equations (2.1), (2.2), do not exhaust all possible singularities of amplitudes in general quantum field theories. There also exist "second-type" singularities (see for example [58, 59]) which are sometimes called "non-Landauian" [60]. These arise in Feynman loop integrals as pinch singularities at infinite loop momentum and must be analyzed by a modified version of Eqs. (2.1), (2.2).

In the next section we turn our attention to the special case of SYM theory, which possesses a remarkable *dual conformal symmetry* [61, 62, 63] implying that there is no invariant notion of "infinity" in momentum space. As pointed out in [4], we therefore expect that second-type singularities should be absent in any dual conformal invariant theory. Because ziggurat graphs are manifestly dual conformal invariant when $D = 4$, this would imply that the first-type Landau singularities of the ziggurat graphs should capture the entire "dual conformally invariant part" of the singularity structure of all massless planar theories in four spacetime dimensions. By this we mean, somewhat more precisely, the singularity loci that do not involve the infinity twistor.

2.6 Planar SYM Theory

In Sec. 2.3 we acknowledged that in certain special theories, the actual set of singularities of amplitudes may be strictly smaller than that of the ziggurat graphs due to cancellations. SYM theory has been shown to possess such rich mathematical structure that it would seem the most promising candidate to exhibit such cancellations. Contrary to this expectation, we now argue that:

$$\boxed{\text{Perturbative amplitudes in SYM theory exhibit first-type Landau singularities on \textit{all} such loci that are possible in any massless planar field theory.}}$$

Moreover, our results suggest that this all-order statement is true separately in each helicity sector. Specifically: for any fixed n and any $0 \leq k \leq n-4$, there is a finite value of $L_{n,k}$ such that the singularity locus of the L-loop n-particle N^{k}MHV amplitude is identical to that of the n-particle ziggurat graph for all $L \geq L_{n,k}$. In order to verify this claim, it suffices to construct an n-particle on-shell diagram with N^{k}MHV support that has the same Landau singularities as the n-particle ziggurat graph; or (conjecturally) equivalently, to write down an appropriate valid configuration of lines inside the amplituhedron [25] $\mathcal{A}_{n,k,L}$ for some sufficiently high L.

To see that this is plausible, note that in general the appearance of a given singularity at some fixed k and L can be shown to imply the existence of the same singularity at lower k but higher L by performing the opposite of a parallel reduction—doubling one or more edges of the relevant Landau graph to make bubbles (see for example Fig. 2 of [2]). For example, while one-loop MHV amplitudes do not have singularities of three-mass box type, it is known by explicit computation [64] that two-loop MHV amplitudes do. Similarly, while two-loop MHV amplitudes do not have singularities of four-mass box type, we expect that three-loop MHV and two-loop NMHV amplitudes do. (To be clear, our analysis is silent on the question of whether the symbol alphabets of these amplitudes contain square roots; see the discussion in Sec. 7 of [6].)

It is indeed simple to check that the n-particle ziggurat graph can be converted into a valid on-shell diagram with MHV support by doubling *each* internal edge to form a bubble. Moreover, in this manner it is relatively simple to write an explicit mutually positive configuration of positive lines inside the MHV amplituhedron. However, we note that while this construction is sufficient to demonstrate the claim, it is certainly overkill; we expect MHV support to be reached at much lower loop level than this argument would require, as can be checked on a case by case basis for relatively small n.

2.7 Symbol Alphabets

Let us comment on the connection of our work to symbol alphabets. In general, the presence of some letter a in the symbol of an amplitude indicates that there exists some sheet on which the analytically continued amplitude has a branch cut from $a = 0$ to $a = \infty$. The symbols of all known six-particle amplitudes in SYM theory can be expressed in terms of a nine-letter alphabet [65] which may be chosen as [66]

$$A_6 = \{u, v, w, 1-u, 1-v, 1-w, y_u, y_v, y_w\}\,, \tag{2.8}$$

where $z = \{y_u, 1/y_u\}$ are the two roots of

$$u(1-v)(1-w)(z^2+1) = \left[u^2-2uvw+(1-v-w)^2\right] z \tag{2.9}$$

and y_v and y_w are defined by cycling $u \to v \to w \to u$. It is evident from Eq. (2.9) that y_u can attain the value 0 or ∞ only if $u = 0$ or $v = 1$ or $w = 1$. We therefore see that the singularity locus encoded in the hexagon alphabet A_6 is precisely equivalent to $\mathcal{S}_6$ given by Eqs. (2.6) and (2.7). Indeed, the hypothesis that six-particle amplitudes in SYM theory do not exhibit singularities on any other loci at any higher loop order (which we now consider to be proven), and the apparently much stronger ansatz that the nine quantities shown in Eq. (2.8) provide a symbol alphabet for all such amplitudes, lies at the heart of a bootstrap program that has made possible impressive explicit computations to high loop order (see for example [66, 67, 68, 69, 70, 71, 57]). An analogous ansatz for $n = 7$ has similarly allowed for the computation of symbols of seven-particle amplitudes [72, 73].

Unfortunately, as the y_u, y_v, y_w letters demonstrate, the connection between Landau singularity loci and symbol alphabets is somewhat indirect. It is not possible to derive A_6 from $\mathcal{S}_6$ alone as knowledge of the latter only tells us about the locus where symbol letters vanish [74] or have branch points (see Sec. 7 of [6]). In order to determine what the symbol letters actually are away from these loci it seems necessary to invoke some other kind of structure; for example, cluster algebras may have a role to play here [35, 75].

2.8 Conclusion

We leave a number of open questions for future work. What is the minimum loop order L_n to which the n-particle ziggurat graph can be reduced? Can one characterize its Landau singularities for arbitrary n, generalizing the result for $n = 6$ in Sec. 2.4? Does there exist a similar framework for classifying second-type singularities, even if only in certain theories? The graph moves reviewed in Sec. 2.2 preserve the (sets of solutions to the) Landau equations even for non-planar graphs; are there results on non-planar Y-Δ reducibility (see for example [76, 77]) that may be useful for non-planar (but still massless) theories?

In Sec. 2.4 we saw that the wheel is a rather remarkable graph. The ziggurat graphs, and those to which they can be reduced, might warrant further study for their own sake. Intriguingly they generalize those studied in [78, 79] and are particular cases of the graphs that have attracted recent interest, for example in [80, 81], in the context of "fishnet" theories. We have only looked at their singularity loci; it would be interesting to explore the structure of their cuts, perhaps in connection with the coaction studied in [82, 83, 84, 85, 86].

In the special case of SYM theory the technology might exist to address more detailed questions. For general n and k, what is the minimum loop order $L_{n,k}$ at which the Landau singularities of the n-particle N^{k}MHV amplitude saturate? Is there a direct connection between Landau singularities, ziggurat graphs, and cluster algebras? For amplitudes of generalized polylogarithm type, now that we know (in principle) the relevant singularity loci, what are the actual symbol letters for general n, and can the symbol alphabet depend on k (even though the singularity loci do not)? How do Landau singularities manifest themselves in general amplitudes that are of more complicated (non-polylogarithmic) functional type?

Chapter 3

Boundaries of amplituhedra and NMHV symbol alphabets at two loops

In this chapter, we classify the boundaries of amplituhedra relevant for determining the branch points of general two-loop amplitudes in SYM theory.We explain the connection to on-shell diagrams, which serves as a useful cross-check. Landau diagrams are assigned to such boundaries, and solved to yield a prediction for the branch points of two-loop NMHV amplitudes. The result, summarized in Sec. 3.4.3, leads to a natural conjecture for the symbol alphabets of these amplitudes which we hope may be employed in the near future by bootstrappers eager to study this class of amplitudes.

We start by introducing the momentum twistor space in which the amplituhedron lives, and reviewing the two formulations of the amplituhedron available in the literature.

3.0.1 The Kinematic Domain

Scattering amplitudes are (in general multivalued) functions of the kinematic data (the energies and momenta) describing some number of particles participating in some scattering process. Specifically, amplitudes are functions only of the kinematic information about the particles entering and exiting the process, called *external data* in order to distinguish it from information about virtual particles which may be created and destroyed during the scattering process itself. A general scattering amplitude in SYM theory is labeled by three integers: the number of particles n, the helicity sector $0 \leq \mathrm{k} \leq n-4$, and the loop order $L \geq 0$, with $L=0$ called *tree level* and $L>0$ called *L-loop level*. Amplitudes with $\mathrm{k}=0$ are called maximally helicity violating (MHV) while those with $\mathrm{k}>0$ are called (next-to-)$^{\mathrm{k}}$maximally helicity violating (N$^{\mathrm{k}}$MHV).

The kinematic configuration space of SYM theory admits a particularly simple characterization: n-particle scattering amplitudes[1] are multivalued functions on $\mathrm{Conf}_n(\mathbb{P}^3)$, the space of configurations of n points in $\mathbb{P}^3$ [35]. A generic point in $\mathrm{Conf}_n(\mathbb{P}^3)$ may be represented by a collection of n homogeneous coordinates Z_a^I on $\mathbb{P}^3$ (here $I \in \{1,\ldots,4\}$ and $a \in \{1,\ldots,n\}$) called *momentum twistors* [56], with two such collections considered equivalent if the corresponding $4\times n$ matrices $Z \equiv (Z_1 \cdots Z_n)$ differ by left-multiplication by an element of (4). We use the standard notation

$$\langle a\, b\, c\, d\rangle = \epsilon_{IJKL} Z_a^I Z_b^J Z_c^K Z_d^L \tag{3.1}$$

for the natural (4)-invariant four-bracket on momentum twistors and use the shorthand $\langle \cdots\, \overline{a}\, \cdots\rangle = \langle \cdots\, a{-}1\, a\, a{+}1 \cdots\rangle$, with the understanding that all particle labels are always taken mod n. We write $(a\, b)$ to denote the line in $\mathbb{P}^3$ containing Z_a and Z_b, $(a\, b\, c)$ to denote the plane containing Z_a, Z_b and Z_c, and so $\overline{a}$ denotes the plane $(a{-}1\, a\, a{+}1)$. The bar notation is motivated by *parity*, which is a $\mathbb{Z}_2$ symmetry of SYM theory that maps N$^{\mathrm{k}}$MHV amplitudes to N$^{n-\mathrm{k}-4}$MHV amplitudes while mapping the momentum twistors according to $\{Z_a\} \mapsto \{W_a = *(a{-}1\, a\, a{+}1)\}$.

When discussing N$^{\mathrm{k}}$MHV amplitudes it is conventional to consider an enlarged kinematic space where the momentum twistors are promoted to homogeneous coordinates $\mathcal{Z}_a$, bosonized momentum twistors [25] on $\mathbb{P}^{\mathrm{k}+3}$ which assemble into an $n \times (\mathrm{k}+4)$ matrix $\mathcal{Z} \equiv (\mathcal{Z}_1 \cdots \mathcal{Z}_n)$. The analog of Eq. (3.1) is then the $(\mathrm{k}+4)$-invariant bracket which we denote by $[\cdot]$ instead of $\langle\cdot\rangle$.

[1]Here and in all that follows, we mean components of superamplitudes suitably normalized by dividing out the tree-level Parke-Taylor-Nair superamplitude [17, 18]. We expect our results to apply equally well to BDS- [19] and BDS-like [20] regulated MHV and non-MHV amplitudes. The set of branch points of a non-MHV ratio function [63] should be a subset of those of the corresponding non-MHV amplitude, but our analysis cannot exclude the possibility that it may be a proper subset due to cancellations.

Given some $\mathcal{Z}$ and an element of the Grassmannian $\mathrm{Gr}(\mathrm{k}, \mathrm{k}+4)$ represented by a $\mathrm{k} \times (\mathrm{k}+4)$ matrix Y, one can obtain an element of $\mathrm{Conf}_n(\mathbb{P}^3)$ by projecting onto the complement of Y. The four-brackets of the *projected external data* obtained in this way are given by

$$\langle a\, b\, c\, d\rangle \equiv [Y\, \mathcal{Z}_a\, \mathcal{Z}_b\, \mathcal{Z}_c\, \mathcal{Z}_d]\,. \tag{3.2}$$

Tree-level amplitudes are rational functions of the brackets while loop-level amplitudes have both poles and branch cuts, and are properly defined on an infinitely-sheeted cover of $\mathrm{Conf}_n(\mathbb{P}^3)$. For each k there exists an open set $\mathcal{D}_{n,\mathrm{k}} \subset \mathrm{Conf}_n(\mathbb{P}^3)$ called the *principal domain* on which amplitudes are known to be holomorphic and non-singular. Amplitudes are initially defined only on $\mathcal{D}_{n,\mathrm{k}}$ and then extended to all of (the appropriate cover of) $\mathrm{Conf}_n(\mathbb{P}^3)$ by analytic continuation.

A simple characterization of the principal domain for n-particle $\mathrm{N^kMHV}$ amplitudes was given in [26]: $\mathcal{D}_{n,\mathrm{k}}$ may be defined as the set of points in $\mathrm{Conf}_n(\mathbb{P}^3)$ that can be represented by a Z-matrix with the properties

1. $\langle a\, a{+}1\, b\, b{+}1\rangle > 0$ for all a and $b \notin \{a{-}1, a, a{+}1\}$[2], and

2. the sequence $\langle 1\, 2\, 3\, \bullet\rangle$ has precisely k sign flips,

where we use the notation $\bullet \in \{1\,, 2\,, \ldots\,, n\}$ so that

$$\langle 1\, 2\, 3\, \bullet\rangle \equiv \{0, 0, 0, \langle 1\, 2\, 3\, 4\rangle, \langle 1\, 2\, 3\, 5\rangle, \ldots, \langle 1\, 2\, 3\, n\rangle\}\,. \tag{3.3}$$

It was also shown that an alternate but equivalent condition is to say that the sequence $\langle a\, a{+}1\, b\, \bullet\rangle$ has precisely k sign flips for all a, b (omitting trivial zeros, and taking appropriate account of the twisted cyclic symmetry where necessary). The authors of [26] showed, and we review in Sec. 3.0.2, that for Y's inside an $\mathrm{N^kMHV}$ amplituhedron, the projected external data have the two properties above.

[2] As explained in [26], the cyclic symmetry on the n particle labels is "twisted", which manifests itself here in the fact that if k is even, and if $a = n$ or $b = n$, then cycling around n back to 1 introduces an extra minus sign. The condition in these cases is therefore $(-1)^{\mathrm{k}+1}\langle c\, c{+}1\, n\, 1\rangle > 0$ for all $c \notin \{1, n{-}1, n\}$.

3.0.2 Amplituhedra

A matrix is said to be *positive* or *non-negative* if all of its ordered maximal minors are positive or non-negative, respectively. In particular, we say that the external data are positive if the $n \times (\mathrm{k}+4)$ matrix $\mathcal{Z}$ described in the previous section is positive.

A point in the n-particle N$^{\mathrm{k}}$MHV L-loop *amplituhedron* $\mathcal{A}_{n,\mathrm{k},L}$ is a collection $(Y, \mathcal{L}^{(\ell)})$ consisting of a point $Y \in \mathrm{Gr}(\mathrm{k}, \mathrm{k}+4)$ and L lines $\mathcal{L}^{(1)}, \ldots, \mathcal{L}^{(L)}$ (called the *loop momenta*) in the four-dimensional complement of Y. We represent each $\mathcal{L}^{(\ell)}$ as a $2 \times (\mathrm{k}+4)$ matrix with the understanding that these are representatives of equivalence classes under the equivalence relation that identifies any linear combination of the rows of Y with zero.

For given positive external data $\mathcal{Z}$, the amplituhedron $\mathcal{A}_{n,\mathrm{k},L}(\mathcal{Z})$ was defined in [25] for $n \geq 4$ as the set of $(Y, \mathcal{L}^{(\ell)})$ that can be represented as

$$Y = C\mathcal{Z}\,, \tag{3.4}$$

$$\mathcal{L}^{(\ell)} = D^{(\ell)}\mathcal{Z}\,, \tag{3.5}$$

in terms of a $\mathrm{k} \times n$ real matrix C and L $2 \times n$ real matrices $D^{(\ell)}$ satisfying the positivity property that for any $0 \leq m \leq L$, all $(2m+\mathrm{k}) \times n$ matrices of the form

$$\begin{pmatrix} D^{(i_1)} \\ D^{(i_2)} \\ \vdots \\ D^{(i_m)} \\ C \end{pmatrix} \tag{3.6}$$

are positive. The D-matrices are understood as representatives of equivalence classes and are defined only up to translations by linear combinations of rows of the C-matrix.

One of the main results of [26] was that amplituhedra can be characterized directly by (projected) four-brackets, Eq. (3.2), without any reference to C or $D^{(\ell)}$'s, by saying that for given positive $\mathcal{Z}$, a collection $(Y, \mathcal{L}^{(\ell)})$ lies inside $\mathcal{A}_{n,\mathrm{k},L}(\mathcal{Z})$ if and only if

1. the projected external data lie in the principal domain $\mathcal{D}_{n,\mathrm{k}}$,
2. $\langle \mathcal{L}^{(\ell)}\, a\, a{+}1\rangle > 0$ for all ℓ and a[3],
3. for each ℓ, the sequence $\langle \mathcal{L}^{(\ell)}\, 1 \bullet\rangle$ has precisely $\mathrm{k}+2$ sign flips, and
4. $\langle \mathcal{L}^{(\ell_1)}\, \mathcal{L}^{(\ell_2)}\rangle > 0$ for all $\ell_1 \neq \ell_2$.

Here the notation $\langle \mathcal{L}\, a\, b\rangle$ means $\langle A\, B\, a\, b\rangle$ if the line $\mathcal{L}$ is represented as $(A\, B)$ for two points A, B. It was also shown that items 2 and 3 above are equivalent to saying that the sequence $\langle \mathcal{L}^{(\ell)}\, a \bullet\rangle$ has precisely $\mathrm{k}+2$ sign flips for any ℓ and a.

3.0.3 Summary: The Algorithm

The Landau equations may be interpreted as defining a map which associates to each boundary of the amplituhedron $\mathcal{A}_{n,\mathrm{k},L}$ a locus in $\mathrm{Conf}_n(\mathbb{P}^3)$ on which the corresponding n-point N$^{\mathrm{k}}$MHV L-loop amplitude has a singularity. The Landau equations themselves have no way to indicate whether a singularity is a pole or branch point. However, it is expected that all poles in SYM theory arise from boundaries that are present already in the tree-level amplituhedra [25]. These occur when some $\langle a\, a{+}1\, b\, b{+}1\rangle$ go to zero. The aim of our work is to understand the loci where amplitudes have branch points, so we confine our attention to the $\mathcal{L}$-boundaries defined in that section.

The algorithm for finding all branch points of the n-particle N$^{\mathrm{k}}$MHV L-loop amplitude is therefore simple in principle:

1. Enumerate all $\mathcal{L}$-boundaries of $\mathcal{A}_{n,\mathrm{k},L}$ for generic projected external data.
2. For each $\mathcal{L}$-boundary, identify the codimension-one loci (if there are any) in $\mathrm{Conf}_n(\mathbb{P}^3)$ on which the corresponding Landau equations admit nontrivial solutions.

[3] Again, the twisted cyclic symmetry implies that the correct condition for the case $a = n$ is $(-1)^{\mathrm{k}+1}\langle \mathcal{L}^{(\ell)}\, n\, 1\rangle > 0$.

3.1 Classification of Two-Loop Boundaries

In this section we classify certain boundaries of two-loop amplituhedra. This analysis builds heavily on Sections 3–5 of [6], and in particular we show how to recycle the one-loop boundaries classified there by "merging" pairs of one-loop boundaries into two-loop boundaries. We find that two different formulations of the amplituhedron — the original formulation in terms of C and D matrices [25], and the reformulation in terms of sign flips [26] — play two complementary roles, exactly as in [6]. Specifically, the former is useful for establishing the existence of boundaries by constructing explicit C and D matrix representatives, while the latter is useful for establishing the non-existence of any other boundaries.

Before proceeding let us dispense of some important details that would otherwise overcomplicate our exposition. There is a parity symmetry between $A_{n,\mathrm{k},L}$, the n-point, N^{k}MHV, L-loop amplitude in SYM theory, and its parity conjugate $A_{n,n-\mathrm{k}-4,L}$. For fixed n, amplitudes become increasingly complicated as k is increased from zero, but after k $\sim n/2$ they must begin to decrease in complexity until the upper bound k $= n-4$. In what follows we will often make use of lower bounds on k, or on constructions that increment k by 1. In making these arguments, we always have in mind that k is sufficiently small compared to n. In other words, unless otherwise stated, we are always working in the "low-k" regime, to use the terminology of [6]. At the very end of our analysis, once we have all of the desired results in this regime, we appeal to parity symmetry in order to translate low-k results into high-k results. However the details of matching these two regimes near the midpoint k $\sim n/2$ can be quite intricate, even moreso at two loops than it was in the one-loop analysis of [6].

3.1.1 Identifying the Relevant Boundaries

In general, a configuration $(Y, \mathcal{L}^{(1)}, \mathcal{L}^{(2)})$ lies on a boundary of a two-loop amplituhedron if at least one item on the following menu is satisfied:

(1) Y is such that some four-brackets of the form $\langle a\, a{+}1\, b\, b{+}1\rangle$ vanish,

(2) $\mathcal{L}^{(1)}$ satisfies some on-shell conditions $\langle \mathcal{L}^{(1)}\, a_1\, a_1{+}1\rangle = \cdots = \langle \mathcal{L}^{(1)}\, a_{d_1}\, a_{d_1}{+}1\rangle = 0$,

(3) $\mathcal{L}^{(2)}$ satisfies some on-shell conditions $\langle \mathcal{L}^{(2)}\, b_1\, b_1{+}1\rangle = \cdots = \langle \mathcal{L}^{(2)}\, b_{d_2}\, b_{d_2}{+}1\rangle = 0$,

(4) or $\langle \mathcal{L}^{(1)}\, \mathcal{L}^{(2)}\rangle = 0$.

Above and through the remainder of the paper, we always take $\langle ABCD\rangle \equiv [YABCD]$ — what we call projected four-brackets following [26].

For the purpose of finding Landau singularities we are always interested only in loop momenta $(\mathcal{L}^{(1)}, \mathcal{L}^{(2)})$ that exist for generic projected external data, i.e., for generic Y, so we disregard possibility (1) in all that follows. Next, we note that for configurations which do not satisfy (4), the Landau equations decouple into two separate sets of equations on the two individual loop momenta, so there can be no new Landau singularities beyond those already found at one loop. Therefore in all that follows we only consider boundaries on which $\langle \mathcal{L}^{(1)}\, \mathcal{L}^{(2)}\rangle = 0$. The Landau equations similarly degenerate if either d_1 or d_2 (defined in the preceeding paragraph) is zero, so we are only interested in configurations with $d_1 d_2 > 0$.

The above considerations motivate us to define an *$\mathcal{L}$-boundary* of a two-loop amplituhedron as a configuration $(Y, \mathcal{L}^{(1)}, \mathcal{L}^{(2)})$ for which Y is such that the projected external data are generic, $\langle \mathcal{L}^{(1)}\, \mathcal{L}^{(2)}\rangle = 0$, and each $\mathcal{L}$ satisfies at least one on-shell condition of the form $\langle \mathcal{L}\, a\, a{+}1\rangle = 0$. In particular, these conditions imply that both $(Y, \mathcal{L}^{(1)})$ and $(Y, \mathcal{L}^{(2)})$ must lie on boundaries of some one-loop amplituhedra; each of these must therefore be one of the 19 branches tabulated in Tab. 1 of [6].

3.1.2 Merging One-Loop Boundaries

The preceding analysis suggests that the boundaries of two-loop amplituhedra can be understood by merging various one-loop boundaries. Let us now see how this works in detail. Suppose that $(Y^{(1)}, \mathcal{L}^{(1)})$ and $(Y^{(2)}, \mathcal{L}^{(2)})$ lie on boundaries of $\mathcal{A}_{n,\mathrm{k}_1,1}$ and $\mathcal{A}_{n,\mathrm{k}_2,1}$, respectively. Then they can be represented as $Y^{(\alpha)} = C^{(\alpha)}\mathcal{Z}$ and $\mathcal{L}^{(\alpha)} = D^{(\alpha)}\mathcal{Z}$, where for each $\alpha \in \{1,2\}$, the matrices $C^{(\alpha)}$, $\left(\begin{smallmatrix} D^{(\alpha)} \\ C^{(\alpha)} \end{smallmatrix}\right)$, and $D^{(\alpha)}$ (as shown in [6]), are all non-negative. In order to streamline the argument we initially consider k_1 and k_2 to be the smallest values of helicity for which boundaries of the desired class exist, and we take each pair $(C^{(\alpha)}, D^{(\alpha)})$ to have the form of one of the 19 branches shown in Secs. 4.2 through 4.4 of [6]. We will show that such a pair of valid one-loop boundary configurations can be uplifted into a valid two-loop boundary configuration $(C, D^{(1)}, D^{(2)})$ satisfying $\langle \mathcal{L}^{(1)}\, \mathcal{L}^{(2)} \rangle = 0$ by constructing an appropriate matrix C from $C^{(1)}$ and $C^{(2)}$.

The process of merging two boundaries depends on whether the two loop momenta $\mathcal{L}^{(1)}$, $\mathcal{L}^{(2)}$ each pass through some common external point Z_i. If they do, then we say that they *manifestly intersect* and the condition that $\langle \mathcal{L}^{(1)}\, \mathcal{L}^{(2)} \rangle = 0$ is automatically satisfied. In this case we can simply stack the two individual C-matrices on top of each other in order to form

$$C = \begin{pmatrix} C^{(1)} \\ C^{(2)} \end{pmatrix}. \tag{3.7}$$

If, on the other hand, the two loop momenta do not manifestly intersect, then we can still ensure that $\langle \mathcal{L}^{(1)}\, \mathcal{L}^{(2)} \rangle = [(C\mathcal{Z})\, \mathcal{L}^{(1)}\, \mathcal{L}^{(2)}] = 0$ by adding one additional suitably crafted row to C. Specifically, if $A^{(\alpha)}$, $B^{(\alpha)}$ are any four points in $\mathbb{P}^n$ such that $\mathcal{L}^{(\alpha)} = (A^{(\alpha)}\mathcal{Z}, B^{(\alpha)}\mathcal{Z})$, then adding a row to C that is any linear combination of these four points will guarantee that $\langle \mathcal{L}^{(1)}\, \mathcal{L}^{(2)} \rangle = 0$.

In this manner we have constructed a candidate for a configuration on the boundary of $\mathcal{A}_{n,\mathrm{k},2}$ with $\mathrm{k} = \mathrm{k}_1 + \mathrm{k}_2$ in the case of manifest intersection, or $\mathrm{k} = \mathrm{k}_1 + \mathrm{k}_2 + 1$ otherwise. It remains to verify that this configuration is *valid*, which means that C can be chosen so that it and the matrices $\begin{pmatrix} D^{(1)} \\ C \end{pmatrix}$, $\begin{pmatrix} D^{(2)} \\ C \end{pmatrix}$, and $\begin{pmatrix} D^{(1)} \\ D^{(2)} \\ C \end{pmatrix}$ are all non-negative.

3.1.3 Planarity from Positivity

Let us begin by analyzing the non-negativity of the C-matrix shown in Eq. (3.7). The nonzero columns of each $C^{(\alpha)}$ (which may be read off from Secs. 4.3 and 4.4 of [6]) are grouped into clusters corresponding to the sets of contiguous indices appearing in the on-shell conditions satisfied by the corresponding $\mathcal{L}^{(\alpha)}$. For example, for a boundary on which the three-mass triangle on-shell conditions $\langle \mathcal{L}\, i\, i{+}1 \rangle = \langle \mathcal{L}\, j\, j{+}1 \rangle = \langle \mathcal{L}\, k\, k{+}1 \rangle = 0$ are satisfied, the C-matrix is zero except in six columns grouped into three clusters $\{i, i{+}1\}$, $\{j, j{+}1\}$ and $\{k, k{+}1\}$.

When we stack two C-matrices together, the result can be one of two different cases depending on whether or not the clusters of $C^{(1)}$ are cyclically adjacent compared to the clusters of $C^{(2)}$. If so, then the stacked C-matrix has the schematic form

$$C = \begin{pmatrix} C^{(1)} \\ C^{(2)} \end{pmatrix} = \begin{array}{c} \left(\begin{array}{cccccccccccc} \cdots & 0 & \star & 0 & \star & 0 & 0 & 0 & 0 & 0 & \cdots \\ \cdots & 0 & 0 & 0 & 0 & 0 & \star & 0 & \star & 0 & \cdots \end{array}\right) \end{array} \begin{array}{l} \}\ \mathrm{k}_1 \text{ rows} \\ \}\ \mathrm{k}_2 \text{ rows} \end{array} \tag{3.8}$$

which we call *planar*; otherwise it is of the form

$$C = \begin{pmatrix} C^{(1)} \\ C^{(2)} \end{pmatrix} = \begin{array}{c} \left(\begin{array}{cccccccccccc} \cdots & 0 & \star & 0 & 0 & 0 & \star & 0 & 0 & 0 & \cdots \\ \cdots & 0 & 0 & 0 & \star & 0 & 0 & 0 & \star & 0 & \cdots \end{array}\right) \end{array} \begin{array}{l} \}\ \mathrm{k}_1 \text{ rows} \\ \}\ \mathrm{k}_2 \text{ rows}\,. \end{array} \tag{3.9}$$

which we call *non-planar*. In Eqns. (3.8) and (3.9) each $\star$ is shorthand for one or more contiguous columns (i.e, clusters) of non-zero entries, and we suppress displaying columns shared by the two C-matrices, which are not relevant to our argument. Also as indicated the top (bottom) row is shorthand for k_1 (k_2) rows. Given that our starting point is a pair of matrices $C^{(1)}$, $C^{(2)}$ that are each non-negative, it is clear that the resulting stacked C-matrix has a chance to be non-negative (for certain values of its parameters) only for planar configurations; the minors of Eq. (3.9) manifestly have non-definite signs.

In cases when $\mathcal{L}^{(1)}$ and $\mathcal{L}^{(2)}$ do not manifestly intersect we need to add an additional row to C as described in the previous section. This additional row can be considered part of either $C^{(1)}$ or $C^{(2)}$. Since the coefficients in this row can be arbitrary and still preserve $\langle \mathcal{L}^{(1)}\, \mathcal{L}^{(2)} \rangle = 0$, the coefficients can always be chosen such that the enlarged C-matrix is non-negative. The conclusion that only planar C's can be made positive still holds.

The nomenclature of 'planar' and 'non-planar' clusters is appropriate in light of the fact that the locations of the clusters precisely correspond to the sets of indices appearing in on-shell conditions listed in points (2) and (3) at the beginning of Sec. 3.1.1. In a configuration like Eq. (3.8) there exist a, b such that all of the on-shell conditions satisfied by $\mathcal{L}^{(1)}$ lie in the range $\{a, a{+}1, \ldots, b, b+1\}$

while all of the on-shell conditions satisfied by $\mathcal{L}^{(2)}$ lie in the range $\{b, b+1, \ldots, a, a+1\}$ (as usual, all indices are always understood mod n). Consequently, the two-loop Landau diagram depicting the merged sets of on-shell conditions (together with the propagator $\langle \mathcal{L}^{(1)}\, \mathcal{L}^{(2)} \rangle$ shared between the two loops) is planar. By the same argument, a nonplanar configuration such as Eq. (3.9) is necessarily associated to a nonplanar Landau diagram.

Now let us consider the non-negative matrices $\begin{pmatrix} D^{(\alpha)} \\ C^{(\alpha)} \end{pmatrix}$ for the two individual initial boundary configurations ($\alpha = 1$ or 2). We require that these matrices stay non-negative when $C^{(\alpha)}$ is replaced by C. By the argument given in Sec. 4.7 of [6], this will be the case if the rows added to $C^{(\alpha)}$ have nonzero entries only in the gaps between clusters of $C^{(\alpha)}$. But this is just another way to phrase the planarity condition described above, so again we see that planarity is enforced, this time by requiring non-negativity of $\begin{pmatrix} D^{(\alpha)} \\ C \end{pmatrix}$.

The final step in establishing the validity of the configuration $(C, D^{(1)}, D^{(2)})$ is checking that the matrix $\begin{pmatrix} D^{(1)} \\ D^{(2)} \\ C \end{pmatrix}$ is non-negative. In the parameterization we have chosen, all of the maximal minors of this matrix actually vanish. If the two loops manifestly intersect this can be checked by looking at the form of the (C, D) matrices tabulated in [6]. If they do not manifestly intersect the analysis is even easier, since in such cases we have included in C a row that is some linear combination of the four rows of $D^{(1)}, D^{(2)}$.

The argument as presented appears to fail if either of the individual one-loop boundaries is MHV, in which case there is no C matrix. However, for MHV boundaries it can be seen from the expressions tabulated in Sec. 4.2 of [6] that the D-matrix serves the same role as the C-matrix played in the above argument. For example, if $\mathrm{k}_1 = 0$ so that $C^{(1)}$ is empty, then $C = C^{(2)}$ so the requirement that $\begin{pmatrix} D^{(1)} \\ C \end{pmatrix} = \begin{pmatrix} D^{(1)} \\ C^{(2)} \end{pmatrix}$ must be non-negative requires that the clusters of $D^{(1)}$ be cyclically adjacent compared to the clusters of $C^{(2)}$. If both k_1 and k_2 are zero then C is empty and the same conclusion follows from consideration of the matrix $\begin{pmatrix} D^{(1)} \\ D^{(2)} \end{pmatrix}$. Therefore, in all cases, the various non-negativity conditions imply that the Landau diagram must be planar. This emergent planarity was discussed in context of MHV amplitudes in [27].

In conclusion, we have established that a boundary of $\mathcal{A}_{n,\mathrm{k},2}$ can be constructed by "merging" a boundary of $\mathcal{A}_{n,\mathrm{k}_1,1}$ with a boundary of $\mathcal{A}_{n,\mathrm{k}_2,1}$, with $\mathrm{k}-\mathrm{k}_1-\mathrm{k}_2=0$ or 1 depending on whether $\mathcal{L}^{(1)}$ and $\mathcal{L}^{(2)}$ manifestly intersect. So far we have considered k_1 and k_2 to saturate the lower bounds shown in Tab. 1 of [6], but once a valid configuration $(C, D^{(1)}, D^{(2)})$ has been constructed as described in this section, it can be lifted to higher values of k by growing the C-matrix according to a suitably modified version of the argument given in Sec. 4.7 of that reference.

3.1.4 Establishing the Lower Bound on Helicity

We have shown that it is possible to merge two one-loop boundaries with (minimal) helicities k_1 and k_2 in order to generate two-loop boundaries with helicities $\mathrm{k} \geq \mathrm{k}_1 + \mathrm{k}_2$. The merging algorithm we have described cannot generate boundaries with k below this lower bound. In this section we prove that we have not overlooked any potential two-loop boundaries. To do so, we use the formulation of amplituhedra in terms of sign flips [26] (reviewed also in Sec. 2.2 of [6]) in order to prove the lower bound.

The proof is essentially a loop-level version of the factorization argument presented in Sec. 6 of [26] for tree-level amplituhedra. Let $(\mathcal{L}^{(1)}, \mathcal{L}^{(2)})$ be some configuration of loop momenta on some codimension $d_1 + d_2 + 1$ boundary of $\mathcal{A}_{n,\mathrm{k},2}$, satisfying the on-shell conditions

$$\langle \mathcal{L}^{(1)}\, a_1\, a_1{+}1 \rangle = \cdots = \langle \mathcal{L}^{(1)}\, a_{d_1}\, a_{d_1}{+}1 \rangle = 0\,, \tag{3.10}$$

$$\langle \mathcal{L}^{(2)}\, b_1\, b_1{+}1 \rangle = \cdots = \langle \mathcal{L}^{(2)}\, b_{d_2}\, b_{d_2}{+}1 \rangle = \langle \mathcal{L}^{(1)}\, \mathcal{L}^{(2)} \rangle = 0\,, \tag{3.11}$$

with the sets of indices $\{a_1, \ldots, a_{d_1}\}$ and $\{b_1, \ldots, b_{d_2}\}$ cyclically ordered and with $1 \leq d_1, d_2 \leq 4$ as detailed in [6]. Planarity requires that all of the b's fall inside an interval between two consecutive a's; specifically, there exists some j such that $a_j \leq b_i \leq a_{j+1}$ for all i. Once we have identified this value of j, let's backtrack and consider factorization (as described in [26]) on the boundary $\langle \mathcal{L}^{(1)}\, a_j\, a_j{+}1 \rangle = \langle \mathcal{L}^{(1)}\, a_{j+1}\, a_{j+1}{+}1 \rangle = 0$. Then $\mathcal{L}^{(1)}$ passes through some point A on the line $(a_j\, a_j{+}1)$ and some point B on the line $(a_{j+1}\, a_{j+1}{+}1)$. With $\mathcal{L}^{(1)} = (A\, B)$ we consider the sets of momentum twistors

$$V = \{A, Z_{a_j+1}, \dots, Z_{a_{j+1}}, B\}\,, \tag{3.12}$$

$$W = \{B, Z_{a_{j+1}+1}, \dots, Z_{a_j}, A\}\,. \tag{3.13}$$

Thinking of V and W separately as "(projected) external data" for sub-amplituhedra describing two smaller sets of scattering particles[4], it follows using arguments analogous to those in Sec. 6 of [26] that they lie in the principal domain for helicities k_V and k_W satisfying $\mathrm{k}_V + \mathrm{k}_W = \mathrm{k}$ where k is the original helicity sector of the (projected) external data $\{Z_i\}$.

Under the assumption that the two-loop configuration $(Y, \mathcal{L}^{(1)}, \mathcal{L}^{(2)})$ is a boundary of $\mathcal{A}_{n,\mathrm{k},2}(Z)$, we prove below the following statements:

- if $\mathcal{L}^{(1)}$ is a solution to the on-shell conditions (3.10) with minimum helicity k_1, then $\mathrm{k}_V \geq \mathrm{k}_1$, and similarly,
- if $\mathcal{L}^{(2)}$ is a solution to the on-shell conditions (3.11) with minimum helicity k_2, then $\mathrm{k}_W \geq \mathrm{k}_2$.

Once we show this, it follows immediately that the two-loop configuration $(\mathcal{L}^{(1)}, \mathcal{L}^{(2)})$ cannot be a valid boundary unless

$$\mathrm{k} = \mathrm{k}_V + \mathrm{k}_W \geq \mathrm{k}_1 + \mathrm{k}_2\,. \tag{3.14}$$

Proof. The minimum values of helicity $\mathrm{k}_{\mathrm{min}}$ for which sets of one-loop one-shell conditions admit solutions inside the closure of $\mathcal{A}_{n,\mathrm{k},1}$ were derived in Sec. 4 of [6]. In that analysis, the fact that a set of on-shell conditions does not have valid solutions of a certain type for $\mathrm{k} < \mathrm{k}_{\mathrm{min}}$ followed from the fact that the non-negativity constraints on the C and $\left(\begin{smallmatrix} D \\ C \end{smallmatrix}\right)$ matrices required certain sequences of (projected) four-brackets to contain at least $\mathrm{k}_{\mathrm{min}}$ sign flips. In analyzing the constraints on the solution $\mathcal{L}^{(1)}$ to Eq. (3.10), the relevant sequences of four-brackets are of the form $\langle \alpha\, \beta\, \gamma\, \bullet \rangle$ where α, β and γ are functions of the momentum twistors belonging to the set $S =$

[4]We put "(projected) external data" in quotation marks when it is (projected) external data only for a sub-amplituhedron, not for the full amplituhedron.

$\{Z_{a_1}, Z_{a_1+1}, \cdots, Z_{a_{d_1}}, Z_{a_{d_1}+1}\}$ only, and the required sign flips occur between adjacent entries in S. Note that there are two points (Z_{a_j} and $Z_{a_{j+1}+1}$) in S that lie outside V, the "(projected) external data" for one of the sub-amplituhedra under consideration. However, because A lies on the line $(a_j\, a_j{+}1)$ and B lies on the line $(a_{j+1}\, a_{j+1}{+}1)$, we clearly have $(a_j\, a_j{+}1) = (a_j\, A)$ and similarly $(a_{j+1}\, a_{j+1}{+}1) = (a_{j+1}\, B)$ so we can choose to express α, β and γ in terms of momentum twistors belonging to

$$S' = \{Z_{a_1}, Z_{a_1+1}, \ldots Z_{a_j}, A, B, Z_{a_{j+1}+1}, \ldots, Z_{a_{d_1}}, Z_{a_{d_1}+1}\} \subset V\,. \tag{3.15}$$

Therefore the abovementioned sequences can all be expressed in terms of the "(projected) external data" associated to the V sub-amplituhedron. Since there are k_1 sign flips in S', it must be the case that $\mathrm{k}_V \geq \mathrm{k}_1$. It follows similarly that $\mathrm{k}_W \geq \mathrm{k}_2$. ■

In Eq. (3.14) we derived an inequality $\mathrm{k} \geq \mathrm{k}_1{+}\mathrm{k}_2$, and at the end of Sec. 3.1.2 we explained that two-loop configurations have support starting from $\mathrm{k} = \mathrm{k}_1 + \mathrm{k}_2$ or $\mathrm{k} = \mathrm{k}_1 + \mathrm{k}_2 + 1$. In Sec. 3.1.2 we effectively defined k_1 and k_2 as the minimum helicities for configurations of loop momenta satisfying sets of disjoint on-shell conditions, not including the shared propagator. However, in this section the definition of k_2 (only) now includes the shared propagator (c.f. Eq. (3.11)). Effectively, this means that the k_2 here is the same as in Sec. 3.1.2 only for manifest intersection, but one greater than the latter in the case of non-manifest intersection.

3.2 Presentation of the Results

It is now a straightforward exercise to explicitly enumerate all possible pairs of one-loop boundaries, using those listed in Tab. 1 of [6], and to determine the minimum value of k such that the merged configuration is a valid boundary of $\mathcal{A}_{n,\mathrm{k},2}$. The resulting set is too large to display in a single figure of the type of Fig. 1 of [6] (which is a summary of the analogous results at one loop), so we focus first on the maximal codimension boundaries. Each involves a total of $d = 8$ on-shell conditions: the shared condition $\langle \mathcal{L}^{(1)}\, \mathcal{L}^{(2)} \rangle = 0$ together with seven conditions on the two loop momenta ($d_1 + d_2 = 7$, in the notation of Sec. 3.1.1).

We find a total of 14 topologically distinct maximal codimension configurations at two loops, which are summarized in Fig. 3.1. The figure emphasizes the fact that all 14 varieties of $\mathcal{L}$-boundaries can be obtained by some sequence of helicity-increasing operations $\mathcal{K}$ (defined in Sec. 5.2 of [6]) acting on just two primitive diagrams, one at MHV level and one at NMHV level. The entirety of this figure should be thought of as the two-loop $d = 8$ analog of the one-loop $d = 4$ column of Fig. 2 of that reference. In the figure, an arrow labeled by i indicates that the diagram at the end of the arrow can be obtained by acting with $\mathcal{K}_i$ on the diagram at the beginning of the arrow. An arrow carries two labels if the result of acting with two different instances of $\mathcal{K}$ gives topologically equivalent diagrams, in which case only the diagram corresponding to the first label on the arrow is shown. Note that for each diagram, the minimal value of k precisely matches the number of non-MHV intersections.

3.2.1 Resolutions

In each of the 14 twistor diagrams shown in Fig. 3.1, the configuration manifestly exhibits a total of $2n_{\text{filled}} + n_{\text{empty}} = 8$ on-shell conditions, where n_{filled} is the number of filled nodes and n_{empty} is the number of empty nodes (including, in each diagram, the node at the intersection of the two loop momenta).

However, on certain sufficiently high codimension boundaries, additional on-shell conditions can be implied by the others and are therefore "accidentally" satisfied. This phenomenon occurs for the four twistor diagrams in Fig. 3.1 that have been drawn with a filled node at the point Z_i and two empty nodes in close proximity (grouped in a faint gray circle in Fig. 3.1), representing the four on-shell conditions

$$\langle \mathcal{L}^{(1)}\, i{-}1\, i\rangle = \langle \mathcal{L}^{(1)}\, i\, i{+}1\rangle = \langle \mathcal{L}^{(2)}\, i\, i{+}1\rangle = \langle \mathcal{L}^{(1)}\, \mathcal{L}^{(2)}\rangle = 0\,. \tag{3.16}$$

The first three conditions are satisfied by $\mathcal{L}^{(1)} = (Z_i, A)$ and $\mathcal{L}^{(2)} = (\alpha Z_i + (1-\alpha)Z_{i+1}, B)$ for

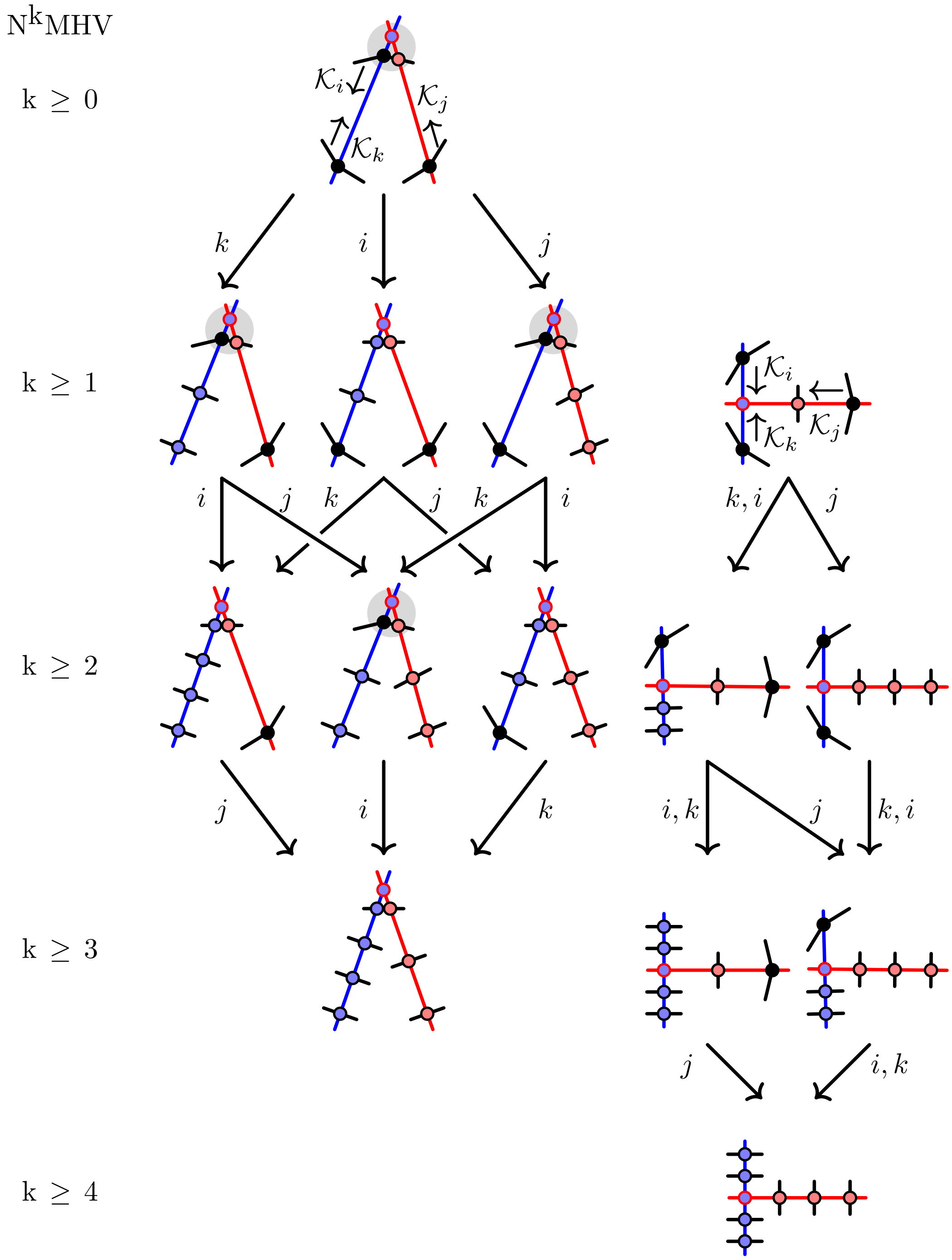

Figure 3.1: The twistor diagrams depicting the 14 distinct maximal codimension boundaries of two-loop $\mathrm{N^kMHV}$ amplituhedra. See the text for more details.

any points A, B. Then, for generic A and B, the fourth condition in Eq. (3.16) implies that $\alpha = 1$, so the line $\mathcal{L}^{(2)}$ is forced to pass through the point Z_i. Therefore, configurations of this type satisfy the additional on-shell condition $\langle \mathcal{L}^{(2)}\, i{-}1\, i \rangle = 0$.

This phenomenon reflects the fact that in general, the on-shell conditions satisfied by a given configuration are not independent: some of them may be implied by the others. In [5] it was found that solving the Landau equations for boundaries of this type was rather subtle, and required first identifying a suitable minimal subset of independent on-shell conditions, a process called *resolution*. It was suggested that a resolution must satisfy two criteria: (1) the chosen subset of on-shell conditions must imply the full set of conditions satisfied for generic (projected) external data, and (2) the Landau diagram corresponding to the subset must be planar.

The example considered above describes a configuration that satisfies five on-shell conditions, the four shown in Eq. (3.16) and also $\langle \mathcal{L}^{(2)}\, i{-}1\, i \rangle = 0$. There are four possible resolutions that satisfy criterion (1): we can simply omit any one of the conditions except for $\langle \mathcal{L}^{(1)}\, \mathcal{L}^{(2)} \rangle = 0$. However not all four choices will satisfy criterion (2), depending on the points A and B. For the four configurations appearing in Fig. 3.1 that require resolution, there are in each case precisely two valid resolutions: we can omit either $\langle \mathcal{L}^{(2)}\, i{-}1\, i \rangle = 0$ (as was done in Eq. (3.16)), or we can omit $\langle \mathcal{L}^{(1)}\, i\, i{+}1 \rangle = 0$.

In Fig. 3.1 we have chosen to always draw a resolved configuration in the four cases where it is necessary. However, in order to avoid clutter we do not draw both resolutions unless they give rise to inequivalent diagrams. There are at least three reasons for preferring the resolved configurations. First of all, it becomes somewhat less clear how to see the action of the three graph operators $\mathcal{K}$, $\mathcal{U}$ and $\mathcal{R}$ on an unresolved configuration. Also, the need for resolution is an accident that occurs only when both loop momenta lie in the low-k branch of solutions to their respective on-shell conditions (or, by parity symmetry, when they both lie in the high-k branch). If one of them lies in the low-k branch and the other lies in the high-k branch, then for generic (projected) external data only the resolved configuration(s) exist; the "extra" on-shell condition would place restrictions on the external data. Finally, when we turn our attention to finding Landau singularities in Sec. 3.4,

	Twistor Diagram	Landau Diagram
(a)	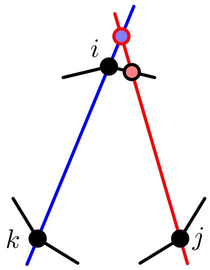	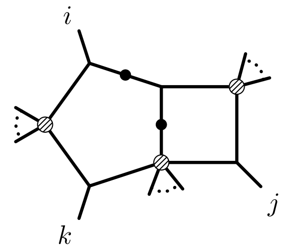

Table 3.1: The twistor and Landau diagram describing a type (the unique type, for $\mathrm{k} = 0$) of resolved maximal codimension boundary of $\mathrm{N}^{\mathrm{k}\geq 0}$MHV amplituhedra.

we will always want to work with resolved diagrams since these give us the independent sets of on-shell conditions for which we will need to solve the Landau equations [5].

3.2.2 Relaxations

All lower-codimension $\mathcal{L}$-boundaries are relaxations: they can be generated by releasing one or more of the seven on-shell conditions (excepting $\langle \mathcal{L}^{(1)} \mathcal{L}^{(2)} \rangle = 0$, which we always preserve) satisfied on the maximal boundaries. Boundaries of this type can be generated by acting on the twistor diagrams in Fig. 3.1 with sequences of the graph operators $\mathcal{U}$ and $\mathcal{R}$. In this way one could imagine uplifting the figure to a three-dimensional generalization of Fig. 2 of [6], with the top layer being a copy of Fig. 3.1 showing the maximal codimension boundaries ($d = 8$), the next layer showing those with $d = 7$, etc. One novelty compared to the one-loop analysis of [6] is that starting at two loops the relaxation of a boundary is not necessarily still a boundary — this will only be the case if the Landau diagram of the relaxation continues to be planar.

Rather than attempting to draw the aforementioned web of interconnected boundaries in a single figure, we summarize our results in terms of the corresponding Landau diagrams in Tabs. 3.1–3.5 grouped according to the minimum helicity for which the configuration is valid, i.e. the minimum k for which $\mathcal{A}_{n,\mathrm{k},2}$ has boundaries of the type shown in the corresponding twistor diagram. Because the maximal codimension singularities have $d_1 + d_2 = 7$, the corresponding Landau diagrams always have the topology of a planar pentagon-box.

As mentioned above the lower codimension singularities can be obtained by acting on the twistor diagrams with sequences of $\mathcal{U}$ and $\mathcal{R}$ operators. As discussed in Sec 5.2 of [6], at one loop these operators generate relaxations that respectively preserve or increase, but can never decrease, the minimum helicity for which a configuration is valid. There is however a subtlety with the $\mathcal{U}$ operator at two loops. Recall that $\mathcal{U}_{i,\mp}$ is the "unpinning" operator which acts on a loop momentum $\mathcal{L}$ passing through some point Z_i by relaxing the on-shell condition $\langle \mathcal{L}\, i\, i{\pm}1\rangle = 0$. This can have the effect of turning what was a manifest intersection between the two loop momenta into a non-manifest intersection, which requires increasing the minimum helicity by 1.

In the tables we have introduced a new graphical notation in order to account for this phenomenon: a propagator with a black dot denotes an on-shell condition that cannot be relaxed without increasing the minimum helicity for which the configuration is valid. (We also always draw a black dot on the $\langle \mathcal{L}^{(1)}\, \mathcal{L}^{(2)}\rangle$ propagator, as a reminder that we never want to relax it.) Consider for example the twistor diagram in Tab. 3.1(a). The two loop momenta manifestly intersect at the point Z_i as explained in the previous section, but this will no longer be the case if we act on this twistor diagram with $\mathcal{U}_{i,-}$. Instead, the configuration would become NMHV rather than MHV (in fact, it would become a relaxation of Tab. 3.2(d), up to relabeling). For this reason we draw a black dot on the $(i\, i{+}1)$ propagator on the pentagon in the Landau diagram of Tab. 3.1(a).

3.2.3 Closing Comments

In summary, to get the full list of Landau diagrams at helicity $\mathrm{k} = 0, 1, 2, 3, 4$, one must therefore consider all of the Landau diagrams in Tables. 3.1 through 3.5, respectively, together with the diagrams generated therefrom by collapsing any subset of undotted propagators.

In Fig. 3.1 and in the tables we have chosen to always draw the loop momentum satisfying $d_1 = 4$ in blue and the one satisfying $d_2 = 3$ in red, but of course the amplituhedron is symmetric under the exchange of any $\mathcal{L}$'s so in each case both assignments $\mathcal{L}^{(1)}$, $\mathcal{L}^{(2)}$ and $\mathcal{L}^{(2)}$, $\mathcal{L}^{(1)}$describe valid boundaries.

The Landau diagrams in Tables 3.1–3.5 are always drawn with the understanding that all indi-

	Twistor Diagram	Landau Diagram
(a)	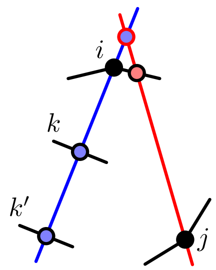	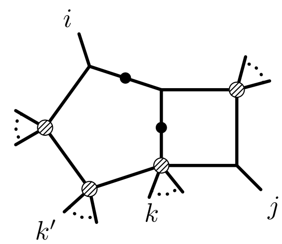
(b)	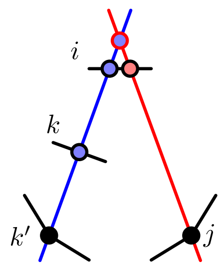	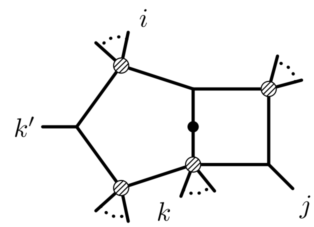
(c)	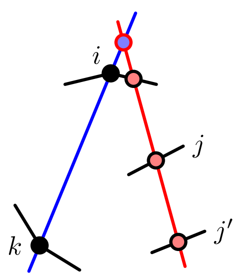	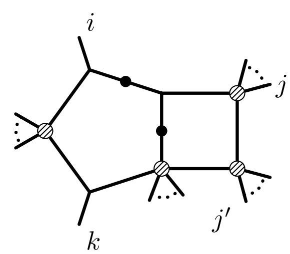
(d)	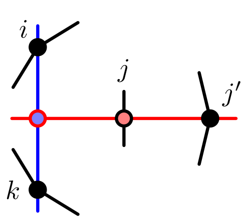	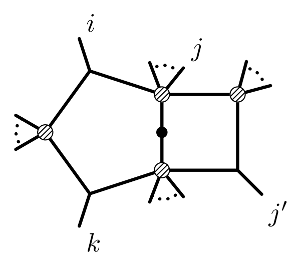

Table 3.2: The twistor and Landau diagrams describing types of (resolved, in (a) and (c)) maximal codimension boundaries of $\mathrm{N}^{k\geq 1}$MHV amplituhedra.

	Twistor Diagram	Landau Diagram
(a)	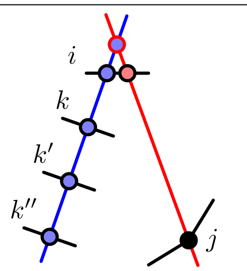	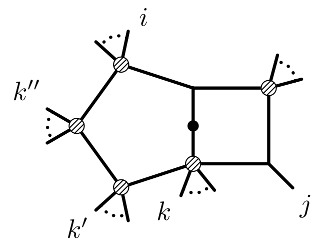
(b)	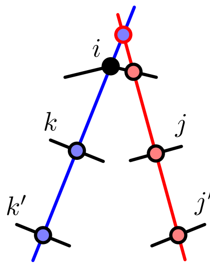	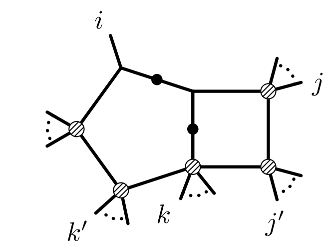
(c)	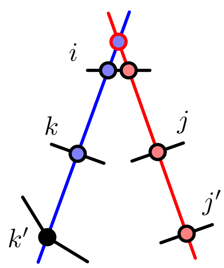	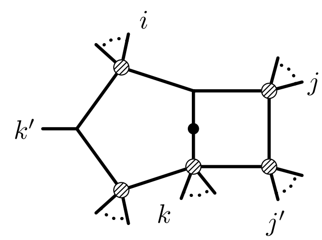
(d)	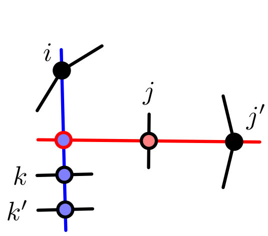	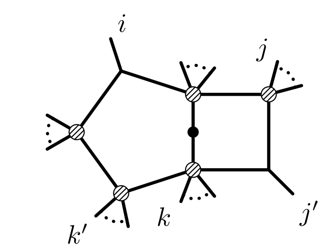
(e)	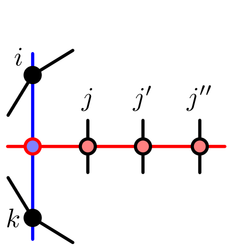	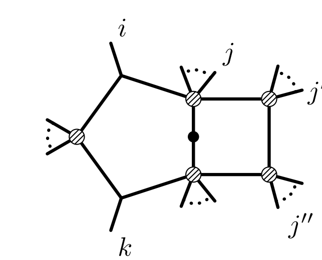

Table 3.3: The twistor and Landau diagrams describing types of (resolved, in (b)) maximal codimension boundaries of $\mathrm{N}^{\mathrm{k}\geq 2}$MHV amplituhedra.

	Twistor Diagram	Landau Diagram
(a)	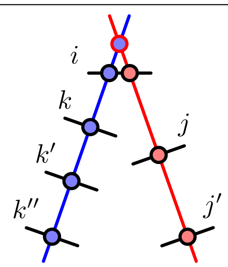	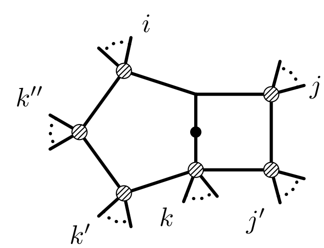
(b)	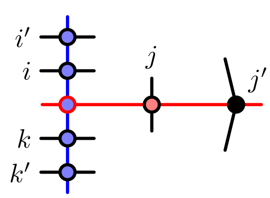	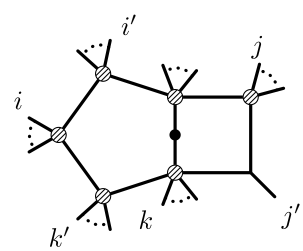
(c)	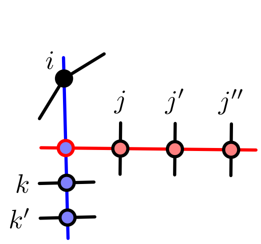	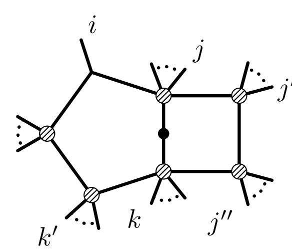

Table 3.4: The twistor and Landau diagrams describing types of maximal codimension boundaries of N$^{k\geq3}$MHV amplituhedra.

	Twistor Diagram	Landau Diagram
(a)	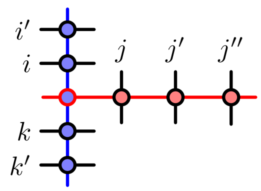	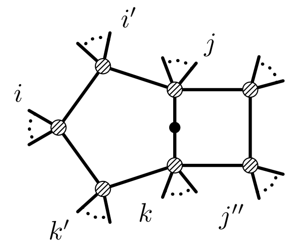

Table 3.5: The twistor and Landau diagram describing a type of maximal codimension boundary of N$^{\mathrm{k}\geq 4}$MHV amplituhedra.

cated labels are cyclically ordered: $i < i' < j < j' < j'' < k < k' < k'' < i$ (mod n). However, the ordering of intersections along the red or blue loop momentum lines carries no significance. Therefore, as described in Sec. 5.1 of [6], there is a second type of ambiguity between the two classes of diagrams. For example, the twistor diagram in Tab. 3.2(a) is agnostic about the cyclic ordering of i, k, and k'; the two independent choices lead to the Landau diagram shown in the table or to its mirror image. In all of the tables we use primes (and, when necessary, also double primes) to indicate pairs (or triplets) of nodes that can be exchanged, as far as the twistor diagram is concerned. Sometimes, as in the example Tab. 3.2(a) just considered, an exchange generates a Landau diagram of the same topology, but in other cases it can generate a new topology. For example, exchanging k and k' in the twistor diagram of Tab. 3.2(b) generates the new Landau diagram

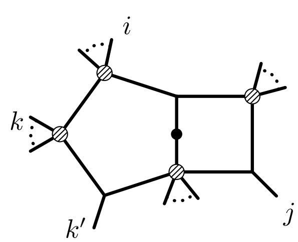

,

where it is to be understood that $i < j < k' < k < i$.

Let us also note that although when interpreted literally as configurations of intersecting lines in $\mathbb{P}^3$ most twistor diagrams only depict the low-k branch of solutions to a given set of on-shell conditions, it is clear that additional, higher-k boundaries can be generated by replacing one or both of the $\mathcal{L}$'s with their parity conjugates. The twistor diagrams appearing in Fig. 3.1 and in the five tables can therefore each be thought of as representing four different types of boundaries corresponding to the same Landau diagram.

Finally, we detail, in Appendix B, how a partial edge-to-node duality maps between the twistor diagrams on the left and the Landau diagrams on the right of these tables, when the two diagrams are treated as graphs. On the one hand, it is not surprising that there exists some map between these two classes of graphs, since both are designed to encode the same information. On the other hand, it is intriguing that there is a straightforward map between a generic Landau diagram and the minimum-helicity solution to the on-shell conditions of said diagram in the very particular choice of loop momentum twistor coordinates. This observation is also reminiscent of the map from Feynman integrals to their duals that aided in exploring the dual conformal invariance of SYM theory amplitudes [61, 62, 63] but here, enticingly, this partial edge-to-node map is well-defined even on nonplanar graphs.

3.3 The Connection With On-Shell Diagrams

So far, we have seen that to each boundary of an amplituhedron one can associate a Landau diagram which encodes information about the singularities of the associated amplitude. In this section we explore the connection between Landau diagrams and a class of closely related diagrams that also encode information about an amplitude's mathematical structure: the on-shell diagrams of [87]. We explain and demonstrate in several examples that for a given amplitude, the information content of certain on-shell diagrams matches the combined information content in the amplituherdon and Landau diagrams. Except possibly for cases of the type discussed in the paragraph following Eq. (3.30), we expect our arguments to also hold for amplitudes at higher loop order and higher helicity.

One reason to shift focus to on-shell diagrams is that anything that can be formulated in terms of the on-shell diagrams discussed here potentially generalizes to more general quantum field theories including less supersymmetric theories as well as the full, non-planar super-Yang–Mills theory. The major difference is that in the planar theory, the relevant Landau diagrams can, in principle, be read off from the boundaries of $\mathcal{A}_{n,\mathrm{k},L}$ for arbitrary n, k, and L, while in the non-planar sector there is currently no known supplier of this list of diagrams. Nevertheless, assuming one has a way to generate a representation for a given non-planar amplitude in terms of Feynman integrals, all of the techniques discussed in this section apply equally well to those non-planar integrals.

Putting that ambitious motivation aside, in the rest of this section we stick to planar SYM theory and show in several examples that a given Landau diagram encodes a singularity of an N$^{\mathrm{k}}$MHV amplitude only if the diagram can be decorated in such a way that it becomes an on-shell diagram associated with an N$^{\mathrm{k}}$MHV amplitude. We begin with a brief review of on-shell diagrams.

3.3.1 On-Shell Diagrams

An *on-shell diagram*, as introduced in [87], is a connected trivalent graph with each node having one of two distinct decorations, traditionally denoted by coloring them black or white. In the application to scattering amplitudes, each edge of the diagram represents an on-shell condition (just like in a Landau diagram) and each black (white) node corresponds to a three-point MHV ($\overline{\mathrm{MHV}}$) tree-level superamplitude. A straightforward generalization allows nodes of higher degree which represent higher-point tree-level superamplitudes. These we depict by a shaded node.

We refer the reader to [87] for details, recalling here only a few basic facts. A *tree-level superamplitude* of *Grassmann weight* κ is a rational function of (projected) external data that is a homogeneous polynomial of degree 4κ in certain Grassmann variables (the fermionic partners of the momentum twistors Z_i). Three-point MHV and $\overline{\mathrm{MHV}}$ amplitudes respectively have $\kappa = 2$ and $\kappa = 1$ while for $n > 3$ an n-point amplitude with helicity k has $\kappa = \mathrm{k} + 2$. To each on-shell diagram there is an associated differential form that is obtained by first multiplying together the tree-level superamplitudes represented by each of the diagram's nodes, and then sewing them together according to a set of simple rules that involve integrating over four Grassmann variables for each internal edge (propagator) in the diagram. Such forms are the values of the residue of the amplitude's integrand at specific loci in loop momentum space.

Consider an on-shell diagram δ. Let ι be the number of internal edges of δ, and for each node ν let κ_ν be the Grassmann weight of the tree-level superamplitude at ν. As a result of the rules just reviewed, the total Grassmann weight of δ is

$$\kappa_\delta = \sum_\nu \kappa_\nu - \iota \,, \tag{3.17}$$

and the total helicity is $\mathrm{k}_\delta = \kappa_\delta - 2$.

To assign a *coloring* to a Landau diagram depicting some set of on-shell conditions means to assign to each trivalent node in the diagram either a white or black coloring, and to assign to each node ν of degree $n > 3$ some helicity $\mathrm{k}_\nu = \kappa_\nu - 2 \in \{0, \ldots, n-4\}$. Since ι is fixed by the propagator structure of the diagram, and each κ_ν is positive, it is clear from Eq. (3.17) that the minimal Grassmann weight of a given Landau diagram results from coloring all trivalent nodes white and from assigning all nodes of higher degree to be MHV ($\kappa_\nu = 2$). In this way we see that the Grassmann weight of an arbitrary coloring of a given Landau diagram is bounded below by

$$\kappa \geq \kappa_{\text{min}} = n_{\text{tri}} + 2n_{\text{high}} - \iota \,, \tag{3.18}$$

where n_{tri} is the number of trivalent nodes and n_{high} is the number of nodes of degree higher than three. This implies a minimal helicity sector $k_{\text{min}} = \kappa_{\text{min}} - 2$ for which the Landau diagram can be relevant.

If a diagram has n_{tri} trivalent indices, there are $2^{n_{\text{tri}}}$ colorings of the trivalent nodes, but in general some of these may lead to on-shell diagrams that evaluate to zero. In practice we count the number of permissible colorings of a diagram by solving the on-shell conditions implied by the diagram and mapping each resulting solution to a specific coloring (see [87]). As discussed in [32], solving a set of on-shell conditions in momentum twistor space amounts to solving a Schubert problem. At one loop these problems have in general two solutions, while for an L-loop Landau diagram we would in general expect 2^L branches of solutions. Given a solution to a

Schubert problem in momentum twistor space, it is straightforward[5] to check if a given trivalent node is MHV or $\overline{\text{MHV}}$ by considering the rank of the three momentum-twistor lines at the node. For an MHV node, the three twistors have full rank, while for an $\overline{\text{MHV}}$ node the rank is less than full. This process is illustrated explicitly in several examples in the following section.

In summary, we have reviewed that a given Landau diagram encodes a set of on-shell conditions, and the various branches of solutions to those conditions correspond in general to different minimum helicity sectors. The permissible colorings of a Landau diagram are in one-one correspondence with those branches, and the Grassmann weight κ of each such Landau-turned-on-shell diagram is related to the minimum helicity sector k of the corresponding solution via $\kappa = \text{k} + 2$.

This observation provides an alternative way to phrase the Landau-equation-based algorithm we employ to identify singularities of amplitudes, compared for example to the way it is phrased in the conclusion of [5] or in Sec. 2.5 of [6]. For one thing, it means we can identify a singularity of a Landau diagram as a singularity of N^{k}MHV amplitudes only if the diagram admits a coloring with total helicity k (equivalently, Grassmann weight $\text{k} + 2$). More specifically, when first solving the on-shell conditions (a subset of the Landau equations) for a given Landau diagram, each solution directly indicates, via the test reviewed in the previous paragraph, the helicity sector for which the singularity associated to that solution is relevant. In the on-shell diagram approach this step is the analog in the amplituhedron approach of identifying the values of k for which the momentum twistor solution lies on the boundary of the N^{k}MHV amplituhedron. In the amplituhedron-based approach, there is potential for confusion because solving the Kirchhoff conditions (the remaining Landau equations) can lead to solutions for loop momenta that lie outside the N^{k}MHV amplituhedron. The on-shell diagram approach bypasses this confusion because the Kirchhoff conditions only further localize a loop momentum solution whose helicity sector has already been identified.

[5]We thank J. Bourjaily for explaining this point to us.

3.3.2 Examples at One and Two Loops

We now consider several examples in order to emphasize the following point:

$$\begin{aligned}&\text{A Landau diagram contributes singularities to an N}^{\text{k}}\text{MHV amplitude}\\&\text{only if the diagram permits a coloring with total Grassmann weight k} + 2.\end{aligned} \tag{3.19}$$

For each of our examples, we also list the values of the loop momenta corresponding to the colorings of the correct Grassmann weight. For the one-loop examples the same information can be read off from Tab. 1 of [6]. We will show how the on-shell diagram and amplituhedron-based methods work in tandem to quickly identify the helicity sector for which a given solution to the set of on-shell conditions is relevant.

One-loop Two-mass Easy Box

The on-shell conditions

$$\langle \mathcal{L}\, i{-}1\, i\rangle = \langle \mathcal{L}\, i\, i{+}1\rangle = \langle \mathcal{L}\, j{-}1\, j\rangle = \langle \mathcal{L}\, j\, j{+}1\rangle = 0 \tag{3.20}$$

admit two solutions, called branches (12) and (13) in [6]. In Tab. 3.6 we pair the momentum twistor representation of each solution with the associated on-shell diagram, i.e. colored Landau diagram. Having this information accessible will prove useful when considering two loops.

In Tab. 3.6(a) the minimum Grassmann weight is computed according to Eq. (3.18) and found to be

$$\kappa_{\text{min}} = \underbrace{1+1}_{\text{white}} + \underbrace{2+2}_{\text{higher}} - 4 = 2 \tag{3.21}$$

so that it is an MHV ($\mathrm{k} = 2 - 2 = 0$) coloring.

In Tab. 3.6(b) the minimum Grassmann weight is

$$\kappa_{\text{min}} = \underbrace{2+2}_{\text{black}} + \underbrace{2+2}_{\text{higher}} - 4 = 4 \tag{3.22}$$

so that it is an N²MHV ($\mathrm{k} = 4 - 2 = 2$) coloring.

Let us now show how to compute the appropriate node colorings directly from the momentum twistor solutions in Tab. 3.6. Consider the trivalent node where external label i connects to the loop. The three lines in momentum twistor space defining the trivalent node are $(i{-}1\, i)$, $(i\, i{+}1)$, and $\mathcal{L}_*$, where $\mathcal{L}_*$ is either $(i\, j)$ or $\bar{i} \cap \bar{j}$. Taking first $\mathcal{L}_* = (i\, j)$, we seek the dimension of the space spanned by the three momentum-twistor lines. One way to compute this is to ask for the rank of the matrix:

$$\text{rank}\begin{pmatrix} (i{-}1\, i) \\ (i\, i{+}1) \\ (i\, j) \end{pmatrix} = \text{rank}\begin{array}{c} \begin{array}{cccc} i{-}1 & i & i{+}1 & j \end{array} \\ \begin{pmatrix} 1 & 0 & 0 & 0 \\ 0 & 1 & 0 & 0 \\ 0 & 1 & 0 & 0 \\ 0 & 0 & 1 & 0 \\ 0 & 1 & 0 & 0 \\ 0 & 0 & 0 & 1 \end{pmatrix} \end{array} = 4 \tag{3.23}$$

which has maximal rank. So the node is MHV, and colored white.

	Coloring	N^{k}MHV	Twistor Solution
(a)	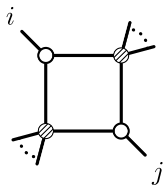	$\mathrm{k} \geq 0$	$\mathcal{L} = (i\,j)$
(b)	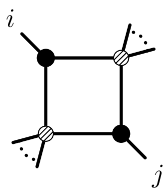	$\mathrm{k} \geq 2$	$\mathcal{L} = \bar{i} \cap \bar{j}$

Table 3.6: Two colorings of the two-mass easy box. Row (a) shows the MHV coloring and momentum twistor solution to the on-shell conditions, and row (b) shows the same for the N^{2}MHV solution.

In contrast, consider the other solution $\mathcal{L}_* = \bar{i} \cap \bar{j}$. The analogous matrix is then

$$\text{rank}\begin{pmatrix} (i{-}1\,i) \\ (i\,i{+}1) \\ \bar{i} \cap \bar{j} \end{pmatrix} = \text{rank}\ \begin{array}{c} \begin{array}{ccc} i{-}1 & i & i{+}1 \end{array} \\ \begin{pmatrix} 1 & 0 & 0 \\ 0 & 1 & 0 \\ 0 & 1 & 0 \\ 0 & 0 & 1 \\ \langle i\,\bar{j}\rangle & -\langle i{-}1\,\bar{j}\rangle & 0 \\ 0 & \langle i{+}1\bar{j}\rangle & -\langle i\,\bar{j}\rangle \end{pmatrix} \end{array} = 3 \tag{3.24}$$

which does not have maximal rank. Thus the second solution is encoded in an $\overline{\text{MHV}}$ node at i, colored black. The colorings of the node at j can be computed analogously.

	Coloring	N$^{\mathrm{k}}$MHV	Twistor Solution
(a)	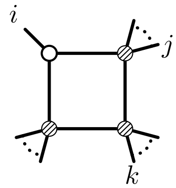	$\mathrm{k} \geq 1$	$\mathcal{L} = (i\,j\,j{+}1) \cap (i\,k\,k{+}1)$
(b)	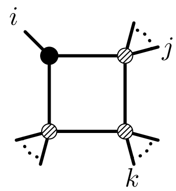	$\mathrm{k} \geq 2$	$\mathcal{L} = (A\,B)$ $A = (j\,j{+}1) \cap \bar{i}$ $B = (k\,k{+}1) \cap \bar{i}$

Table 3.7: Two colorings of the three-mass box. Row (a) shows the NMHV coloring and momentum twistor solution to the on-shell conditions, and row (b) shows the same for the N^{2}MHV solution.

One-loop Three-mass Box

We perform the same exercise for the three-mass box on-shell conditions

$$\langle \mathcal{L}\, i{-}1\, i \rangle = \langle \mathcal{L}\, i\, i{+}1 \rangle = \langle \mathcal{L}\, j\, j{+}1 \rangle = \langle \mathcal{L}\, k\, k{+}1 \rangle = 0\,. \tag{3.25}$$

The solutions of the on-shell conditions are matched to the two on-shell diagram colorings in Tab. 3.7, and the corresponding minimum Grassmann weights are computed using Eq. (3.18). The colorings are also directly calculable from the momentum twistor solutions as in the previous two-mass easy box example. The three-mass box is worth pointing out because in this case neither coloring is MHV, in contrast to the previous example.

Two-loop Pentagon-box

We can recycle our knowledge of one-loop solutions to determine the helicity sectors to which a given two-loop Landau diagram contributes its singularities. We consider the pentagon-box of Tab. 3.2(a) as an exemplar. We solve the pentagon-box on-shell conditions as follows. We first solve the subsystem of four propagators that depend on only $\mathcal{L}^{(2)}$:

$$\langle \mathcal{L}^{(2)}\, i{-}1\, i\rangle = \langle \mathcal{L}^{(2)}\, i\, i{+}1\rangle = \langle \mathcal{L}^{(2)}\, k\, k{+}1\rangle = \langle \mathcal{L}^{(2)}\, k'\, k'{+}1\rangle = 0 \tag{3.26}$$

using either of the two three-mass box solutions shown in Tab. 3.7, after an appropriate exchange of the external labels in order to match to Eq. (3.26). This means there are two branches of colorings: one were the trivalent node at i is white, and one where it is black. The two corresponding solutions $\mathcal{L}_*^{(2)}$ are shown in the first row of Tab. 3.8. For each choice of $\mathcal{L}_*^{(2)}$ we then solve the remaining four on-shell conditions

$$\langle \mathcal{L}^{(1)}\, i\, i{+}1\rangle = \langle \mathcal{L}^{(1)}\, j{-}1\, j\rangle = \langle \mathcal{L}^{(1)}\, j\, j{+}1\rangle = \langle \mathcal{L}^{(1)}\, \mathcal{L}_*^{(2)}\rangle\,. \tag{3.27}$$

These four conditions constitute a two-mass easy box problem, so we can utilize Tab. 3.6 to identify the two solutions $\mathcal{L}_*^{(1)}$, which color the trivalent nodes of the box either both white or both black. These two solutions are tabulated in the first column of Tab. 3.8. Altogether the table shows a grid containing a total of four distinct solutions, and the four associated distinct colorings. From this analysis we conclude that only the solution

$$\mathcal{L}_{*,1}^{(2)} = (i\, k\, k{+}1) \cap (i\, k'\, k'{+}1)\,,\ \mathcal{L}_{*,1}^{(1)} = (j\, i\, i{+}1) \cap (j\, \mathcal{L}_{*,1}^{(2)}) = (i\, j) \tag{3.28}$$

shown in the top left of Tab. 3.8 is relevant to the NMHV sector. This means that when we turn in the following section to the problem of finding singularities of NMHV amplitudes by solving the Landau equations, we can disregard the other three solutions. Were we to attempt an amplituhedron-based answer to this same question, we would find that the other solutions to the on-shell conditions do not lie on a boundary of $\mathcal{A}_{n,1,2}$.

$\mathcal{L}_*^{(1)} \backslash \mathcal{L}_*^{(2)}$	$(i\,k\,k{+}1) \cap (i\,k'\,k'{+}1)$	$((k\,k{+}1) \cap \bar{i}\,(k'\,k'{+}1) \cap \bar{i})$
$(i\,j)$	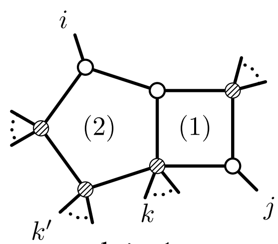 k ≥ 1	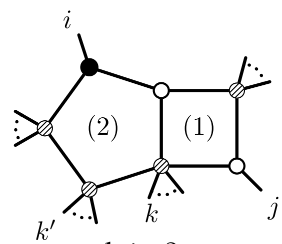 k ≥ 2
$\bar{i} \cap \bar{j}$	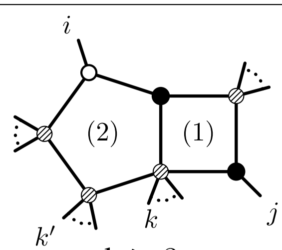 k ≥ 3	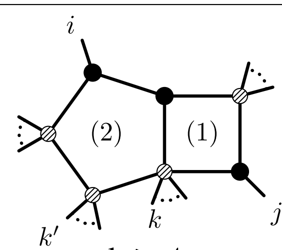 k ≥ 4

Table 3.8: All permissible colorings of the trivalent nodes of the two-loop pentagon-box Landau diagram from Tab. 3.2(a). The first row shows the two possible solutions to the three-mass on-shell conditions (Eq. (3.26)) satisfied by $\mathcal{L}^{(2)}$, the loop momentum in the pentagon. The first column shows the two possible solutions to the two-mass easy on-shell conditions (Eq. (3.27)) satisfied by $\mathcal{L}^{(1)}$, the loop momentum in the box. The cell at the intersection of a row and a column is the colored Landau diagram that results from the two solutions. Also indicated in each cell is the minimum helicity sector of the colored Landau diagram, which is achieved only if the gray nodes are taken to be MHV.

General Two-Loop Pentagon-Boxes

By using the same simple counting arguments applied to the results in Tables 3.1–3.5, it is a straightforward exercise to show that

- the set of Landau diagrams corresponding to the maximal codimension boundaries of $\mathcal{A}_{n,\mathrm{k},2}$ and
- the set of on-shell diagrams of pentagon-box topology that admit an $\mathrm{N^kMHV}$ coloring

are the same. Specifically, the second set may be constructed by starting with a pentagon-box diagram with no external edges or coloring, then placing all possible combinations of massive and massless edges on nodes of the diagram in all possible ways, and finally enumerating all colorings of the resulting Landau diagrams to identify the minimum possible value of k.

3.4 Landau Singularities of Two-Loop NMHV Amplitudes

Finally we come to step 2 of the algorithm summarized in Sec. 2.5 of [6]: in order to determine the locations of Landau singularities of the two-loop $\mathrm{N^kMHV}$ amplitude in SYM theory, we must identify, for each $\mathcal{L}$-boundary of $\mathcal{A}_{n,\mathrm{k},2}$ tabulated in Sec. 3.2, the codimension-one loci (if there are any) in $\mathrm{Conf}_n(\mathbb{P}^3)$ on which the corresponding Landau equations admit nontrivial solutions.

The ultimate aim of this project has been to derive (or at least to conjecture) symbol alphabets for two-loop amplitudes. However, as discussed in Sec. 7 of [6], guessing a symbol alphabet from a list of singularity loci can require a nontrivial extrapolation. At one loop the extrapolation is straightforward for all Landau diagrams except the four-mass box.

At two loops, four-mass box subdiagrams become prevalent starting at $\mathrm{k} = 2$, where they appear in the maximal codimension Landau diagram shown in Tab. 3.2(e), as well as in many of the relaxations of the other Landau diagrams in Tab. 3.2. At $\mathrm{k} = 1$ there is a single four-mass bubble-box Landau diagram, Fig. 3.2, relevant to two-loop NMHV amplitudes. As shown in the Appendix of [5], Landau diagrams containing bubble subdiagrams are equivalent to the same

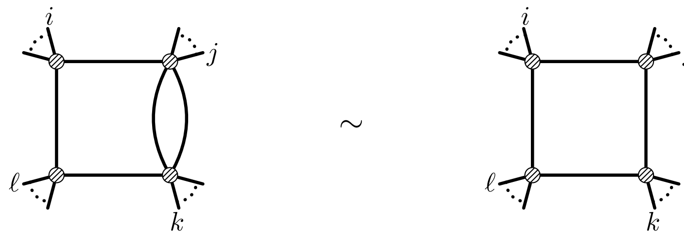

Figure 3.2: The Landau equations of a Landau diagram containing a bubble are identical to the equations of a Landau diagram with one propagator of the bubble removed. The two-loop four-mass bubble-box on the left is the only Landau diagram with a four-mass box contributing to the branch points of the NMHV amplitude. It has the same well-known branch points as the one-loop four-mass box on the right.

diagram with one of the propagators of the bubble removed. So we expect the one-loop four-mass box singularity to reappear as a singularity of the two-loop NMHV amplitude. Though we are only guaranteed from this analysis that the singularities match, we can throw caution to the wind and conjecture that the same symbol entries that appear in the one-loop four-mass box integral appear also in two-loop NMHV amplitudes. Of note here: the four-mass box has support starting at $\mathrm{k} = 2$, so there is shared singularity structure between the two-loop NMHV and one-loop N^2MHV amplitudes.

Having dealt with this single caveat, we restrict our analysis to the remaining NMHV singularities, where we may hope that our approach allows us to read off symbol alphabets directly from lists of singularity loci.

3.4.1 Computational Approaches

Sec. 2.4 of [6] reviews the Landau equations and Sec. 6 of that reference details the process of solving them in several one-loop examples. Beyond one loop, one approach for seeking solutions is to perform the analysis "one loop at a time", by considering each one-loop subdiagram and writing down the constraints on the values of other loop and external momenta imposed by the on-shell and Kirchhoff conditions of the subdiagram. After taking the union of those constraints, one may conclude that a solution exists for generic external data, or that the solution exists only when the external data satisfy some set of equations. Solutions of the former type were associated with the infrared singularities of an amplitude in [4], and solutions of the latter type indicate branch points of the amplitude when they live on codimension-one loci in $\mathrm{Conf}_n(\mathbb{P}^3)$.

Here we recall a few basic facts about this loop-by-loop approach, which has been carried out for several cases in [4, 5].

First, as mentioned above, one edge of a bubble subdiagram can always be removed without affecting Landau analysis.

Second, as shown in the Appendix of [5], a generic triangle subdiagram has seven different branches of solutions that should be considered separately. All of the solutions demand that the squared sum of momenta on "external" edges attached to at least one of the triangle's corners vanish, and the seven branches of solutions are classified according to the number of null corners[6]. There are three branches of "codimension-one" solutions (any one of the three corners vanishing), three branches of "codimension two" (any two of the three corners vanishing) and one of "codimension three" (all corners vanishing). In a Landau diagram analysis, it will often be the case that one of a triangle's corners is null by fiat; in this case, the solution space will be reduced. For example, a "two-mass" triangle subdiagram has only one codimension-one solution. In the examples we detail in Sec. 3.4.2, all triangle subdiagrams we describe are of this two-mass variety.

Finally, the Kirchhoff conditions associated to a box subdiagram constitute four homogeneous equations on four Feynman parameters, so the existence of nontrivial solutions requires the vanishing of a certain four-by-four determinant called the *Kirchhoff constraint* for the box. The Kirchhoff constraints for the four different cases of box diagrams are summarized in Eqns. (2.7) through (2.11) of [4].

It is worth noting one detail regarding the "one loop at a time" approach. Because the method starts by enumerating the constraints imposed by the existence of nontrivial solutions to the Landau equations of each subdiagram, it will miss the solutions which set all Feynman parameters

[6]These corners can be read off as the factors of the Landau singularity locus, for example in the rightmost column of Tab. 1, branch (9), of [6].

corresponding to some one-loop subdiagram to zero. However, Landau singularities obtained this way will always be those already present at lower loop order. So the "one loop at a time" approach neglects no novel branch points. We comment on a specific example of this phenomenon in the next section.

Let us also describe a conceptually simpler but computationally less effective alternative approach which we have used as a cross-check on our results. For a given branch of solutions to a set of on-shell conditions, or equivalently, for a given on-shell diagram, one can reduce the Landau equations "all at once" to see whether they impose codimension-one constraints on the external data. This approach is of course usually feasible only with the aid of a computer algebra system such as Mathematica. It also lends itself well to numerical experimentation: one can probe the presence or absence of a putative singularity at some locus $a = 0$ by generating random numeric values for the external data except for one free parameter z, and then reducing the Landau equations to see if the existence of nontrivial solutions forces z to take a value that sets $a = 0$.

Before proceeding to the examples and results, let us address the question: how do we confirm that we have detected all singularities? Starting from the maximal codimension boundaries of the NMHV amplituhedron shown in Tab. 3.2, we determine all corresponding Landau diagrams keeping in mind the ambiguity mentioned in Sec. 3.2.3. From there it is straightforward to produce all possible relaxed Landau diagrams. And from the diagrams we compute the singularities using the "one loop at a time" approach outlined above. Once we have a list of potential singularities, we turn to the "all at once" numerical probing. Doing so we directly confirm on a diagram-by-diagram basis not only that the set of singularities is correct, but also that there are no additional singularities. We have performed these steps to confirm the NMHV singularities presented in Sec. 3.4.3.

We will focus only on Landau diagrams that have minimally-NMHV coloring, as defined in Sec. 3.3.1, or equivalently, diagrams that come from a boundary of a two-loop NMHV amplituhedron. A priori, we cannot dismiss the possibility that a minimally-MHV diagram may have novel singularities coming from an NMHV branch of solutions, but we have explicitly checked that this does not occur in the two-loop NMHV amplitudes we consider here. We will demonstrate our "one loop at a time" approach to solving Landau equations on an example in the next section, and then proceed to list the full set of singularities in Sec. 3.4.3.

3.4.2 A Sample Two-Loop Diagram

We now turn to the Landau analysis of the boundaries displayed in Tab. 3.2. The analysis is very similar to that of the many examples that have been considered in [4, 5], to which we refer the reader for additional details. Therefore we only carry out the analysis in detail for the case of Tab. 3.2(a), and summarize all of the results in the following section.

At maximal codimension the on-shell conditions encapsulated in the Landau diagram of Tab. 3.2(a) are shown in Eqns. (3.26) and (3.27). These have a total of four discrete solutions, as summarized in Tab. 3.8, but the only one relevant at NMHV order is the one displayed in Eq. (3.28). The Landau equations (specifically, the Kirchhoff constraint for the box subdiagram defined by Eq. (3.27)) admit a solution only if [4]

$$\langle j(j{-}1\,j{+}1)(i\,i{+}1)\,\mathcal{L}_*^{(2)}\rangle = 0\,. \tag{3.29}$$

Substituting in the lower-helicity solution $\mathcal{L}_{*,1}^{(2)}$ and simplifying turns the constraint into

$$\langle i\,\bar{j}\rangle\langle i\,(i{+}1\,j)\,(k\,k{+}1)\,(k'\,k'{+}1)\rangle = 0\,. \tag{3.30}$$

Now we must address a subtlety of the result (3.30) that is analogous to the one encountered for the maximal codimension MHV configuration under Eq. (3.29) of [5]. Like in that case, the eight-propagator Landau diagram under consideration here, shown in Tab. 3.2(a), corresponds to a resolution of a configuration that actually satisfies nine on-shell conditions, as reviewed in Sec. 3.2.1. It was proposed in [5] that we should trust the resulting Landau analysis only to the extent that the eight on-shell conditions imply the ninth for generic external data. Let us note that if we put

$\langle \mathcal{L}^{(1)}\,\mathcal{L}^{(2)}\rangle = 0$ aside for a moment, the NMHV solution to the seven other on-shell conditions is

$$\mathcal{L}^{(2)} = (i\,k\,k{+}1) \cap (i\,k'\,k'{+}1)\,, \qquad \mathcal{L}^{(1)} = (\alpha Z_i + (1-\alpha) Z_{i+1}, Z_j)\,, \tag{3.31}$$

from which we find

$$\langle \mathcal{L}^{(1)}\,\mathcal{L}^{(2)}\rangle = (1-\alpha)\langle i(i{+}1\,j)(k\,k{+}1)(k'\,k'{+}1)\rangle\,. \tag{3.32}$$

Therefore the conclusion that $\alpha = 1$, and hence that the ninth condition $\langle \mathcal{L}^{(1)}\,i{-}1\,i\rangle = 0$ is also satisfied, actually only follows if $\langle i(i{+}1\,j)(k\,k{+}1)(k'\,k'{+}1)\rangle \neq 0$. This observation introduces controversy about whether the second quantity on the left-hand side of Eq. (3.30) is a valid singularity. However, note that from the on-shell diagram point of view there is no apparent reason why this singularity should be excluded, since the diagram can be assigned a valid NMHV coloring as shown in Tab. 3.8. Absent a rigorous argument resolving the matter, we remain agnostic about the status of this singularity.

It is easy to see that another solution to the Landau equations with $\mathcal{L}^{(1)} = (i\,j)$ and $\mathcal{L}^{(2)} = (i\,k\,k{+}1) \cap (i\,k'\,k'{+}1)$ exists if the four Feynman parameters associated to the box subdiagram are set to zero. In this case the box completely decouples and the pentagon subdiagram reduces to a three-mass box, so this branch exists if the external data satisfy the corresponding Kirchhoff constraint

$$\langle i(i{-}1\,i{+}1)(k\,k{+}1)(k'\,k'{+}1)\rangle = 0\,. \tag{3.33}$$

This illustrates the point highlighted in the previous section that the "one loop at a time" approach can miss certain solutions to the Landau equations associated entirely with one-loop subdiagrams. As mentioned, we are only seeking new singularities, whereas Eq. (3.33) is already known from one loop.

Next we move on to codimension seven. There are four inequivalent relaxations, which we now discuss in turn. These relaxations result from collapsing any of the undotted propagators of Tab. 3.2(a). We list only the minimally-NMHV diagrams; see Fig. 3.3.

Relaxing $\langle \mathcal{L}^{(2)}\, i{-}1\, i\rangle = 0$ leads to a double-box Landau diagram, Fig. 3.3(a).

There are two Kirchhoff constraints (one per box), one of which is easier to determine than the other. The easier-to-find Kirchhoff constraint comes from the box formed of the $\mathcal{L}^{(1)}$-dependent propagators (including the shared propagator). It reads

$$\langle j\,(j{-}1\,j{+}1)\,(i\,i{+}1)\,\mathcal{L}^{(2)}_{*}\rangle = 0\,, \tag{3.34}$$

where we write $\mathcal{L}^{(2)}_{*}$ to emphasize the loop momentum is on-shell when all Landau equations are satisfied.

The second Kirchhoff constraint is easiest to find after solving the three $\mathcal{L}^{(1)}$-dependent on-shell conditions via $\mathcal{L}^{(1)}_{*,1} = (Z_j, B)$, with $B = \alpha Z_i + (1-\alpha) Z_{i+1}$. Using this form of $\mathcal{L}^{(1)}$ in the $\mathcal{L}^{(2)}$-dependent propagators (including the shared one) results in

$$\langle \mathcal{L}^{(2)}\, i\, B\rangle = \langle \mathcal{L}^{(2)}\, k\, k{+}1\rangle = \langle \mathcal{L}^{(2)}\, k'\, k'{+}1\rangle = \langle \mathcal{L}^{(2)}\, j\, B\rangle = 0\,, \tag{3.35}$$

which are now effectively the propagators of a three-mass box. The second Kirchhoff constraint is therefore

$$\langle B\,(i\,j)\,(k\,k{+}1)\,(k'\,k'{+}1)\rangle = 0\,. \tag{3.36}$$

Solving the remaining on-shell and Kirchhoff constraints (recall that the three $\mathcal{L}^{(1)}$-dependent conditions were solved already) fixes

$$\mathcal{L}^{(2)}_{*,1} = (A\,k\,k{+}1) \cap (A\,k'\,k'{+}1)\,, \quad A = (i\,i{+}1) \cap \bar{j}\,, \quad \text{and} \tag{3.37}$$

$$B = (i\,i{+}1) \cap (j\,\mathcal{L}^{(2)}_{*,1})\,. \tag{3.38}$$

This constraint on B turns Eq. (3.36) into a codimension-one constraint on the external data:

$$\langle A\,(i\,j)\,(k\,k{+}1)\,(k'\,k'{+}1)\rangle = 0\,, \quad A = (i\,i{+}1) \cap \bar{j}\,, \tag{3.39}$$

which is a new, genuinely two-loop, singularity.

Relaxing $\langle \mathcal{L}^{(1)}\, j{-}1\, j\rangle = 0$ leads to a pentagon-triangle Landau diagram, Fig. 3.3(b).

There is a single codimension-one branch for the triangle subdiagram since there is an on-shell line at one of its corners. This branch leads to Landau equations with a solution locus that is a Kirchhoff constraint of three-mass box type:

$$\langle i\,(i{-}1\,i{+}1)\,(k\,k{+}1)\,(k'\,k'{+}1)\rangle = 0\,. \tag{3.40}$$

We do not focus on these already familiar singularities.

Following any codimension-two branch of the triangle subdiagram leads to Landau singularities that exist only on codimension-two loci in the space of external data, which are not of interest to us.

Following the single codimension-three branch for the triangle leads to a branch of solutions to the Landau equations that exists only if

$$\langle i\,(j\,j{+}1)\,(k\,k{+}1)\,(k'\,k'{+}1)\rangle = 0\,, \tag{3.41}$$

which is a new type of singularity.

Relaxing $\langle \mathcal{L}^{(1)}\, i\, i{+}1\rangle = 0$ leads to a pentagon-triangle Landau diagram, Fig. 3.3(c).

There is again a single codimension-one branch for the triangle subdiagram leading to an effective decoupling of the two loop momenta and an overall Landau constraint of the same form (up to relabeling) as Eq. (3.40).

Following the codimension-two branches for the triangle subdiagram uncovers constraints of

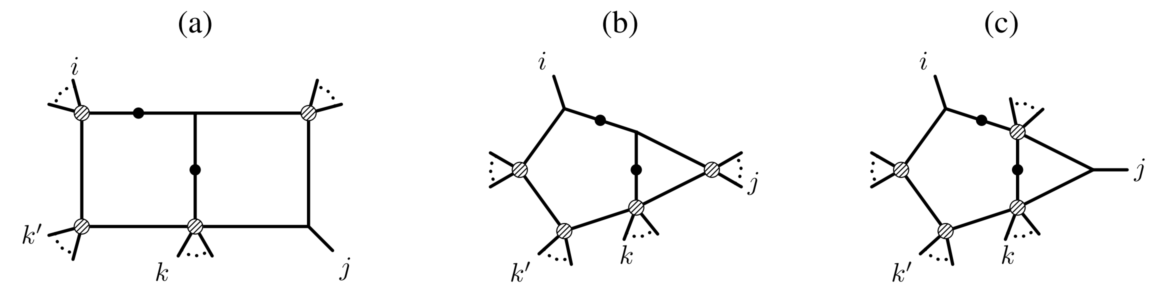

$\langle \mathcal{L}^{(2)}\, i{-}1\, i\rangle \neq 0$ $\qquad$ $\langle \mathcal{L}^{(1)}\, j{-}1\, j\rangle \neq 0$ $\qquad$ $\langle \mathcal{L}^{(1)}\, i\, i{+}1\rangle \neq 0$

Figure 3.3: These are the unique single-relaxations of Tab. 3.2(a) that result in NMHV Landau diagrams. The computation of the associated Landau singularities is discussed in the text.

codimension higher than one on the external data, which cannot sensibly be associated with branch points.

Following the codimension-three branch for the triangle subdiagram leads to the same Landau singularity as in Eq. (3.41) (up to relabeling).

At codimension six there are three inequivalent relaxations, shown in Fig. 3.4, that do not reduce the Landau diagram to an MHV one. Collapsing any of the undotted propagators of a box subdiagram in Fig. 3.4 results in a minimally-MHV Landau diagram, as one of the external labels would necessarily drop out. Any additional relaxations of a propagator in a triangle subdiagram of Fig. 3.4 will yield a bubble subdiagram, which cannot yield a new singularity as we have already emphasized.

Relaxing both $\langle \mathcal{L}^{(1)}\, i\, i{+}1\rangle$ **=** $\langle \mathcal{L}^{(2)}\, i{-}1\, i\rangle = 0$ leads to a box-triangle Landau diagram, Fig. 3.4(a).

The single codimension-one branch of the triangle leads to the effective decoupling of the two loops and results in Landau singularities at Mandelstam-type loci:

$$\langle i\, i{+}1\, k\, k{+}1\rangle \langle i\, i{+}1\, k'\, k'{+}1\rangle \langle k\, k{+}1\, k'\, k'{+}1\rangle = 0\,. \tag{3.42}$$

The same Landau singularities are obtained by following the codimension-two branches for the triangle.

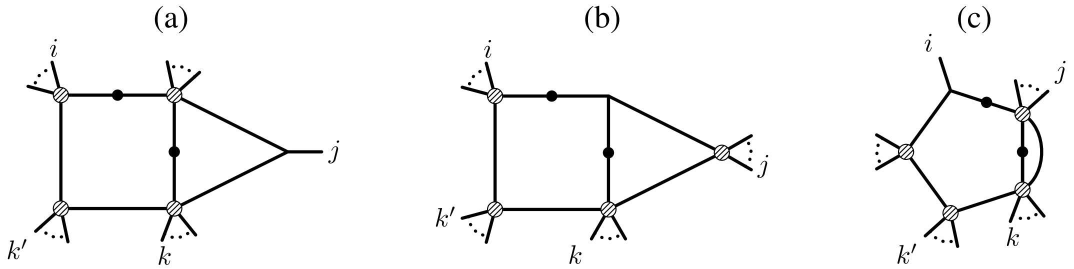

$\langle \mathcal{L}^{(2)}\, i{-}1\, i \rangle \neq 0$ $\langle \mathcal{L}^{(1)}\, i\, i{+}1 \rangle \neq 0$

$\langle \mathcal{L}^{(2)}\, i{-}1\, i \rangle \neq 0$ $\langle \mathcal{L}^{(1)}\, j{-}1\, j \rangle \neq 0$

$\langle \mathcal{L}^{(1)}\, i\, i{+}1 \rangle \neq 0$ $\langle \mathcal{L}^{(1)}\, j{-}1\, j \rangle \neq 0$

Figure 3.4: These are the unique minimally NMHV relaxations of the diagrams Fig. 3.3. As such, these are also double-relaxations of Tab. 3.2(a). Computing the associated singularities is discussed in the text. Any further relaxations of triangles yield bubble subdiagrams. In (c), relaxing either of $\langle \mathcal{L}^{(2)}\, i\, i{\pm}1 \rangle = 0$ yields the four-mass bubble-box of Fig. 3.2.

Following the codimension-three branch for the triangle leads to the constraint

$$\langle j\,(i\,i{+}1)\,(k\,k{+}1)\,(k'\,k'{+}1) \rangle = 0\,. \tag{3.43}$$

Relaxing both $\langle \mathcal{L}^{(2)}\, i{-}1\, i \rangle = \langle \mathcal{L}^{(1)}\, j{-}1\, j \rangle = 0$ leads to a box-triangle Landau diagram, Fig. 3.4(b). All branches of the triangle subdiagram result in bubble-type singularities, $\langle a\, a{+}1\, b\, b{+}1 \rangle$, or higher codimension constraints.

Relaxing both $\langle \mathcal{L}^{(1)}\, i\, i{+}1 \rangle = \langle \mathcal{L}^{(1)}\, j{-}1\, j \rangle = 0$ leads to a pentagon-bubble Landau diagram, Fig. 3.4(c), as discussed above and displayed in Fig. 3.2, with a singularity on the locus

$$\langle i\,(j\,j{+}1)\,(k\,k{+}1)\,(k'\,k'{+}1) \rangle = 0\,. \tag{3.44}$$

Relaxing both $\langle \mathcal{L}^{(1)}\, j{-}1\, j \rangle = \langle \mathcal{L}^{(1)}\, j\, j{+}1 \rangle = 0$ is displayed in Fig. 3.5. This case is interesting because it emphasizes the interplay between on-shell diagrams and the amplituhedron.

From the on-shell diagram perspective, this diagram naively has a minimally MHV coloring, Fig. 3.5(b). However the graph moves that preserve on-shell functions (particularly the "collapse and re-expand" and "bubble deletion" of Sec. 2.6 of [87]) permit redrawing the coloring as a three-

(a) (b) (c)

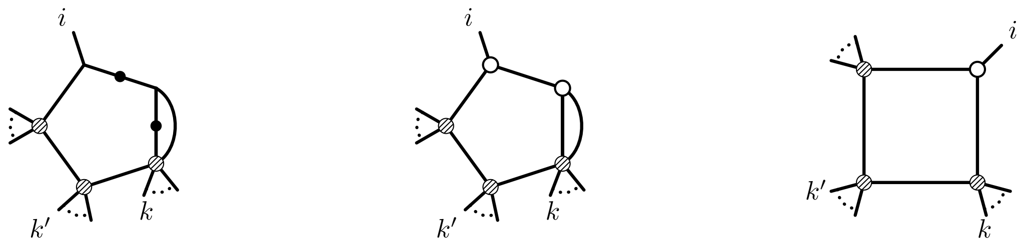

$\langle \mathcal{L}^{(1)}\, j{-}1\, j\rangle \neq 0$
$\langle \mathcal{L}^{(1)}\, j\, j{+}1\rangle \neq 0$

Minimal Coloring

After Graph Moves

Figure 3.5: The Landau diagram (a) appears to have a minimally MHV coloring (b). Yet the corresponding on-shell function is related by the on-shell diagram moves of [87] to one in the NMHV helicity sector (c).

mass box on-shell diagram Fig. 3.5(c), colored in its minimal helicity manner, k ≥ 1 . Since the graph moves preserve the on-shell function, the original on-shell diagram must also be minimally NMHV.

It is straightforward to check that the momentum twistor solution corresponding to this minimal coloring Fig. 3.5(a) is in fact a boundary of an NMHV amplituhedron, not an MHV one, and so the on-shell diagram and amplituhedron perspectives align.

For the two-loop amplitude, this diagram does not contribute new possible branch points, but this phenomenon is something to keep in mind for future studies.

There are no new NMHV triple relaxations, but we revisit a case discussed earlier to show how it naturally arises in this organizational scheme.

Relaxing all of $\langle \mathcal{L}^{(2)}\, i{-}1\, i\rangle = \langle \mathcal{L}^{(1)}\, i\, i{+}1\rangle = \langle \mathcal{L}^{(1)}\, j{-}1\, j\rangle = 0$ leads to the bubble-box Landau diagram discussed above and displayed in Fig. 3.2. As mentioned above, this does not contribute a new two-loop singularity but it does indicate that two-loop NMHV amplitudes inherit the four-mass box singularity that appears at one loop only starting at k $= 2$. Our analysis indicates this is a fairly common phenomenon: Landau diagrams for an L-loop N$^{\text{k}}$MHV amplitude that contain bubble or triangle subdiagrams will often contain singularities that also contribute to $(L-1)$-loop $\mathrm{N}^{\mathrm{k}+1}$MHV amplitudes.

3.4.3 Two-Loop NMHV Symbol Alphabets

The full set of loci in the external kinematic space $\mathrm{Conf}_n(\mathbb{P}^3)$ where two-loop NMHV amplitudes have Landau singularities is obtained by carrying out the analysis of the previous section for all Landau diagrams appearing in Tabs. 3.1 and 3.2, together with all of their (still NMHV) relaxations. Among the set of singularities generated in this way are the two-loop MHV singularities that arise from the configuration shown in Tab. 3.1, which live on the loci

$$\begin{aligned} \langle a\, a{+}1\, b\, c\rangle &= 0\,, \\ \langle a\, a{+}1\, \bar{b} \cap \bar{c}\rangle &= 0\,, \end{aligned} \tag{3.45}$$

for arbitrary indices a, b, c. The set of brackets appearing on the left-hand sides of Eq. (3.45) correspond exactly to the set of symbol letters of two-loop MHV amplitudes originally found in [64].

For the NMHV configurations shown in Tab. 3.2 we find additional singularities that live on loci of the form[7]

$$\begin{aligned} \langle i\,(i{\pm}1\,\ell)(j\,j{+}1)(k\,k{+}1)\rangle &= 0\,, \\ \langle j\,(j{-}1\,j{+}1)\,(j'\,j'{+}1)\,(i\,\ell)\rangle &= 0\,, \\ \langle i\,(j\,j{+}1)(k\,k{+}1)(\ell\,\ell{+}1)\rangle &= 0\,, \\ \langle i\,i{+}1\,\bar{j} \cap (k\,k'\,k'{+}1)\rangle &= 0\,, \\ \langle \bar{i} \cap (i\,i'\,i'{+}1)\, \cap\, \bar{j} \cap (j\,j'\,j'{+}1)\rangle &= 0\,, \\ (i\,i{+}1) \cap \bar{j}; (i\,j)(k\,k{+}1)(\ell\,\ell{+}1) &= 0\,, \end{aligned} \tag{3.46}$$

[7] Out of caution we have included on the first line the singularities of the type shown in Eq. (3.30); but we remind the reader of the discussion in the subsequent paragraph; for $n = 8$ it happens that the first line is necessarily a particular case of the second and/or fourth so there is no controversy.

using notation explained in Appendix A. The indices are restricted (as a consequence of planarity) to have the cyclic ordering $\ell \leq \{i, i'\} \leq \{j, j'\} \leq \{k, k'\} \leq \ell$ (or the reflection of this, with all $\leq$'s replaced by $\geq$'s) where the curly bracket notation means that the relative ordering of an index with its primed partner is not fixed (tracing back to the ambiguity discussed in Sec. 3.2.3).

In addition to singularities of the type listed in Eq. (3.46), two-loop NMHV amplitudes also have four-mass box singularities as discussed in the beginning of Sec. 3.4 and illustrated in Fig. 3.2. Although guessing symbol letters from knowledge of singularity loci is in general nontrivial (see Sec. 7 of [6]), we conjecture that the quantities appearing on the left-hand sides of Eqns. (3.45) and (3.46), together with appropriate symbol letters of four-mass box type (see the example in the following section), constitute the symbol alphabet of two-loop NMHV amplitudes in SYM theory. It is to be understood that all degenerations of the indicated forms are meant to be included as well, for example such as taking $j = j' - 1$ in the first line. For certain values of some indices the expressions can degenerate into symbol letters (or products of symbol letters) that already appear in Eq. (3.45), or elsewhere in Eq. (3.46), but other degenerate cases are valid, new NMHV letters.

It is interesting to note that for arbitrary n the conjectural set of symbol letters in Eq. (3.46) is not closed under parity, unlike the two in Eq. (3.45) which are parity conjugates of each other[8]. We know of no a priori reason why the symbol alphabet for a given amplitude in SYM theory should be closed under parity; in principle, the parity symmetry of the theory requires only that the symbol alphabet of $\mathrm{N^kMHV}$ amplitudes must be the parity conjugate of the symbol alphabet of $\mathrm{N}^{n-\mathrm{k}-4}$MHV amplitudes.

The absence of parity symmetry is a simple consequence of the fact that different branches of solutions to the Landau equations give non-zero support to amplitudes in different helicity sectors (or, equivalently, overlap boundaries of amplituhedra in different helicity sectors). From this point of view it appears to be an accident that the two-loop MHV symbol alphabet is closed under parity; we guess that this will continue to hold at arbitrary loop order. It is also an interesting consistency

[8]More precisely, the parity conjugate of the first quantity in Eq. (3.45) is $\langle a{-}1\, a\, a{+}1\, a{+}2\rangle$ times the second; they become exactly parity conjugate in a gauge where the momentum twistors are scaled so that all four-brackets of four adjacent indices are set to 1.

check that for $n < 8$ the symbol letters in Eq. (3.46) necessarily degenerate into letters of the type already present at MHV order. This is consistent with all results available to date from the hexagon and heptagon amplitude bootstrap programs, which are based on the hypothesis that the symbol alphabet for all amplitudes with $n < 8$ is given by Eq. (3.45) to all loop order. Genuinely new NMHV letters begin to appear only starting at $n = 8$, to which we now turn our attention.

3.4.4 Eight-point Example

For the sake of illustration let us conclude by explicitly enumerating our conjecture for the two-loop NMHV symbol alphabet for the case $n = 8$. First let us recall that the corresponding MHV symbol alphabet [64] is comprised of 116 letters:

- 68 four-brackets of the form $\langle a\, a{+}1\, b\, c\rangle$ (there are altogether of $\binom{8}{4} = 70$ four-brackets of the more general form $\langle a\, b\, c\, d\rangle$, but at $n = 8$ both $\langle 1\,3\,5\,7\rangle$ and $\langle 2\,4\,6\,8\rangle$ are excluded by the requirement that at least one pair of indices must be adjacent),
- 8 cyclic images of $\langle 1\,2\,\overline{4} \cap \overline{6}\rangle$,
- and 40 degenerate cases of $\langle a\, a{+}1\, \overline{b} {\cap} \overline{c}\rangle$ consisting of 8 cyclic images each of $\langle 1\,(2\,3)(4\,5)(7\,8)\rangle$, $\langle 1\,(2\,3)(5\,6)(7\,8)\rangle$, $\langle 1\,(2\,8)(3\,4)(5\,6)\rangle$, $\langle 1\,(2\,8)(3\,4)(6\,7)\rangle$, as well as $\langle 1\,(2\,8)(4\,5)(6\,7)\rangle$.

Referring the reader again to Appendix A for details on our notation, we conjecture that an additional 88 letters appear in the symbol alphabet of the two-loop $n = 8$ NMHV amplitude[9]

- 48 degenerate cases consisting of 16 dihedral images each of $\langle 1\,(2\,3)(4\,5)(6\,7)\rangle$, $\langle 1\,(2\,3)(4\,5)(6\,8)\rangle$, as well as $\langle 1\,(2\,8)(3\,4)(5\,7)\rangle$,
- 8 cyclic images of $\langle \overline{2} \cap (2\,4\,5) \cap \overline{8} \cap (8\,5\,6)\rangle$ (this set is closed under reflections, so adding all dihedral images would be overcounting),

[9]The $116 + 88 = 204$ symbol letters of this amplitude can be assembled into $204 - 8 = 196$ dual conformally invariant cross-ratios in many different ways. We cannot *a priori* rule out the possibility that the symbol of this amplitude might be expressible in terms of an even smaller set of carefully chosen multiplicatively independent cross-ratios, though this type of reduction is not possible in any known six- or seven-point examples.

- the 8 distinct dihedral images of $\langle\bar{2}\cap(2\,4\,5)\cap\bar{6}\cap(6\,8\,1)\rangle$ (which is distinct from its reflection but comes back to itself after cycling the indices by four),
- 16 dihedral images of $(1\,2)\cap\bar{4};(1\,4)(5\,6)(7\,8)$,
- and finally 8 four-mass box-type letters.

The last of these were displayed in Eq. (7.1) of [6] and take the form

$$f_{i\ell}f_{jk} \pm (f_{ik}f_{j\ell} - f_{ij}f_{k\ell}) \pm \sqrt{(f_{ij}f_{k\ell} - f_{ik}f_{j\ell} + f_{i\ell}f_{jk})^2 - 4f_{ij}f_{jk}f_{k\ell}f_{i\ell}}\,, \tag{3.47}$$

where $f_{ij} \equiv \langle i\,i{+}1\,j\,j{+}1\rangle$ and the signs may be chosen independently. For $n = 8$ there are two inequivalent choices $\{i, j, k, \ell\} = \{1, 3, 5, 7\}$ or $\{2, 4, 6, 8\}$, for a total of eight possible symbol letters of this type.

3.5 Conclusion

The symbol alphabets for all two-loop MHV amplitudes in SYM theory were first found in [64]. In [67, 34] it was found that two-loop NMHV amplitudes have the same symbol alphabets as the corresponding MHV amplitudes for $n = 6, 7$, which is now believed to be true to all loop order. However, the question of whether two-loop NMHV amplitudes for $n > 7$ have the same symbol alphabets as their MHV cousins has remained open. In this paper we find that the former have branch points (of the type shown in Eq. (3.46)) not shared by the latter, answering this question in the negative.

Our conjectures for the two-loop NMHV symbol alphabets are formulated in terms of quantities analogous to the cluster $\mathcal{A}$-coordinates of [35], although it is simple to confirm that at least some of them are not cluster coordinates of the $\mathrm{Gr}(4, n)$ cluster algebra (it is possible that none of them are, but some of them are more difficult to check). For the purpose of carrying out the amplitude bootstrap, it is however more convenient to assemble these letters into dual conformally invariant cross-ratios. In the literature considerable effort (see for example [40, 38, 36, 39, 75]) has gone into divining deep mathematical structure of amplitudes hidden in the particular kinds of cross-ratios that might appear, especially when they can be taken to cluster $\mathcal{X}$-coordinates (or Fock-Goncharov coordinates) of the type reviewed in [35]. However, we see no hint in the Landau analysis or inherent to the twistor or on-shell diagrams employed in this paper that suggests any preferred way of building such cross-ratios.

It is inherent in the approach taken here following [5, 6] (as well as in the amplitude bootstrap program itself) that we eschew knowledge of or interest in explicit representations of amplitudes in terms of local Feynman integrals. However, as mentioned in the conclusion of [6], the procedure of identifying relevant boundaries of amplituhedra and then solving the Landau equations associated to each one as if it literally represented some Feynman integral is suggestive that this approach might be thought of as naturally generating integrand expansions around the highest codimension amplituhedron boundaries[10]. This approach might lead to a resolution of the controversy regarding the status of Landau singularities of the type Eq. (3.30) obtained from maximal codimension boundaries. This analysis is, however, beyond the scope of our paper and we remain agnostic about the status of this branch point in anticipation of empirical data. If this singularity is shown to be spurious, this would be an interesting result not easily explainable using on-shell diagram techniques, and it would signal that boundaries of amplituhedra contain more information waiting to be explored.

These observations highlight a point that we have emphasized several times in this paper and the prequel [6]. Namely, several threads in this tapestry, including the connection to on-shell diagrams reviewed in Sec. 3.3 and the simple relation between twistor diagrams and Landau diagrams in Appendix B, do not inherently rely on planarity. This hints at the tantalizing possibility that some of our toolbox may be useful for studying non-planar amplitudes about which much less is known (see [41, 42, 43]).

One of the stronger hints — the relationship between on-shell diagrams and Landau diagrams — also aids in corroborating results. A vanishing on-shell diagram indicates a location where the

[10] We are grateful to N. Arkani-Hamed for extensive discussions on this point.

analytic structure of an amplitude is trivial; that is exactly the same information encoded by the boundaries of the amplituhedron. The simple connection between the results tabulated in Sec. 3.2 and those obtained via the on-shell diagram approach provides an important cross-check supporting the validity of our analysis, as well as giving additional corroboration to the definition of amplituhedra.

Chapter 4

Scattering amplitudes and simple canonical forms for simple polytopes

In the last few years it has been understood that the novel geometrical picture for scattering amplitudes utilized in the previous chapter extends beyond the very special SYM theory. Amplituhedra have been found to underlie amplitudes in bi-adjoint scalar theory at tree level [88], integrands at 1-loop level [98], and constituents of planar tree level amplitudes in a host of scalar theories with polynomial interactions [90],[99],[100], as well as in non-planar ones [101]. It is promising to discover that the same set of ideas can be used to describe amplitudes in theories as vastly different as SYM and bi-adjoint ϕ^3. On the other hand, it is perhaps not surprising that the role of the amplituhedron in these elementary theories is played directly by convex polytopes which, in the language of [92], are the most basic instances of *Positive Geometries*, whereas the SYM amplituhedron sits on the wildest end of the spectrum of these geometries.

It is probably wise at this point to caution the reader, especially the physicist reader, that the elementary nature of convex polytopes can be deceptive. The study of polytopes is indeed a rich branch of mathematics, with connections to combinatorics, geometry and abstract algebra, where foundational results were established only recently. Just to give an example, to this day it is not understood whether a putative "combinatorial" polytope can be realized as the face lattice of an actual convex polytope. Because of this, the existence of infinite families of polytopes associated with the theories described above should be appreciated for being a very non-trivial fact.

A common trait of the newly discovered amplituhedra is that they all are *simple* polytopes, which means that each of their vertices lies at the intersection of precisely d facets [1], d being the dimension of the polytope itself. The canonical form of these polytopes can be immediately written, following [88], as a sum over its vertices

$$\Omega = \sum_{v \in \text{vertices}} \text{sgn}(v) \bigwedge_{\substack{f \in \text{facets} \\ v \in f}} d\log(X_f), \tag{4.1}$$

where X_f is the variable associated to a facet f. When a convex realization of the polytope is known, all the variables X_f are given by affine linear functions. However, it will be enlightening for the moment to think of the X_f as independent variables and Ω as a differential form defined on the space spanned by all of them, which we collectively call X. We still have to decide how to assign the relative signs of the $d$logs appearing in (4.1). This can be done uniquely up to an overall sign by requiring Ω to be *projective*, i.e. invariant under local rescaling of the variables $X \to \alpha(X)X$. We can give an appealing interpretation for the projectivity of a form by introducing the projective variation operator defined as

$$d\log\alpha \wedge \delta(\Omega) := \Omega|_{X \to \alpha(X)} - \Omega.$$

It is not difficult to see that for any form Ω written as a linear combination of $d$logs, the form

$$\tilde{\Omega} = \Omega - d\log(M) \wedge \delta(\Omega),$$

where M is a new variable not already appearing in Ω, is projective. It follows that $\tilde{\Omega}$ is well defined as a top form on the projective space with homogeneous coordinates $Y = (M, X)$. Clearly, it reduces to Ω in the affine chart where $M = 1$; however, it also develops a pole along the plane at

[1] By facet we mean a codimension one boundary of the polytope

infinity $M = 0$ with residue $\delta(\Omega)$. In conclusion, the projectivity of Ω is equivalent to the absence of a pole at infinity when the variables X are projectivized, a fact which is strongly reminiscent of dual conformal invariance in $\mathcal{N} = 4$ SYM.

For a simple polytope the projectivity of Ω is a remarkable property which is, however, obscured in (4.1): the $d\log$ terms are not individually invariant and the projectivity is hidden in the fact that relative signs can be coherently assigned to all vertices in such a way that their projective variations cancel each other. En passant we recall that vertices are associated to Feynman diagrams, so we can rephrase this fact as saying that there is a symmetry of the amplitude obscured term-by-term in the Feynman diagramatic expansion. It is natural to try and make manifest this symmetry by finding a representation for Ω which is manifestly invariant under δ.

We will see shortly that such a representation exists, but first let us start with a few illustrative examples. The simplest polytope is a segment for which the canonical form can be trivially made manifestly projective,

$$\Omega_2 = d\log(X_1) - d\log(X_2) = d\log\left(\frac{X_1}{X_2}\right), \tag{4.2}$$

since it depends only on the ratio X_1/X_2.

The first non-trivial shape that we encounter is a 2-dimensional pentagon as in Fig. 4.1 whose canonical form is

$$\begin{aligned}\Omega_5 = {} & d\log(X_1)d\log(X_2) - d\log(X_3)d\log(X_2) \\ & + d\log(X_3)d\log(X_4) - d\log(X_5)d\log(X_4) + d\log(X_5)d\log(X_1),\end{aligned} \tag{4.3}$$

and now there is no obvious way of recombining the $d\log$s in a manifestly projective way. However, we can decompose the pentagon in the two squares as in Fig. 4.1 and, accordingly, write its canonical form as the sum of the two forms associated to each square. We introduce an extra boundary which, in order to be internal to the pentagon, must be of the form $X_{\text{spurious}} \sim X_1 - \epsilon X_2$ for some positive ϵ; it will be sufficient to make the simplest choice $X_{\text{spurious}} = X_1 - X_2$. We

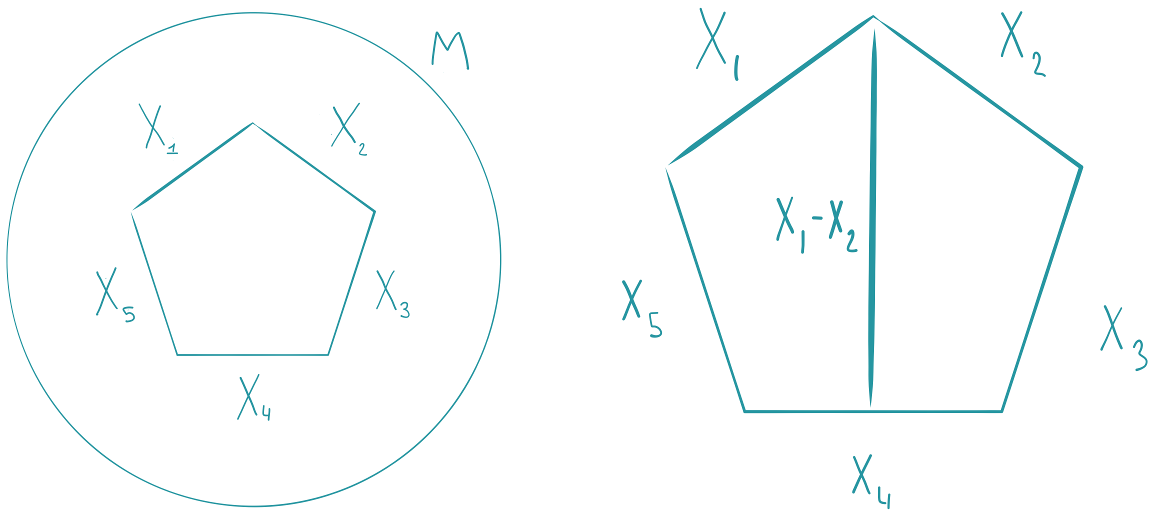

Figure 4.1: A pentagon with the line at infinity $\{M = 0\}$ (left) and its decomposition into two squares (right).

obtain the expression

$$\begin{aligned}\Omega_5 &= [d\log(X_1) - d\log(X_4)] \wedge [d\log(X_5) - d\log(X_2 - X_1)] + \\ &+ [d\log(X_2) - d\log(X_4)] \wedge [d\log(X_3) - d\log(X_1 - X_2)] = \\ &= d\log\left(\frac{X_1}{X_4}\right) \wedge d\log\left(\frac{X_5}{X_2 - X_1}\right) + d\log\left(\frac{X_2}{X_4}\right) \wedge d\log\left(\frac{X_3}{X_1 - X_2}\right),\end{aligned} \tag{4.4}$$

which is manifestly projective. Before going further, we wish to emphasize that in the above computation the details of the particular convex realization of the pentagon do not appear. In particular, there was no real motivation to draw the line X_{spurious} in Fig. 4.1 as intersecting the facet X_4 inside of the pentagon. Nevertheless, the equality in (4.4) stands as an equality between differential forms on the space of *independent* variables X. We should also emphasize a fact which might have gone unnoticed in the derivation of (4.4) because of the particularly simple geometry in consideration. Each of the squares can be thought of as a $prism$, by which we mean a polytope with two combinatorically equivalent facets - let us call them $\mathcal{U}$pper and $\mathcal{B}$ottom - plus many $\mathcal{S}$ide facets joining them. Because of its simple structure, it is easy to guess that the canonical form of a prism is

$$\Omega_{\mathcal{P}} = d\log\left(\frac{X_{\mathcal{B}}}{X_{\mathcal{U}}}\right) \wedge D_u \Omega_{\mathcal{U}}, \tag{4.5}$$

where $\Omega_{\mathcal{U}}$ is the canonical form of the upper facet (we could also choose to use the bottom facet) and D_u is an operator that must promote the poles that in $\Omega_{\mathcal{U}}$ are associated to the intersections $\mathcal{U} \cap \mathcal{S}$ to poles along the higher dimensional facets $\mathcal{S}$. Therefore in (4.4) we are both recursively computing Ω_5, by recycling the result of (4.2), and making it manifestly projective in one fell swoop.

This is not the end of the story. Most (presumably all) of the newly discovered Amplituhedra admit a convex realization, i.e. a subspace H where all the variables X are given by affine linear functions, such that the pullback of Ω on this space is given by

$$\Omega|_H = dX_1 \wedge \cdots \wedge dX_d \left(\sum_{v \in \text{vertices}} \prod_{\substack{f \in \text{facets} \\ v \in f}} \frac{1}{X_f} \right), \tag{4.6}$$

where $(X_1, \ldots, X_d)$ is an arbitrary choice of coordinates for H. The rational function

$$\underline{\Omega} = \frac{\Omega|_H}{dx_1 \ldots dx_d},$$

is then immediately recognised as the Feynman diagramatic expansion of the amplitude. For example, in the case of the pentagon one obtains

$$\underline{\Omega}_5 = \sum_{i=1}^{5} \frac{1}{X_i X_{i+1}}. \tag{4.7}$$

Note that the relative signs required for the projectivity of Ω get miracolously balanced by the pullback on H. Staring at (4.4) is then tempting to guess a recursive expression for the rational function of the pentagon

$$\underline{\Omega}_5 \stackrel{?}{=} \left(\frac{1}{X_1} + \frac{1}{X_4}\right)\left(\frac{1}{X_5} + \frac{1}{X_1 - X_2}\right) + \left(\frac{1}{X_2} + \frac{1}{X_4}\right)\left(\frac{1}{X_3} + \frac{1}{X_2 - X_1}\right), \tag{4.8}$$

by direct comparison with (4.7) it is easy to see that, indeed, (4.8) yields an identity between rational functions in the variables X_i.

Once again, we wish to stress that the details of the convex realization of the pentagon drop out, and one is left with recursive formulae for amplitudes which are correct on the space of independent variables X_i. The above constructions were inspired by a remarkable projection property satisfied by the so called generalized ABHY Associahedra, which will be discussed elsewhere [102]. However, it was later understood that they hold in greater generality for arbitrary simple polytopes.

In the rest of the paper we will state and prove the recursive formulae for Ω and $\underline{\Omega}$ in full generality. As an illustrative example we will apply it to Stokes polytopes obtaining novel representations for their rational functions. As we will argue later, the simple structure of the recursions also suggests a natural way to get rid of double countings of Feynman diagrams across different polytopes by taking suitable limits, a fact that we will use to obtain new expression for the full planar amplitude as well.

This paper is structured as follows. In Section 4.1 we offer a self-contained review of the definition of positive geometries and canonical forms focused on the case of simple polytopes. In Section 4.2 we present and prove our main results, as well as providing a few simple examples. In Section 4.3 we apply our formulae to the case of Stokes polytopes, obtaning recursive representation for their rational functions, as well as for the full ϕ^4 amplitude. Finally, in Section 4.4 we draw our conclusions.

4.1 A brief review of positive geometries

We review in more details some of the ideas put forward in [92] which we touched in the introduction. We then state and prove a simple recursive formula to compute the canonical form of simple polytopes. Remarkably, a naive guess allows to extend this to a recursive formula for rational functions canonically associated to simple polytopes. As we will see, however, this latter formula requires some extra combinatorical requirement on the polytope.

4.1.1 Polytopes and their canonical forms

Let $\mathcal{P}$ be a d-dimensional simple polytope. If we label the facets of $\mathcal{P}$ using variables X_f, $f = 1, \ldots, F$, then each vertex v of $\mathcal{P}$ is uniquely identified by a d-tuple of variables X. Note that $F \geq d+1$, the inequality being saturated if and only if $\mathcal{P}$ is a simplex. Without loss of generality, we assume that $\mathcal{P}$ is given a convex realization as the intersection of the positive region $\mathbb{R}^F_{\geq 0}\{X_f \geq 0\}$ with an appropriate d-dimensional affine subspace H. Thinking projectively, we introduce a homogeneous vector $\mathcal{Y} = (M, X_1, \ldots, X_F)$, then H is defined by the constraint $\mathcal{C} \cdot \mathcal{Y} = 0$ where $\mathcal{C}$ is a $(F-d) \times (F+1)$ matrix. The subspace H can alternatively be encoded by writing each of the F variables X_f as an affine function, i.e. by writing $X = W \cdot Y$, where Y is a $(d+1)$-vector of homogeneous coordinates for H. By performing a $\mathrm{GL}(d+1)$ transformation we can always choose d compatible variables X_f to be the affine coordinates for H, which means that we center the origin of our space at one of the vertices v of $\mathcal{P}$. Then we have to specify only $F-d$ rows of W; they are the in-ward normal vectors of $F-d$ corresponding facets of $\mathcal{P}$.

To any convex polytope $\mathcal{P}$, or more generally to any positive geometry, we can uniquely associate a meromorphic top-dimensional differential form $\Omega_{\mathcal{P}}$, which is defined in a iterative way by the requirements

$$\mathrm{Res}_{X_f}(\Omega_{\mathcal{P}}) = \Omega_{X_f}, \text{ and } \Omega_{\text{point}} = \pm 1, \tag{4.9}$$

By further requiring that $\Omega_{\mathcal{P}}$ is holomorphic elsewhere, Ω_P is fixed up to a sign. We recall that the residue[2] of a top degree differential form along an affine subspace $\{X_f = 0\}$ is defined by

$$\mathrm{Res}_{X_f}(d\log(X_f) \wedge \omega + \eta) = \omega|_{X_f=0}(\Omega), \tag{4.10}$$

where ω (which may be zero) and η are regular along $\{X_f = 0\}$. The residue operator yields a differential form on the subspace $\{X_f = 0\}$. The operation of taking residues can be iterated and one can define the operator

$$\mathrm{Res}_{(X_{f_1},\ldots,X_{f_m})}(\Omega)\mathrm{Res}_{X_{f_1}}\ldots\mathrm{Res}_{X_{f_m}}, \tag{4.11}$$

where we stress that the functions X_{f_i} have to be restricted to the subspaces on which residues have already been taken.

As we anticipated in the introduction, the canonical form of a simple polytope $\mathcal{P}$ is given by

$$\Omega_{\mathcal{P}} = \sum_{v\in\text{vertices}} \mathrm{sgn}(v) \bigwedge_{\substack{f\in\text{facets}\\ v\in f}} d\log(X_f), \tag{4.12}$$

where the signs are fixed by projectivity. More precisely, the statement is that the pullback of $\Omega_{\mathcal{P}}$ on the subspace H defining the convex realization of $\mathcal{P}$ yields its canonical form. The proof is by comparison with a known representation of $\underline{\Omega}$ as integral over the dual polytope $\mathcal{P}^*$, in this language the plane at infinity $\{M = 0\}$ is dual to a point in the interior of $\mathcal{P}^*$, which proves that neither Ω or its pullback on H develops a pole there. In practice, the signs can be fixed as follows. Any 1-dimensional face of $\mathcal{P}$ is uniquely associated to a collection of $d-1$ facets $(X_{a_1}, \ldots, X_{a_{d-1}})$ and it touches $\mathcal{P}$ at two vertices specified by two additional variables X and X'. In order not to

[2]In the mathematical literature there are several notions of multivariate generalizations of the familiar residue from complex analysis. The one invoked here is known as *Poincare Residue*.

develop a pole at infinity along the line $(X_{a_1}, \ldots, X_{a_{d-1}})$ we must have

$$\mathrm{Res}_{(X_{a_1},\ldots,X_{a_m},X)}(\Omega) = -\mathrm{Res}_{(X_{a_1},\ldots,X_{a_m},X')}(\Omega). \tag{4.13}$$

We can start from any vertex v_0, choose an arbitrary sign for the corresponding $d\log$, then explore all the vertices of $\mathcal{P}$ by moving along its 1-dimensional faces and fix the signs according to (4.13).

A priori it is not obvious that the procedure just described is going to be consistent, i.e. that the the assignment of signs will not depend on a particular path chosen to get to a far away vertex. However, we know that this must be the case because $\mathcal{P}$ is a polytope, in particular it admits a dual $\mathcal{P}^*$ which gives an independent proof of the projectivity of $\Omega_{\mathcal{P}}$. Note, however, that the procedure only requires the knowledge of the graph of $\mathcal{P}$, i.e. the collection of its one dimensional faces. For example, the particular subspace H does not effectively appear in Ω. It is tempting to try and define a form for an arbitrary graph G and it is then an interesting question to understand what are the topological properties of G that guarantee the projectivity of Ω.

Because the particular realization of the polytope $\mathcal{P}$ does not effectively appear in the definition of $\Omega_{\mathcal{P}}$ it is natural to study it as a differential form on the affine space generated by all the facet variables, thought of as independent variables. This poses an obvious problem, in that the usual residue operator is well defined on top-degree forms, e.g. the residue $\mathrm{Res}_y \frac{dx}{y}$ would not make sense. However, if we restrict ourselves to forms which are given by linear combinations of $d\mathrm{log}$s one can still define a well behaved Res operator. We will review this construction in the following section.

If on one hand differential forms are very natural objects to consider in order to speak of residues, on the other scattering amplitudes are ultimately functions of the kinematical data. When dealing with top degree differential forms on a projective space the distinction is irrelevant since any such form can be written as $\Omega = \langle Y d^d Y\rangle \underline{\Omega}(Y)$, where $\underline{\Omega}(Y)$ is an homogeneous function of weight $-(d+1)$ and $\langle Y d^d Y\rangle \det(Y dY \ldots dY)$ is a standard measure on $\mathbb{P}^d$. Therefore we can unambiguosly pass from the differential form Ω to the rational function $\underline{\Omega}$. However, the number of facets of any polytope $\mathcal{P}$ is always greater than its dimension so that the canonical form $\Omega_{\mathcal{P}}$ is never a top degree form. The obvious solution is to consider its pullback Ω_H on the space H on which $\mathcal{P}$ is geometrically realized, which is now a top degree form and is thus associated to a rational function. In the case of a simple polytope from (4.12) we get

$$\underline{\Omega}|_H = \left(\sum_{v \in \text{vertices}} \text{sgn}(v) \langle W_M W_{f_1} \dots W_{f_d} \rangle \prod_{\substack{f \in \text{facets} \\ v \in f}} \frac{1}{X_f} \right), \tag{4.14}$$

where $(X_1, \dots, X_d)$ are affine coordinates for H, the variables X_f are now given by linear functions $X_f = W_f \cdot (1, X_1, \dots, X_d)$ and $W_M = (1, 0, \dots, 0)$. Furthermore, in all cases encountered so far, the pullback space H is such that the signs $\text{sgn}(v)$ conspired with the determinants in (4.14) to produce unit numerators. In this case. the rational function associated to $\mathcal{P}$ is given by

$$\underline{\Omega}_{\mathcal{P}}|_H = \left(\sum_{v \in \text{vertices}} \prod_{\substack{f \in \text{facets} \\ v \in f}} \frac{1}{X_f} \right). \tag{4.15}$$

As for Ω, we find natural to associate to $\mathcal{P}$ a rational function defined on the space of all facet variables by

$$\underline{\Omega}_{\mathcal{P}} = \left(\sum_{v \in \text{vertices}} \prod_{\substack{f \in \text{facets} \\ v \in f}} \frac{1}{X_f} \right), \tag{4.16}$$

we reiterate that in (4.16) the variables X_f are thought of as independent variables on an affine space.

4.1.2 $d\log$ forms and Res operator

On the affine space V with coordinates $(X_1, \dots, X_n)$ consider a family $\mathcal{A}$ of codimension one planes passing through the origin, we denote by ℓ the linear equations defining these planes. We will always assume that $\mathcal{A}$ contains all of the hyperplanes $\{X_i = 0\}$. Then we define the following vector space of differential forms

$$R_V^p(\mathcal{A})\{\Omega \mid \Omega = \sum_{\substack{\ell \subset D \\ |\ell|=p}} c_\ell \, d\log(\ell_1) \wedge \cdots \wedge d\log(\ell_p), c_\ell \in \mathbb{C}\}. \tag{4.17}$$

$R_V^p(\mathcal{A})$ is a finitely generated vector space, a set of generators is provided by the simple p-forms $d\log(\ell_1) \wedge \cdots \wedge d\log(\ell_p)$, which are overcomplete because of partial fractions identities such as

$$d\log\left(\frac{\ell}{\ell'}\right) \wedge d\log(\alpha\ell + \beta\ell') = d\log(\ell) \wedge d\log(\ell') \quad \alpha, \beta \in \mathbb{C}. \tag{4.18}$$

Note that (4.18) can be interpreted geometrically in terms of the triangulation depicted in Fig. 4.2. A detailed study of the algebraic structure of the space $R_V^p(\mathcal{A})$ and its connection with the combi-

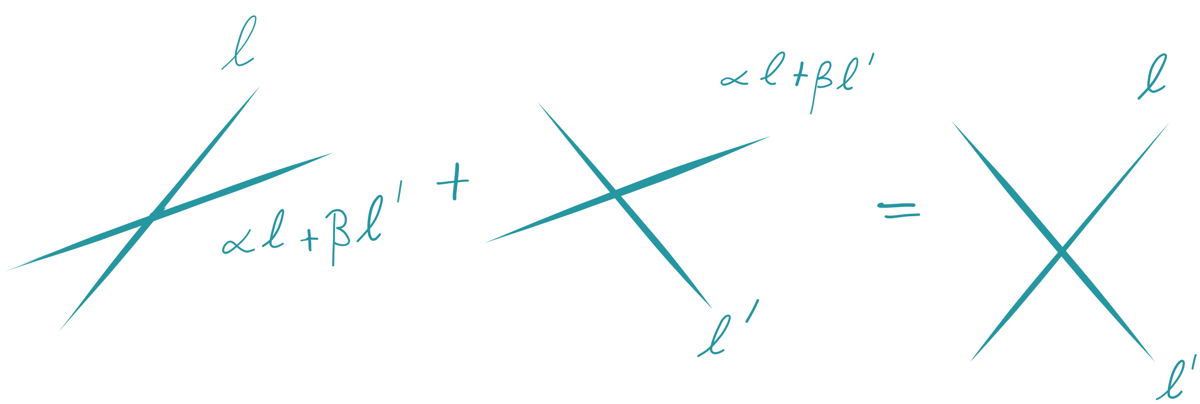

Figure 4.2: Geometric interpretation of the identities between $d\log$ forms

natorics of $\mathcal{A}$ can be found in [103]. An important fact for us is that the forms

$$\omega_I = d\log(X_{I_1}) \wedge \cdots \wedge d\log(X_{I_p}) \quad \text{for any } I \subset (1, \ldots, n), \tag{4.19}$$

are all independent. For any $\ell \in \mathcal{A}$, we define the residue operator as a map

$$\mathrm{Res}_\ell : R_V^p(\mathcal{A}) \to R_\ell^{p-1}(\mathcal{A})$$

defined by writing any form Ω as $\Omega = d\log\ell \wedge \eta + \omega$, with η, ω regular in $\{\ell = 0\}$ and then posing $\mathrm{Res}_\ell \Omega = \eta|_{\{\ell=0\}}$. If it is not possible to write Ω in this way, then the residue is zero.

Suppose that $\Omega \in R^p_V(\mathcal{A})$ lies in the kernel of Res_ℓ for some $\ell \in D$, then one can show that $\Omega \in R^p_V(\mathcal{A}')$ where $\mathcal{A}' = \mathcal{A} \setminus \{\ell\}$, in other words we can eliminate the variable ℓ from Ω. For example, the LHS of (4.18) has zero residue on the plane $\{\alpha\ell + \beta\ell' = 0\}$ and indeed this plane does not appear on the RHS. However, in general the elimination of the variable may require more complicated identities, such as

$$\begin{aligned} d\log(\ell_1)d\log(\ell_2)d\log(\ell_3) = d\log(\ell_1+\ell_2+\ell_3)\wedge \\ [d\log(\ell_1)d\log(\ell_2) - d\log(\ell_1)d\log(\ell_3) + d\log(\ell_2)d\log(\ell_3)]\,. \end{aligned}$$

By iterated application of this fact one can deduce that if $\mathrm{Res}_\ell\Omega = 0$ for any ℓ, then Ω must be zero. Finally, if Ω is written as a linear combination of the forms defined in (4.19), i.e. if

$$\Omega = \sum_I c_I \omega_I, \tag{4.20}$$

then we can define an iterated residue operator by $\mathrm{Res}_{X_J}\mathrm{Res}_{J_1} \circ \cdots \circ \mathrm{Res}_{J_p}$ whose action is clearly $\mathrm{Res}_{X_J}\Omega = c_J$. Note that Res_{X_J}, when it acts on forms such as (4.20) is antisymmetric with respect to the planes X_{J_i}.

In what follows we will interested in the particularly simple case where $\mathcal{A}$ is composed by the hyperplanes $\{X_i = 0\}$, $\{X_i - X_j = 0\}$ and $\{X_i + X_j = 0\}$ and $p < n$. Looking back at (4.12) and at our naïve guess for the canonical form of a prism (4.5) we see that this is the minimal choice required.

4.2 The recursive formulae

We are now in position to state and prove our main result, a recursive formula to compute the canonical form of a simple polytope in terms of the canonical forms of its facets. In the case of amplituhedra facets factorize into lower dimensional amplituhedra, mimicking the factorization of amplitudes into product of lower point amplitudes, so that the recursion for Ω yields novel, BCFW-like, expressions for the corresponding amplitudes.

4.2.1 Recursive formula for Ω

Let $\mathcal{P}$ be a d-dimensional simple polytope, partition its facets into a distinguished one X_b, which can be chosen arbitrarily, and the remaining ones which we collectively denote by $\mathcal{U}$. For each of the facet X_u in $\mathcal{U}$ we introduce the operator D_u that acts on differential forms by replacing $X_{u'} \to X_{u'} - X_u$, for $X_{u'} \in \mathcal{U} \setminus \{X_u\}$ and $X_b \to X_b + X_u$ [3]. We claim that the canonical form of $\mathcal{P}$ is given by

$$\Omega_{\mathcal{P}} = \sum_{X_u \in \mathcal{U}} d\log\left(\frac{X_u}{X_b}\right) \wedge D_u(\pm\Omega_{X_u}) \tag{4.21}$$

where we wrote $(\pm\Omega_{X_u})$ to emphasize that the canonical forms of the facets are defined only up to an overall sign. This ambiguity is fixed by the requirement that the spurious poles along $\{X_u' - X_u = 0\}$, introduced by D_u, cancel each other. In order to do so, one can arbitrarily choose the sign for one of the facets in $\mathcal{U}$ and then fix the orientation of the remaining facets accordingly. We remark that (4.21) makes manifest the projectivity of $\Omega_{\mathcal{P}}$, since it can be recursed to compute the canonical forms Ω_{X_u}. On the other hand, it is not obvious that the sign-fixing procedure will be consistent, therefore the cancellation of spurious poles is not manifest. This is in complete analogy with (4.12), where no spurious poles were introduced, but the sign-fixing procedure to ensure projectivity was not obviously consistent.

Let us now prove the correctness of (4.21), by showing that it satisfies the definition (4.9). We assume that signs have been chosen so that $\mathrm{Res}_{(X_u'-X_u)}\Omega_{\mathcal{P}} = 0$. We also have spurious poles at $\{X_u + X_b = 0\}$, but their cancellation is clear due to the prefactor $d\log\left(\frac{X_u}{X_b}\right)$. From the absence of spurious poles follows, in particular, that $\Omega_{\mathcal{P}}$ is written in terms of $d\log$s involving only the facet

[3]One could more generally define D_u so that it sends $X \to \alpha X + \beta X_u$, but for simplicity of notation we stick to our more restrictive choice.

variables X and thus any iterated residue $\mathrm{Res}_{X_J}(\Omega_{\mathcal{P}})$ is anti-symmetric with respect to the facet variables X_{J_i}. The pole in $\{X_u = 0\}$ appear in (4.21) only through the prefactor $d\log\left(\frac{X_u}{X_b}\right)$ and since evaluating the residue there undo the action of the operator D_u, we have $\mathrm{Res}_{X_u}\Omega_{\mathcal{P}} = \Omega_{X_u}$. It is left to check that $\mathrm{Res}_{X_b}\Omega_{\mathcal{P}} = \Omega_{X_b}$, applying the definition (4.9) to Ω_{X_b} this is equivalent to $\mathrm{Res}_{X_u}\mathrm{Res}_{X_b}\Omega_{\mathcal{P}} = \Omega_{X_u \cap X_b}$ or zero if $X_u \cap X_b = \emptyset$. Since iterated residues are anti-symmetric we can invert the order of the residues and then the result follows from $\mathrm{Res}_{X_u}\Omega_{\mathcal{P}} = \Omega_{X_u}$.

As it stands (4.21) is a recursion formula that requires as input the knowledge of the canonical forms of all but one the facets. It turns out that the recursion can be made dramatically more efficient. After a distinguished facet X_b is chosen, let us now further partition the remaining facets in two sets $\mathcal{U}$ and $\mathcal{S}$ in such a way that every vertex of $\mathcal{P}$ lies in at least one of the facets $\{X_b\} \cup \mathcal{U}$. Surprisingly, (4.21) gives again the correct canonical form. However, first one has to decide how to fix the relative signs of the forms Ω_{X_u}, since now the X_u facets might not be joined to each other by a sequence of adjacencies. In order to overcome this problem, one has to further require that if two facets X_u and $X_{u'}$ are connected by a one-dimensional edge, then Ω_{X_u} and $\Omega_{X'_u}$ must have opposite residues at the vertices of that edge. The only new element in the proof of (4.21) is that now one has to consider residues of the form

$$\mathrm{Res}_{X_S, X_b}\Omega_{\mathcal{P}} = -\sum_{X_u \in \mathcal{U}} \mathrm{Res}_{X_S} D_u \Omega_{X_u} = -\sum_{X_u \in \mathcal{U}} \mathrm{Res}_{X_S}\Omega_{X_u}, \tag{4.22}$$

where X_S is a (d-1)-tuple of facets in $\mathcal{S}$ and in the second passage we used the fact that D_u does not deform the variables $\mathcal{S}$, so that $\mathrm{Res}_{X_s} D_u = D_u \mathrm{Res}_{X_s}$ for any pair $s \in \mathcal{S}$ and $u \in \mathcal{U}$. Let us write $\cap X_S$ for the intersection of the corresponding facets, then there are three cases to be considered: $\cap X_S$ is empty, $\cap X_S$ defines a one dimensional edge of $\mathcal{P}$ which is incident to two facets in $\mathcal{U}$ and $\cap X_S$ defines a one dimensional edge incident to a facet X_u in $\mathcal{U}$ and to the facet X_b. In the first case, each of the terms in the RHS of (4.22) is zero, in the second case the sum is zero and in the third case (4.22) gives $\mathrm{Res}_{X_S, X_b}\Omega_{\mathcal{P}} = -\mathrm{Res}_{X_S, X_u}\Omega_{\mathcal{P}}$. In every case, the result is correct.

We conclude this section with a few explicit examples of (4.21). The simplest example is a segment with facets X_1 and X_2, and we trivially get $\Omega = d\log\left(\frac{X_1}{X_2}\right)$. Already the case of a 2-simplex with facets $\{X_1, X_2, X_3\}$ is slightly interesting, we can choose either $X_b = X_1$, $\mathcal{U} = \{X_2, X_3\}$ and $\mathcal{S}$ empty or $\mathcal{U} = \{X_2\}$ and $\mathcal{S} = \{X_3\}$. We obtain, respectively,

$$\Omega = d\log\left(\frac{X_2}{X_1}\right) \wedge d\log\left(\frac{X_3 - X_2}{X_2 + X_1}\right) - d\log\left(\frac{X_3}{X_1}\right) \wedge d\log\left(\frac{X_2 - X_3}{X_3 + X_1}\right),$$

and

$$\Omega = d\log\left(\frac{X_2}{X_1}\right) \wedge d\log\left(\frac{X_3}{X_2 + X_1}\right),$$

using (4.18) it is easy to see that both agree with (4.12), which would give

$$\Omega = d\log X_1 \wedge d\log X_2 - d\log X_3 \wedge d\log X_2 - d\log X_1 \wedge d\log X_3. \tag{4.23}$$

A more interesting example is provided by a two dimensional square with facets $\{X_1, X_2, X_3, X_4\}$, see Fig. 4.3. We consider $X_b = X_1$, and either $\mathcal{U} = \{X_3\}$ or $\mathcal{U} = \{X_2, X_4\}$.

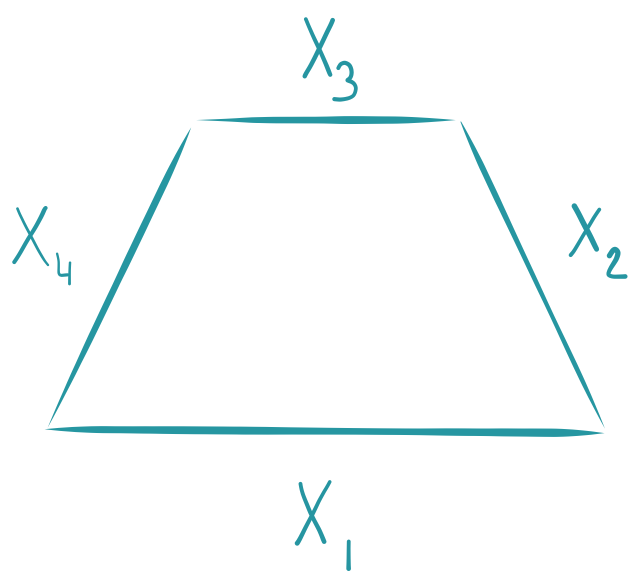

Figure 4.3: A square

In the first case we get

$$\Omega = d\log\left(\frac{X_3}{X_1}\right) \wedge d\log\left(\frac{X_2}{X_4}\right), \tag{4.24}$$

which is clearly the form of the square $[X_1, X_3] \times [X_2, X_4]$. In the other case we get

$$\Omega_{\pm} = d\log\left(\frac{X_2}{X_1}\right) \wedge d\log\left(\frac{X_3}{X_1+X_2}\right) \pm d\log\left(\frac{X_4}{X_1}\right) \wedge d\log\left(\frac{X_3}{X_1+X_4}\right), \tag{4.25}$$

we wish to emphasize that, regardless of the relative signs we choose, $\Omega_{\pm}$ does not have spurious poles along $\{X_4 - X_2 = 0\}$, but $\mathrm{Res}_{X_2,X_1}\Omega_+ = \mathrm{Res}_{X_4,X_1}\Omega_+ = 1$, so that we have to pick Ω_- to satisfy the sign fixing rule.

4.2.2 Recursive formula for $\underline{\Omega}$

We recall the expression (4.16) for the canonical rational function $\underline{\Omega}_{\mathcal{P}}$ associated to a simple polytope $\mathcal{P}$,

$$\underline{\Omega}_{\mathcal{P}} = \left(\sum_{v\in\text{vertices}} \prod_{\substack{f\in\text{facets}\\ v\in f}} \frac{1}{X_f}\right). \tag{4.26}$$

Suppose that the facets of $\mathcal{P}$ are partitioned in X_b and two sets $\mathcal{U}, \mathcal{S}$, as described in the previous section. Staring at the recursive formula (4.21) for Ω one would naïvely guess that a similar expression should exist for $\underline{\Omega}_{\mathcal{P}}$, since after all the proof of (4.21) relies on partial fraction identities, such as (4.18), which also hold at the level of functions. We consider, then, the following expression

$$\underline{\Omega} = \sum_{X_u\in\mathcal{U}} \left(\frac{1}{X_b} + \frac{1}{X_u}\right) D_u \underline{\Omega}_u \tag{4.27}$$

where the deformation operators D_u are again defined by $X_{u'} \to X_{u'} - X_u$ for $u \neq u'$ and $X_b \to X_b + X_u$. Note that differential forms carry a notion of an orientation, which is crucial in the cancellation of spurious poles in Ω. At the level of $\underline{\Omega}$ this notion is translated in the positivity of the functions appearing in (4.27), that is in the fact that $D_u X'_u = -D'_u X_u$. It turns out, however, that (4.27) holds only if the choice of $\mathcal{U}$ and $\mathcal{S}$ is such that there is no $(d-1)$-tuple of facets $X_s \in \mathcal{S}$ whose intersection defines a one dimensional edge of $\mathcal{P}$ adjacent to two facets in $\mathcal{U}$. This should not be suprising thinking back at the proof of (4.21), the existence of such an edge requires to orient the forms Ω_{X_u} so that they have opposite residues at its vertices, a requirement which is not easily translated at the level of $\underline{\Omega}$.

Before proving (4.27) in full generality, let us give an example to better illustrate both the formula and the aforementioned extra condition. We will consider once again the square of Fig. 4.3, with the same choices of $\mathcal{U}$ and $\mathcal{B}$. The canonical form of the square is given by

$$\Omega = \frac{1}{X_1 X_2} + \frac{1}{X_2 X_3} + \frac{1}{X_3 X_4} + \frac{1}{X_1 X_4}. \tag{4.28}$$

In the case where $\mathcal{U} = \{X_3\}$ and $\mathcal{S}$ is empty the recursive formula reads

$$\Omega = \left(\frac{1}{X_1} + \frac{1}{X_3}\right)\left(\frac{1}{X_2} + \frac{1}{X_4}\right), \tag{4.29}$$

while if we chose $\mathcal{U} = \{X_2, X_4\}$ and $\mathcal{S} = \{X_3\}$ we would *incorrectly* get

$$\Omega = \left(\frac{1}{X_1} + \frac{1}{X_2}\right)\left(\frac{1}{X_1 + X_2} + \frac{1}{X_3}\right) + \left(\frac{1}{X_1} + \frac{1}{X_4}\right)\left(\frac{1}{X_1 + X_4} + \frac{1}{X_3}\right), \tag{4.30}$$

the mismatch is due to the contributions from the vertices on the facet $\{X_3 = 0\}$. Indeed, this choice of $\mathcal{U}$ and $\mathcal{S}$ does not satisfy the new requirement because the one dimensional edge $X_3 \in \mathcal{S}$ is incident to both facets in $\mathcal{U}$.

We now prove that $\underline{\Omega}_{\mathcal{P}}$ as defined by (4.26) is the same as computed in (4.27). Our strategy will be to consider the contribution of every vertex v in $\mathcal{P}$ to both expressions. There are several types of vertices to consider:

1. Vertex $v \notin X_b$ belongs to only one of the elements of $\mathcal{U}$. Then, there is only one term in

(4.27) to consider, of the form

$$\left(\frac{1}{X_b}+\frac{1}{X_{u_i}}\right)\frac{1}{X_{s_1}\dots X_{s_{d-1}}}=\frac{1}{X_bX_{s_1}\dots X_{s_{d-1}}}+\frac{1}{X_{u_i}X_{s_1}\dots X_{s_{d-1}}} \tag{4.31}$$

reproducing both the term in (4.26) corresponding to v and the term in (4.26) corresponding to $B=\bigcap_{a=1}^{d-1}X_{s_i}\cap X_b$. Since $d-1$ facets in $\mathcal{S}$ can not intersect along an edge adjacent to two vertices in $\mathcal{U}$, B will be one of the vertices of $\mathcal{P}$, and it is easy to check that its corresponding term will not appear again in (4.27).

2. Vertex $v\notin X_b$ belongs to a collection of $n\geq 2$ facets in $\mathcal{U}$, X_{u_1}, X_{u_2}, ... ,X_{u_n}. Then, we need to consider the sum of n terms in (4.27) of the form

$$\sum_{i=1}^{n}\left(\frac{1}{X_b}+\frac{1}{X_{u_i}}\right)\prod_{\substack{j=1\\j\neq i}}^{n}\left(\frac{1}{X_{u_j}}-\frac{1}{X_{u_i}}\right)\frac{1}{X_{s_1}\dots X_{s_{d-n}}} \tag{4.32}$$

Now, we can use the following two identities,

$$\sum_{i=1}^{n}\frac{1}{X_{u_i}}\prod_{\substack{j=1\\j\neq i}}^{n}\frac{1}{X_{u_j}-X_{u_i}}=\frac{1}{X_{u_1}X_{u_2}\dots X_{u_n}} \tag{4.33}$$

$$\sum_{i=1}^{n}\prod_{\substack{j=1\\j\neq i}}^{n}\frac{1}{X_{u_j}-X_{u_i}}=0 \tag{4.34}$$

to conclude that the sum from (4.32) will reproduce the term corresponding to v in (4.26).

3. Vertex $v\in X_b$ is shared with only one element of $\mathcal{U}$, which we will denote as X_{u_i}. Then, there will only be one term in (4.27) to consider,

$$\left(\frac{1}{X_b}+\frac{1}{X_{u_i}}\right)\frac{1}{(X_b+X_{u_i})X_{s_1}\ldots X_{s_{d-2}}}=\frac{1}{X_bX_{u_i}X_{s_1}\ldots X_{s_{d-2}}} \tag{4.35}$$

reproducing the term corresponding to v in (4.26).

4. Vertex $v \in X_b$ is shared with a collection of n elements of $\mathcal{U}$, which we will denote as X_{u_1}, $X_{u_2}, \ldots, X_{u_n}$. Then, there are n terms of (4.27) to consider,

$$\sum_{i=1}^{n}\left(\frac{1}{X_b}+\frac{1}{X_{u_i}}\right)\prod_{\substack{j=1\\ j\neq i}}^{n}\left(\frac{1}{X_{u_j}-X_{u_i}}\right)\frac{1}{X_b+X_{u_i}}\frac{1}{X_{s_1}\ldots X_{s_{d-n-1}}}=$$
$$\sum_{i=1}^{n}\frac{1}{X_{u_i}}\prod_{\substack{j=1\\ j\neq i}}^{n}\left(\frac{1}{X_{u_j}-X_{u_i}}\right)\frac{1}{X_bX_{s_1}\ldots X_{s_{d-n-1}}}=\frac{1}{X_bX_{u_1}X_{u_2}\ldots X_{u_n}X_{s_1}\ldots X_{s_{d-n-1}}} \tag{4.36}$$

where the identity in (4.33) was used in the second term. We can see that the result matches the appropriate term of (4.26).

4.3 Application to planar ϕ^4 amplitudes

In the context of planar ϕ^4 amplitudes, Feynman diagrams for n - particle amplitudes correspond to the quadrangulations of an n - gon. Unlike the bi-adjoint ϕ^3 theory, a single polytope whose vertices are in correspondence with the full set of quadrangulations does not exist. Instead, a notion of *compatibility* with a reference quadrangulation Q is used to select a set of quadrangulations with the appropriate poset structure, corresponding to the Stokes polytope, as introduced in [94]. The properties of Stokes polytopes have been studied by mathematicians in [95],[96], and used by physicists to describe the planar ϕ^4 amplitudes in [90], [93].

Before defining Q-compatibility, we choose an alternating assignment of '+' and '-' to the

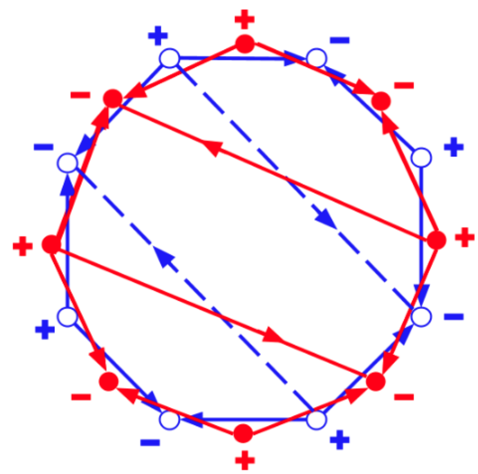

Figure 4.4: An example of a red quadrangulation compatible with a blue one

vertices of our polygon [4] and assign an arrow to each diagonal, pointing from a '+' vertex to a '-' one. Then, we consider a slight clockwise rotation of our polygon superimposed onto itself, as in Fig. 4.4. If our reference quadrangulation Q is assigned a blue color, and a quadrangulation Q', drawn to correspond to the rotated polygon is assigned a red color, then Q' is defined to be compatible with Q if each blue arrow that crosses a red arrow is oriented counter-clockwise from the said red arrow.

All quadrangulations Q' compatible with Q correspond to vertices of a Stokes polytope S_Q. A mutation rule replacing a diagonal Q'_i with the Q-compatible diagonal of a hexagon obtained by deleting Q'_i will take us along the edges of S_Q. Facets of Stokes polytope are in correspondence with Q - compatible diagonals of the polygon, and more generally, codimension - d boundaries are in correspondence with sets of d non-crossing Q-compatible diagonals.

It is important to note that Q-compatibility is not an equivalence relation. It turns out that for $2n+2$ - gon, we will have $\frac{1}{2n+2}\binom{3n}{n}$ distinct Stokes polytopes, one for each of the quadrangulations of the $2n+2$ - gon taken as a reference.

Stokes polytopes are simple polytopes with the property that each facet X_{ij} factorizes as $\partial_{X_{ij}} S_Q = S_{Q'} \times S_{Q''}$, for some suitably chosen reference quadrangulations Q', Q'' [91]. Hence, they are a natural playground on which we can explore our recursive formulae.

[4] We will choose an assignment of '+' to odd and '-' to even - numbered vertices

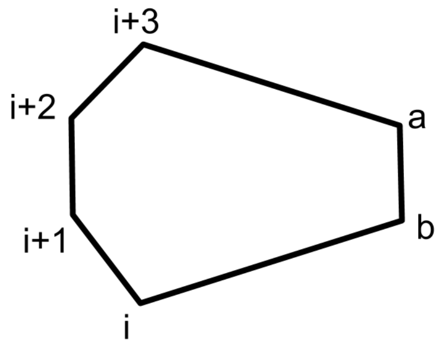

Figure 4.5: The hexagon carved out by a collection of diagonals corresponding to facets in $\mathcal{S}$

4.3.1 Choosing the $\mathcal{U}$ facets

We start by noting that any Stokes polytope S_Q has a face corresponding to the diagonal of the n - gon of the form $(i, i+3)$. For illustration purposes, let us take this to be our face X_b. Then, we will define $\mathcal{U}$ to be the set of faces of S_Q whose corresponding diagonals cross $(i, i+3)$. It is then easy to check that every quadrangulation will contain either the quadrangle $(i, i+1, i+2, i+3)$ or a diagonal crossing $(i, i+3)$, hence every vertex will be contained in either one of the $\mathcal{U}$ facets or X_b. We may also note that no element of thus chosen $\mathcal{U}$ has intersection with X_b.

As usual, we will denote by $\mathcal{S}$ the complement of $\mathcal{U} \cup \{X_b\}$. In order to be able to use our choice of $X_b, \mathcal{U}$ to recursively compute the canonical function, we also need to check that no edge adjacent to two facets in $\mathcal{U}$ can be given as an intersection of $d-1$ facets in $\mathcal{S}$. The facets $\mathcal{S}$ correspond to Q-compatible diagonals other than $(i, i+3)$ which do not cross $(i, i+3)$. For a d - dimensional S_Q, any subset of $d-1$ such elements of $\mathcal{S}$ will either contain a pair of crossing diagonals, in which case the intersection of such faces will be an empty set, or will form a partial quadrangulation of the form shown in Fig. 4.5. It is now easy to see that this quadrangulation can be completed by either adding the diagonal $(i, i+3)$ (corresponding to X_b), or one of the diagonals $(i+1, a)$, $(i+2, b)$ (corresponding to one of the facets in $\mathcal{U}$) selected by the Q-compatibility, and the desired property is satisfied.

4.3.2 Recursion for $\underline{\Omega}_{S_Q}$

Note that, up to cyclic shifts of the number labels, any reference quadrangulation Q will contain a facet of the form $X_{1,4}$. Let us pick $X_b = X_{1,4}$ and choose the $\mathcal{U}$ facets as those corresponding to Q - compatible variables crossing $X_{1,4}$. It is easy to check that all $\mathcal{U}$ variables must be of the form $X_{3,2i}$ and the recursive formula for canonical function of $\mathcal{S}_Q$ takes the form

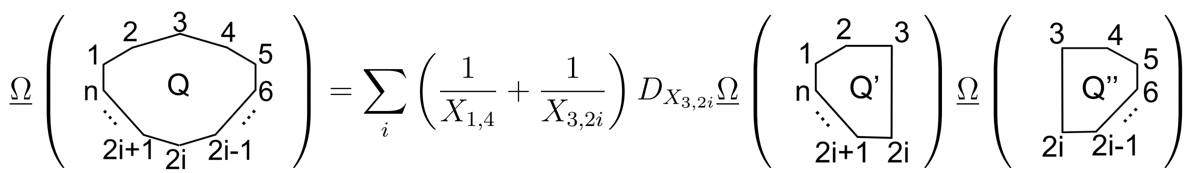

(4.37)

where we are summing over all Q-compatible $X_{3,2i}$. The new reference quadrangulations Q', Q'' are chosen by keeping the diagonals of Q not crossing $X_{3,2i}$ and choosing their completion in the two regions such as to obtain the top quadrangulation corresponding to facet $X_{3,2i}$ of the oriented flip graph[5], as defined in [95]. We have verified that this produces correct results for $n \leq 10$ particles.

Since the facet X_b only enters (4.37) through the prefactors, it is particularly simple to take the limit $X_b \to \infty$, a fact we will exploit as we piece together the scattering amplitude from the limits of Stokes polytopes.

4.3.3 Examples

The canonical function of a Stokes polytope corresponding to an $n = 4$ particle amplitude is trivial and can form the basis of the recursion,

[5] We thank F.Chapoton for explaining how factorisation can be seen from the oriented flip graphs

$\underline{\Omega}\Bigg($ 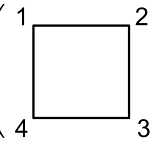 $\Bigg) = 1$ (4.38)

For the case of quadrangulations of a hexagon, it is straightforward to use the recursive formula to get the correct answer, as in the following example,

$\underline{\Omega}\Bigg($ 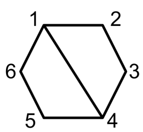 $\Bigg) = \left(\frac{1}{X_{1,4}}+\frac{1}{X_{3,6}}\right) D_{X_{3,6}}\underline{\Omega}\Bigg($ 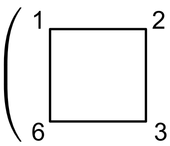 $\Bigg) D_{X_{3,6}}\underline{\Omega}\Bigg($ 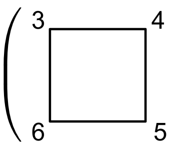 $\Bigg)$

$$= \frac{1}{X_{1,4}}+\frac{1}{X_{3,6}} \tag{4.39}$$

The set of quadrangulations of octagon has 12 elements corresponding to vertices of the two different types of Stokes polytopes, a box and a pentagon [90]. The canonical function of a representative of the box class is given by

$\underline{\Omega}\Bigg($ 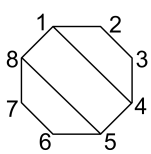 $\Bigg) = \left(\frac{1}{X_{1,4}}+\frac{1}{X_{3,8}}\right) D_{X_{3,8}}\underline{\Omega}\Bigg($ 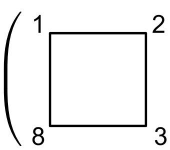 $\Bigg) D_{X_{3,8}}\underline{\Omega}\Bigg($ 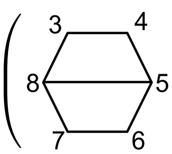 $\Bigg)$

$$= \left(\frac{1}{X_{1,4}}+\frac{1}{X_{3,8}}\right)\left(\frac{1}{X_{4,7}}+\frac{1}{X_{5,8}}\right) \tag{4.40}$$

The canonical function of a representative pentagon is given by

$$\underline{\Omega}\left(\vphantom{\frac{1}{X}}\right.$$
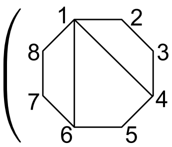

$$\left.\vphantom{\frac{1}{X}}\right) = \left(\frac{1}{X_{1,4}} + \frac{1}{X_{3,6}}\right) D_{X_{3,6}}\underline{\Omega}\left(\vphantom{\frac{1}{X}}\right.$$
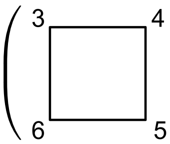

$$\left.\vphantom{\frac{1}{X}}\right) D_{X_{3,6}}\underline{\Omega}\left(\vphantom{\frac{1}{X}}\right.$$
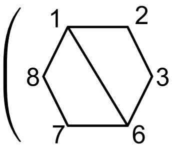

$$\left.\vphantom{\frac{1}{X}}\right) + \left(\frac{1}{X_{1,4}} + \frac{1}{X_{3,8}}\right) D_{X_{3,8}}\underline{\Omega}\left(\vphantom{\frac{1}{X}}\right.$$
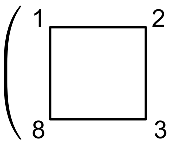

$$\left.\vphantom{\frac{1}{X}}\right) D_{X_{3,8}}\underline{\Omega}\left(\vphantom{\frac{1}{X}}\right.$$
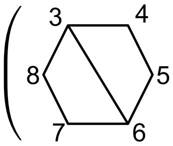

$$\left.\vphantom{\frac{1}{X}}\right) = \left(\frac{1}{X_{1,4}} + \frac{1}{X_{3,6}}\right)\left(\frac{1}{X_{1,6}} + \frac{1}{X_{3,8} - X_{3,6}}\right) + \left(\frac{1}{X_{1,4}} + \frac{1}{X_{3,8}}\right)\left(\frac{1}{X_{5,8}} + \frac{1}{X_{3,6} - X_{3,8}}\right) \quad (4.41)$$

We can illustrate the application of (4.37) for $n = 10$ on the following example,

$$\underline{\Omega}\left(\vphantom{\frac{1}{X}}\right.$$
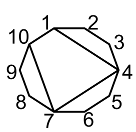

$$\left.\vphantom{\frac{1}{X}}\right) = \left(\frac{1}{X_{1,4}} + \frac{1}{X_{3,6}}\right) D_{X_{3,6}}\underline{\Omega}\left(\vphantom{\frac{1}{X}}\right.$$
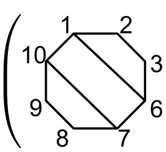

$$\left.\vphantom{\frac{1}{X}}\right) D_{X_{3,6}}\underline{\Omega}\left(\vphantom{\frac{1}{X}}\right.$$
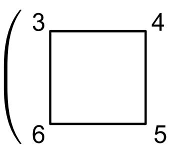

$$\left.\vphantom{\frac{1}{X}}\right) + \left(\frac{1}{X_{1,4}} + \frac{1}{X_{3,10}}\right) D_{X_{3,10}}\underline{\Omega}\left(\vphantom{\frac{1}{X}}\right.$$
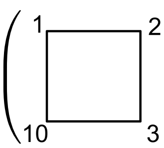

$$\left.\vphantom{\frac{1}{X}}\right) D_{X_{3,10}}\underline{\Omega}\left(\vphantom{\frac{1}{X}}\right.$$
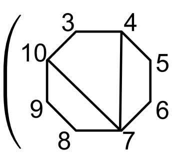

$$\left.\vphantom{\frac{1}{X}}\right) \quad (4.42)$$

4.3.4 Assembling the amplitude

As a warmup exercise, let us consider the case of $n = 6$. For orientations of diagonals defined by assigning '+' to odd and '-' to even vertices, it is easy to check that diagonals $X_{1,4}$ and $X_{3,6}$ are compatible with $X_{1,4}$; $X_{2,5}$ and $X_{1,4}$ are compatible with $X_{2,5}$. Let us then write the amplitude in the form

$$A_6 = \frac{1}{X_{1,4}} + \frac{1}{X_{2,5}} + \frac{1}{X_{3,6}} = \underline{\Omega}\left(\vphantom{\frac{1}{X}}\right.$$
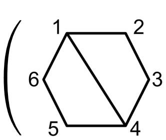

$$\left.\vphantom{\frac{1}{X}}\right) + \lim_{X_{1,4}\to\infty} \underline{\Omega}\left(\vphantom{\frac{1}{X}}\right.$$
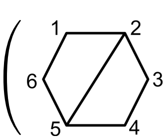

$$\left.\vphantom{\frac{1}{X}}\right) \quad (4.43)$$

In order to piece together the amplitude for $n = 8$, in addition to (4.40), (4.41) we will need to consider three more Stokes polytopes. Those functions are obtained by picking $X_b = X_{1,4}$, $X_b = X_{3,8}$, $X_b = X_{1,6}$, respectively, and are given by

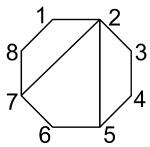

$$\underline{\Omega}\left(\quad \right) = \left(\frac{1}{X_{1,4}} + \frac{1}{X_{2,5}}\right)\left(\frac{1}{X_{1,6}} + \frac{1}{X_{2,7} - X_{2,5}}\right) + \left(\frac{1}{X_{1,4}} + \frac{1}{X_{2,7}}\right)\left(\frac{1}{X_{4,7}} + \frac{1}{X_{2,5} - X_{2,7}}\right)$$

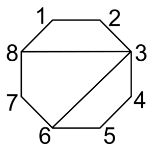

$$\underline{\Omega}\left(\quad \right) = \left(\frac{1}{X_{3,8}} + \frac{1}{X_{2,5}}\right)\left(\frac{1}{X_{5,8}} + \frac{1}{X_{2,7} - X_{2,5}}\right) + \left(\frac{1}{X_{3,8}} + \frac{1}{X_{2,7}}\right)\left(\frac{1}{X_{3,6}} + \frac{1}{X_{2,5} - X_{2,7}}\right)$$

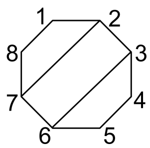

$$\underline{\Omega}\left(\quad \right) = \left(\frac{1}{X_{1,6}} + \frac{1}{X_{2,7}}\right)\left(\frac{1}{X_{2,5}} + \frac{1}{X_{3,6}}\right) \tag{4.44}$$

Then, the 8-particle amplitude can be obtained as

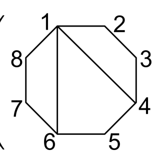

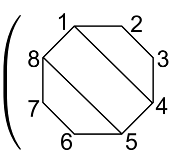

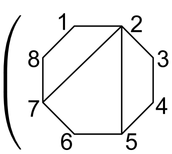

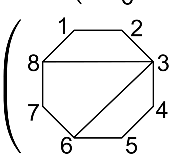

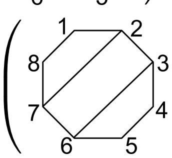

$$A_8 = \underline{\Omega}\left(\quad \right) + \lim_{X_{5,8}\to\infty} \underline{\Omega}\left(\quad \right) + \lim_{X_{1,4}\to\infty} \underline{\Omega}\left(\quad \right) + \\ + \lim_{X_{3,8}\to\infty} \underline{\Omega}\left(\quad \right) - \lim_{X_{3,6}\to\infty} \lim_{X_{1,6}\to\infty} \underline{\Omega}\left(\quad \right) \tag{4.45}$$

A nice feature of this formula is that the limits taken in Eq. (4.45) match the X_b facets of Eq. (4.40), Eq. (4.41), Eq. (4.44). The fact that the facet X_b appears only in the prefactors of the recursive formula Eq. (4.37) results in a simple expression for the amplitude.

4.4 Conclusions

In this paper we presented a simple way to compute recursively both the canonical form and the canonical rational function associated to simple polytopes, motivated by the desire of making manifest the projectivity of the former. As it is familiar from the case of BCFW formulae [89], this is done at the cost of introducing spurious poles.

Compared to more standard recursive formulae, such as those in [97], based on triangulations which do not involve other vertices other than those of the polytope itself, our formula have the advantage of introducing only linear spurious poles[6]. This fact might turn out to be helpful especially in the case of polytopes associated to integrands when addressing the loop integration. Furthermore, it is not always obvious how to uplift identities which are true on the subspace where a given polytope is realized to the space of all its facet variables. Our formulae, however, are proved to hold directly in this space. In particular, although it is important to know that a convex realization of the polytope exists, one can setup recursive formulae without the explicit knowledge of such realization.

For illustrational purposes we applied our results to Stokes polytopes, which are known to be related to a planar theory with quartic interactions. A convex realization of these polytopes was presented in [91], see also [93] for connections with ABHY associahedra. As already discussed, however, we can write down recursive formulae for both the canonical forms and the rational functions of Stokes polytope without making explicit use of these geometric data. Also, the structure of the recursion makes manifest how to perform certain limits on the rational function of Stokes polytopes which could be used to assemble them together in a planar quartic amplitudes in a more efficient way.

An interesting direction for further investigation would be to consider canonical forms of non simple polytopes. Dually one has to consider volumes of non simplicial polytopes which can be computed by iterating the standard triangulation method described in [88] for all non simplicial facets. The simplest example is that of the pyramid shown in Fig. 4.6, whose canonical form is given by

$$\Omega = d\log\left(\frac{X_b}{X_0}\right) \wedge d\log\left(\frac{X_1}{X_3}\right) \wedge d\log\left(\frac{X_2}{X_4}\right)\Bigg|_H , \tag{4.46}$$

where H is the subspace defined by $\{X_2 = X_1 + \alpha X_3 + \beta X_0,\ X_4 = X_1 + \alpha' X_3 + \beta' X_0\}$. The

[6]We would like to thank Song He for pointing at us the importance of this fact.

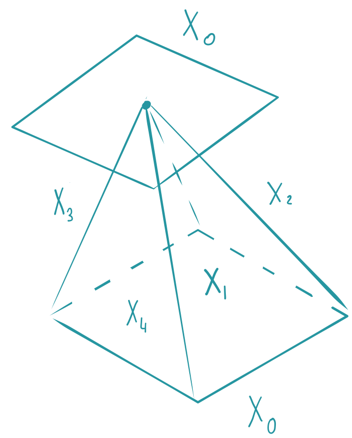

Figure 4.6: A square pyramid is not simple because the four facets X_1, X_2, X_3 and X_4 meet at a common vertex. The standard triangulation of the dual involves the external facet X_0 in addition to the plane at infinity.

novelty with respect to 4.12 is that we cannot think of facet Ω as living in the space of independent variables otherwise Ω would develop a spurious pole along the plane X_0. Because of this a generalization of our formula is not immediate and we leave it for a future work.

Appendix A

Twistor Notation

Here we recall some standard momentum twistor notation and define some new notation used in Sec. 3.4. The momentum twistors Z_a^I are n homogeneous coordinates on $\mathrm{Conf}_n(\mathbb{P}^3)$ (so $I \in \{1, \ldots, 4\}$ and $a \in \{1, \ldots, n\}$) in terms of which we have the natural four-brackets

$$\langle a\, b\, c\, d\rangle \equiv \epsilon_{IJKL} Z_a^I Z_b^J Z_c^K Z_d^L \,. \tag{A.1}$$

We use (see for example Eq. (2.38) of [32])

$$\langle x\, y\, (a\, b\, c) \cap (d\, e\, f)\rangle \equiv \langle x\, a\, b\, c\rangle\langle y\, d\, e\, f\rangle - \langle y\, a\, b\, c\rangle\langle x\, d\, e\, f\rangle \tag{A.2}$$

and in the special case when the two planes $(a\, b\, c)$, $(d\, e\, f)$ share a common point, say $f = c$, we use the shorthand

$$\langle c\, (x\, y)(a\, b)(d\, e)\rangle \equiv \langle x\, y\, (a\, b\, c) \cap (d\, e\, c)\rangle \tag{A.3}$$

to emphasize the otherwise non-manifest fact that this quantity is fully antisymmetric under the exchange of any two of the three lines $(x\, y)$, $(a\, b)$, and $(d\, e)$. In Sec. 3.4 we introduce a bracket for the intersection of four planes which is related by the obvious duality to an intersection of four points. Specifically, if we represent a plane $(a\,b\,c)$ by its dual point

$$(a\,b\,c)_I \equiv \epsilon_{IJLK} Z_a^J Z_b^K Z_c^L \tag{A.4}$$

then we define

$$\begin{aligned}&\langle (a_1\,a_2\,a_3) \cap (b_1\,b_2\,b_3) \cap (c_1\,c_2\,c_3) \cap (d_1\,d_2\,d_3) \rangle \\ &\qquad\qquad \equiv \epsilon^{IJKL} (a_1\,a_2\,a_3)_I (b_1\,b_2\,b_3)_J (c_1\,c_2\,c_3)_K (d_1\,d_2\,d_3)_L\,.\end{aligned} \tag{A.5}$$

Our final new definition

$$(a\,a{+}1) \cap \bar{b}; (a\,b)(c\,d)(e\,f) \equiv \frac{\langle ((a\,a{+}1) \cap \bar{b})(a\,b)(c\,d)(e\,f) \rangle}{\langle a\,\bar{b} \rangle} \tag{A.6}$$

requires a little bit of explanation. The first quantity in the numerator recalls that the intersection of a line $(a\,b)$ and a plane $(c\,d\,e)$ can be represented by the point (see for example p. 33 of [32])

$$(a\,b) \cap (c\,d\,e) \equiv Z_a \langle b\,c\,d\,e \rangle + Z_b \langle c\,d\,e\,a \rangle\,. \tag{A.7}$$

Using this definition, the $(a\,a{+}1) \cap \bar{b}$ in the numerator of Eq. (A.6) defines a point that feeds into "c" in the definition (A.3). By following the trail of definitions it is easy to check that the resulting bracket in the numerator of Eq. (A.6) always has an overall factor of $\langle a\,\bar{b} \rangle$, which we divide out in order to make . irreducible (for general arguments).

Appendix B

Twistor Diagrams to Landau Diagrams

In this appendix, we explain how twistor diagrams and Landau diagrams are partial edge-to-node duals of each other. This map straightforwardly generalizes to any number of loops, and is easily inverted to map a Landau diagram into a twistor diagram.

We first note that the edges in a twistor diagram associated with the external labels are redundant, since the "empty" or "filled" property of the node already tracks the same information. So we can drop such edges. Then the following steps map a twistor diagram, τ, to a Landau diagram, λ:

1. For each loop line $\mathcal{L}^{(i)}$ in τ, identify one endpoint of $\mathcal{L}^{(i)}$ with the other endpoint of $\mathcal{L}^{(i)}$. Since τ are graphs, this identification preserves the order of the nodes along all $\mathcal{L}^{(i)}$.

2. Map each empty τ-node into a λ-edge. Identify the two λ-nodes defining the λ-edge as massive corners of λ.

3. Map each filled τ-node into two λ-edges sharing one common λ-node. Identify the common λ-node as a massless corner of λ, and the other two λ-nodes as massive corners of λ.

4. The external labels map from τ to λ such that:

    - the label of an empty τ-node maps to one of the two massless corners defining the new λ-edge, and

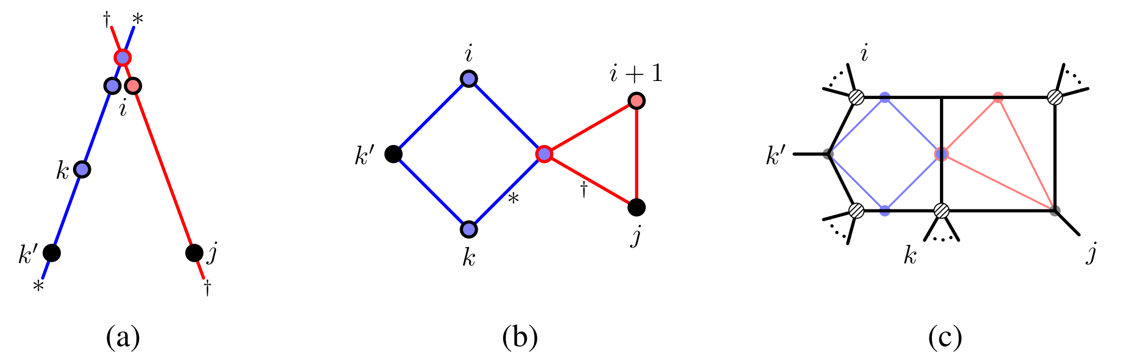

Figure B.1: Figure (a) is momentum twistor diagram (with the superfluous edges associated with the external labels dropped), with the endpoints of $\mathcal{L}^{(1)}$ (denoted with †) identified, and with the endpoints of $\mathcal{L}^{(2)}$ (denoted with *) identified. The resulting graph (b) comes from preserving the ordering of nodes along the line. Note we have used the ambiguity in ordering between k and k' to consider the case $k < k' < i$. Mapping any empty node to an edge between massive corners and mapping any filled node to a massless corner with two edges between massive corners, results in the Landau diagram (c). There would be a massive corner along the top of the Landau diagram, but the indices fix that corner to be zero.

- the label of a filled τ-node maps into a massless corner of λ.

This is a partial edge-to-node map because only the empty τ-nodes obey a proper edge-to-node exchange as they map to a λ-edge, while the filled τ-nodes are effectively unchanged as they map to λ-nodes. It is always possible to consistently assign the labels of τ to λ, though so doing may cause a massive corner of λ to completely vanish, as happens in the following concrete example.

We turn now to detailing how the two-loop twistor diagram, Fig. B.1(a), (also the first column of Tab. 3.2(b)) maps into one of its corresponding Landau diagrams, Fig. B.1(c) (the second column of Tab. 3.2(b)).

The first step is to identify the two nodes corresponding to the end-points of each $\mathcal{L}^{(i)}$, $i = 1, 2$. This closes the two lines into loops, and we formally think of the diagram as a graph, specified by its edges, nodes, and decorations of its nodes. The result is Fig. B.1(b), with identified endpoints marked by * and †.

In this instance, there is an ambiguity in choosing $k' < k$ or $k < k'$. We demonstrate the latter case here to highlight that k' and k can be swapped with respect to how they appear on the loop line. The $k' < k$ differs from what we detail here by swapping ordering of the two nodes along the loop. Then the filled k' node would be on the bottom of the box in Fig. B.1(b), while the empty k node would be on the left of the box.

In the $k < k'$ case we are considering, the resulting graph becomes the Landau diagram, Fig. B.1(c) under the partial edge-to-node dual map, as described in the steps above. Note in Fig. B.1(c) that the empty nodes of the original twistor diagram are identified with edges of the resulting Landau diagram. In contrast, the filled nodes are identified with massless corners, which are themselves nodes. So this is only a partial edge-to-node map.

Appendix C

Explicit derivation of the recursive formula for Ω

In this Appendix we provide an alternative, and somewhat more explicit, proof of our recursive formula. We focus on each of the vertices of our polytope $\mathcal{P}$ and show that every term in (4.1) is reproduced by a sum of the corresponding terms in (4.21). Like in the derivation of Section 4.2.1, there will be several types of vertices to consider.

1. Vertex $v \notin X_b$, such that $(v, B) = \bigcap_{a=1}^{d-1} X_{s_a}$, for some vertex $B \in X_b$ and a collection of $d-1$ facets $X_{s_a} \in \mathcal{S}$. Here, v will belong to only one element of $\mathcal{U}$, which we may denote as X_{u_i}. Let the corresponding terms of Ω evaluated as in (4.1) be

$$\begin{aligned}\Omega_v &= d\log X_{u_i} \bigwedge_{a=1}^{d-1} d\log X_{s_a} \\ \Omega_B &= -d\log X_b \bigwedge_{a=1}^{d-1} d\log X_{s_a}\end{aligned} \tag{C.1}$$

Here, we have chosen the ordering of X_{s_a} in the wedge product in such a way as to absorb any possible overall minus sign in the first line. There is only one term in (4.21) to consider, giving

$$\tilde{\Omega}_v = d\log X_{u_i} \bigwedge_{a=1}^{d-1} d\log X_{s_a} - d\log X_b \bigwedge_{a=1}^{d-1} d\log X_{s_a} \tag{C.2}$$

producing precisely the sum of the two terms of (C.1). Note that the relative minus sign between two terms is in accordance with the sign flip rule as described in the Section 4.1.1.

2. Vertex $v \notin X_b$, such that $(v, U) = \bigcap_{a=1}^{d-1} X_{s_a}, X_{s_a} \in \mathcal{S}$, where v belongs to some element X_{u_i} of $\mathcal{U}$ and U belongs to some element X_{u_j} of $\mathcal{U}$. When we were studying the recursive formula for canonical rational functions, this is precisely the choice of $\mathcal{U}$ we aimed to avoid. When working with canonical forms, however, signs conspire in such a way that the troublesome term is canceled between v and U. Let the sum of terms of (4.1) corresponding to v and U (written in accordance with the sign flip rule) be

$$\Omega_v + \Omega_U = d\log X_{u_i} \bigwedge_{a=1}^{d-1} d\log X_{s_a} - d\log X_{u_j} \bigwedge_{a=1}^{d-1} d\log X_{s_a} \tag{C.3}$$

Note that we have again chosen the ordering of X_{s_a} in the wedge product in such a way that any potential minus sign of the first term is absorbed. This expression is to be compared with the sum of terms corresponding to vertices v and U on the right hand side of (4.21),

$$\begin{aligned}\tilde{\Omega}_v + \tilde{\Omega}_U = &\left(d\log X_{u_i} \bigwedge_{a=1}^{d-1} d\log X_{s_a} - d\log X_b \bigwedge_{a=1}^{d-1} d\log X_{s_a}\right) - \\ &\left(d\log X_{u_j} \bigwedge_{a=1}^{d-1} d\log X_{s_a} - d\log X_b \bigwedge_{a=1}^{d-1} d\log X_{s_a}\right)\end{aligned} \tag{C.4}$$

The relative sign of the two terms has to be a minus sign, in order to ensure the projectivity of form Ω on the line $\bigcap_{a=1}^{d-1} X_{s_a}$. To say it differently, the minus sign comes from the flip rule described in Section 4.1.1, considering that a mutation of X_{u_i} takes us from vertex v to vertex U. Now the unwanted X_b - dependent term cancels and we can see that $\Omega_v + \Omega_U = \tilde{\Omega}_v + \tilde{\Omega}_U$.

3. Vertex $v \notin X_b$, such that v belongs to some collection of facets in $\mathcal{U}$, $X_{u_1}, \ldots, X_{u_n}$. Let the corresponding term in (4.1) be

$$\Omega_v = \bigwedge_{i=1}^{n} d\log X_{u_i} \bigwedge_{a=1}^{d-n} d\log X_{s_a} \tag{C.5}$$

Then, we will need to consider the sum of n terms in (4.21), giving us

$$\begin{aligned}\tilde{\Omega}_v = &\sum_{i=1}^{n} \bigwedge_{j=1}^{i-1} d\log\left(X_{u_j} - X_{u_i}\right) \wedge d\log X_{u_i} \bigwedge_{k=i+1}^{n} d\log\left(X_{u_k} - X_{u_i}\right) \bigwedge_{a=1}^{d-n} d\log X_{s_a} - \\ &\sum_{i=1}^{n} \bigwedge_{j=1}^{i-1} d\log\left(X_{u_j} - X_{u_i}\right) \wedge d\log X_b \bigwedge_{k=i+1}^{n} d\log\left(X_{u_k} - X_{u_i}\right) \bigwedge_{a=1}^{d-n} d\log X_{s_a}\end{aligned} \tag{C.6}$$

Now, we can see that the second line vanishes after expanding out the wedge products and using the identity in (4.34). Similarly, using the identity in (4.33), we can see that the first line simplifies to the form $\tilde{\Omega}_v = \Omega_v$.

4. Vertex $v \in X_b$, such that v belongs to only one element of $\mathcal{U}$, which we will denote as X_{u_i}. Let us write the corresponding term of Ω as

$$\Omega_v = d\log X_{u_i} \wedge d\log X_b \bigwedge_{j=1}^{n-2} d\log X_{s_j} \tag{C.7}$$

Then, there is only one term in (4.21) to consider, giving us

$$\tilde{\Omega}_v = (d\log X_{u_i} - d\log X_b) \wedge d\log(X_b + X_{u_i}) \bigwedge_{j=1}^{n-2} d\log X_{s_j} = \Omega_v \tag{C.8}$$

where we used the identity

$$d\log\left(\frac{a}{b}\right) \wedge d\log(a+b) = d\log a \wedge d\log b \tag{C.9}$$

5. Vertex $v \in X_b$, such that v belongs to some collection of n elements of $\mathcal{U}$, denoted as X_{u_1}, $X_{u_2}, \ldots, X_{u_n}$. Let us write the corresponding term of Ω as

$$\Omega_v = d\log X_b \bigwedge_{i=1}^{n} d\log X_{u_i} \bigwedge_{a=1}^{d-n-1} d\log X_{s_a} \tag{C.10}$$

Now, there are n terms in (4.21) to consider, which after using the identity in (C.9) give

$$\tilde{\Omega}_v = \sum_{i=1}^{n} d\log X_b \bigwedge_{j=1}^{i-1} d\log\left(X_{u_j} - X_{u_i}\right) \wedge d\log X_{u_i} \bigwedge_{k=i+1}^{n} d\log\left(X_{u_k} - X_{u_i}\right) \bigwedge_{a=1}^{d-n-1} d\log X_{s_a} \tag{C.11}$$

which after expanding the wedge products and using the identity in (4.34), in the same manner as before, gives $\tilde{\Omega}_v = \Omega_v$.

Bibliography

[1] I. Prlina, M. Spradlin and S. Stanojevic, Phys. Rev. Lett. **121**, no. 8, 081601 (2018) doi:10.1103/PhysRevLett.121.081601 [arXiv:1805.11617 [hep-th]].

[2] I. Prlina, M. Spradlin, J. Stankowicz and S. Stanojevic, JHEP **1804**, 049 (2018) [arXiv:1712.08049].

[3] G. Salvatori and S. Stanojevic, arXiv:1912.06125 [hep-th].

[4] T. Dennen, M. Spradlin and A. Volovich, JHEP **1603**, 069 (2016) [arXiv:1512.07909 [hep-th]].

[5] T. Dennen, I. Prlina, M. Spradlin, S. Stanojevic and A. Volovich, JHEP **1706**, 152 (2017) [arXiv:1612.02708 [hep-th]].

[6] I. Prlina, M. Spradlin, J. Stankowicz, S. Stanojevic and A. Volovich, arXiv:1711.11507 [hep-th].

[7] A. B. Goncharov, M. Spradlin, C. Vergu and A. Volovich, Phys. Rev. Lett. **105**, 151605 (2010) [arXiv:1006.5703 [hep-th]].

[8] J. Maldacena, D. Simmons-Duffin and A. Zhiboedov, JHEP **1701**, 013 (2017) [arXiv:1509.03612 [hep-th]].

[9] L. D. Landau, Nucl. Phys. **13**, 181 (1959).

[10] R. J. Eden, P. V. Landshoff, D. I. Olive and J. C. Polkinghorne, Cambridge University Press, 1966.

[11] L. J. Dixon, J. M. Drummond and J. M. Henn, JHEP **1111**, 023 (2011) [arXiv:1108.4461 [hep-th]].

[12] L. J. Dixon, J. M. Drummond and J. M. Henn, JHEP **1201**, 024 (2012) [arXiv:1111.1704 [hep-th]].

[13] L. J. Dixon, J. M. Drummond, M. von Hippel and J. Pennington, JHEP **1312**, 049 (2013) [arXiv:1308.2276 [hep-th]].

[14] L. J. Dixon, M. von Hippel and A. J. McLeod, JHEP **1601**, 053 (2016) [arXiv:1509.08127 [hep-th]].

[15] S. Caron-Huot, L. J. Dixon, A. McLeod and M. von Hippel, Phys. Rev. Lett. **117**, no. 24, 241601 (2016) [arXiv:1609.00669 [hep-th]].

[16] J. M. Drummond, G. Papathanasiou and M. Spradlin, JHEP **1503**, 072 (2015) [arXiv:1412.3763 [hep-th]].

[17] S. J. Parke and T. R. Taylor, Phys. Rev. Lett. **56**, 2459 (1986).

[18] V. P. Nair, Phys. Lett. B **214**, 215 (1988).

[19] Z. Bern, L. J. Dixon and V. A. Smirnov, Phys. Rev. D **72**, 085001 (2005) [hep-th/0505205].

[20] L. F. Alday, D. Gaiotto and J. Maldacena, JHEP **1109**, 032 (2011) [arXiv:0911.4708 [hep-th]].

[21] L. J. Dixon, J. Drummond, T. Harrington, A. J. McLeod, G. Papathanasiou and M. Spradlin, JHEP **1702**, 137 (2017) [arXiv:1612.08976 [hep-th]].

[22] J. L. Bourjaily, A. J. McLeod, M. Spradlin, M. von Hippel and M. Wilhelm, Phys. Rev. Lett. **120**, no. 12, 121603 (2018) [arXiv:1712.02785 [hep-th]].

[23] D. Nandan, M. F. Paulos, M. Spradlin and A. Volovich, JHEP **1305**, 105 (2013) [arXiv:1301.2500 [hep-th]].

[24] S. Caron-Huot and K. J. Larsen, JHEP **1210**, 026 (2012) [arXiv:1205.0801 [hep-ph]].

[25] N. Arkani-Hamed and J. Trnka, JHEP **1410**, 030 (2014) [arXiv:1312.2007 [hep-th]].

[26] N. Arkani-Hamed, H. Thomas and J. Trnka, JHEP **1801**, 016 (2018) [arXiv:1704.05069 [hep-th]].

[27] N. Arkani-Hamed and J. Trnka, JHEP **1412**, 182 (2014) [arXiv:1312.7878 [hep-th]].

[28] J. M. Drummond, J. Henn, V. A. Smirnov and E. Sokatchev, JHEP **0701**, 064 (2007) [hep-th/0607160].

[29] L. F. Alday and J. M. Maldacena, JHEP **0706**, 064 (2007) [arXiv:0705.0303 [hep-th]].

[30] J. M. Drummond, J. Henn, G. P. Korchemsky and E. Sokatchev, Nucl. Phys. B **828**, 317 (2010) [arXiv:0807.1095 [hep-th]].

[31] N. Arkani-Hamed, J. L. Bourjaily, F. Cachazo, A. B. Goncharov, A. Postnikov and J. Trnka, arXiv:1212.5605 [hep-th].

[32] N. Arkani-Hamed, J. L. Bourjaily, F. Cachazo and J. Trnka, JHEP **1206**, 125 (2012) [arXiv:1012.6032 [hep-th]].

[33] S. Caron-Huot, JHEP **1112**, 066 (2011) [arXiv:1105.5606 [hep-th]].

[34] S. Caron-Huot and S. He, JHEP **1207**, 174 (2012) [arXiv:1112.1060 [hep-th]].

[35] J. Golden, A. B. Goncharov, M. Spradlin, C. Vergu and A. Volovich, JHEP **1401**, 091 (2014) [arXiv:1305.1617 [hep-th]].

[36] J. Golden and M. Spradlin, JHEP **1502**, 002 (2015) [arXiv:1411.3289 [hep-th]].

[37] J. Drummond, J. Foster and O. Gurdogan, Phys. Rev. Lett. **120**, no. 16, 161601 (2018) [arXiv:1710.10953 [hep-th]].

[38] J. Golden, M. F. Paulos, M. Spradlin and A. Volovich, J. Phys. A **47**, no. 47, 474005 (2014) [arXiv:1401.6446 [hep-th]].

[39] T. Harrington and M. Spradlin, JHEP **1707**, 016 (2017) [arXiv:1512.07910 [hep-th]].

[40] J. Golden and M. Spradlin, JHEP **1309**, 111 (2013) [arXiv:1306.1833 [hep-th]].

[41] N. Arkani-Hamed, J. L. Bourjaily, F. Cachazo and J. Trnka, Phys. Rev. Lett. **113**, no. 26, 261603 (2014) [arXiv:1410.0354 [hep-th]].

[42] Z. Bern, E. Herrmann, S. Litsey, J. Stankowicz and J. Trnka, JHEP **1506**, 202 (2015) [arXiv:1412.8584 [hep-th]].

[43] Z. Bern, E. Herrmann, S. Litsey, J. Stankowicz and J. Trnka, JHEP **1606**, 098 (2016) [arXiv:1512.08591 [hep-th]].

[44] J. Mathews, Phys. Rev. **113**, 381 (1959).

[45] T. T. Wu, Phys. Rev. **123**, 678 (1961).

[46] T. T. Wu, Phys. Rev. **123**, 689 (1961).

[47] J. Bjorken and S. Drell, “Relativistic Quantum Fields,” McGraw-Hill, 1965.

[48] I. Gitler, “Delta-wye-delta transformations: algorithms and applications,” Ph.D. Thesis, University of Waterloo, 1991.

[49] I. Gitler and F. Sagols, Networks **57**, 174 (2011).

[50] S. B. Akers, Oper. Res. **8**, 311 (1960).

[51] T. A. Feo and J. S. Provan, Oper. Res. **41**, 572 (1993).

[52] Y. C. Verdière, I. Gitler and D. Vertigan, Comment. Math. Helv. **71** (144) (1996).

[53] D. Archdeacon, C. J. Colbourn, I. Gitler and J. S. Provan, J. Graph Theory **33**, 83 (2000).

[54] L. Demasi and B. Mohar, Proceedings of the Twenty-Sixth Annual ACM-SIAM Symposium on Discrete Algorithms 1728 (2014).

[55] A. T. Suzuki, Can. J. Phys. **92**, 131 (2014) arXiv:1112.1332].

[56] A. Hodges, JHEP **1305**, 135 (2013) [arXiv:0905.1473].

[57] S. Caron-Huot, L. J. Dixon, A. McLeod and M. von Hippel, Phys. Rev. Lett. **117**, no. 24, 241601 (2016) [arXiv:1609.00669].

[58] D. B. Fairlie, P. V. Landshoff, J. Nuttall and J. C. Polkinghorne, J. Math. Phys. **3**, 594 (1962).

[59] R. J. Eden, P. V. Landshoff, D. I. Olive and J. C. Polkinghorne, "The Analytic S-Matrix," Cambridge University Press, 1966.

[60] R. E. Cutkosky, J. Math. Phys. **1**, 429 (1960).

[61] J. M. Drummond, J. Henn, V. A. Smirnov and E. Sokatchev, JHEP **0701**, 064 (2007) [hep-th/0607160].

[62] L. F. Alday and J. M. Maldacena, JHEP **0706**, 064 (2007) [arXiv:0705.0303].

[63] J. M. Drummond, J. Henn, G. P. Korchemsky and E. Sokatchev, Nucl. Phys. B **828**, 317 (2010) [arXiv:0807.1095].

[64] S. Caron-Huot, JHEP **1112**, 066 (2011) [arXiv:1105.5606].

[65] A. B. Goncharov, M. Spradlin, C. Vergu and A. Volovich, Phys. Rev. Lett. **105**, 151605 (2010) [arXiv:1006.5703].

[66] L. J. Dixon, J. M. Drummond and J. M. Henn, JHEP **1111**, 023 (2011) [arXiv:1108.4461].

[67] L. J. Dixon, J. M. Drummond and J. M. Henn, JHEP **1201**, 024 (2012) [arXiv:1111.1704].

[68] L. J. Dixon, J. M. Drummond, M. von Hippel and J. Pennington, JHEP **1312**, 049 (2013) [arXiv:1308.2276].

[69] L. J. Dixon, J. M. Drummond, C. Duhr, M. von Hippel and J. Pennington, PoS LL **2014**, 077 (2014) [arXiv:1407.4724].

[70] L. J. Dixon and M. von Hippel, JHEP **1410**, 065 (2014) [arXiv:1408.1505].

[71] L. J. Dixon, M. von Hippel and A. J. McLeod, JHEP **1601**, 053 (2016) [arXiv:1509.08127].

[72] J. M. Drummond, G. Papathanasiou and M. Spradlin, JHEP **1503**, 072 (2015) [arXiv:1412.3763].

[73] L. J. Dixon, J. Drummond, T. Harrington, A. J. McLeod, G. Papathanasiou and M. Spradlin, JHEP **1702**, 137 (2017) [arXiv:1612.08976].

[74] J. Maldacena, D. Simmons-Duffin and A. Zhiboedov, JHEP **1701**, 013 (2017) [arXiv:1509.03612].

[75] J. Drummond, J. Foster and Ö. Gürdoğan, Phys. Rev. Lett. **120**, no. 16, 161601 (2018) [arXiv:1710.10953].

[76] D. K. Wagner, Discrete Appl. Math. **180**, 158 (2015).

[77] I. Gitler and G. Sandoval-Angeles, ENDM **62**, 129 (2017).

[78] J. L. Bourjaily, A. J. McLeod, M. Spradlin, M. von Hippel and M. Wilhelm, Phys. Rev. Lett. **120**, no. 12, 121603 (2018) [arXiv:1712.02785].

[79] J. L. Bourjaily, Y. H. He, A. J. McLeod, M. Von Hippel and M. Wilhelm, arXiv:1805.09326 [hep-th].

[80] D. Chicherin, V. Kazakov, F. Loebbert, D. Müller and D. l. Zhong, JHEP **1805**, 003 (2018) [arXiv:1704.01967].

[81] B. Basso and L. J. Dixon, Phys. Rev. Lett. **119**, no. 7, 071601 (2017) [arXiv:1705.03545].

[82] S. Abreu, R. Britto, C. Duhr and E. Gardi, JHEP **1410**, 125 (2014) [arXiv:1401.3546].

[83] S. Abreu, R. Britto, C. Duhr and E. Gardi, JHEP **1706**, 114 (2017) [arXiv:1702.03163].

[84] S. Abreu, R. Britto, C. Duhr and E. Gardi, Phys. Rev. Lett. **119**, no. 5, 051601 (2017) [arXiv:1703.05064].

[85] S. Abreu, R. Britto, C. Duhr and E. Gardi, JHEP **1712**, 090 (2017) [arXiv:1704.07931].

[86] S. Abreu, R. Britto, C. Duhr and E. Gardi, PoS RADCOR **2017**, 002 (2018) [arXiv:1803.05894 [hep-th]].

[87] N. Arkani-Hamed, J. L. Bourjaily, F. Cachazo, A. B. Goncharov, A. Postnikov and J. Trnka, doi:10.1017/CBO9781316091548 arXiv:1212.5605 [hep-th].

[88] N. Arkani-Hamed, Y. Bai, S. He and G. Yan, JHEP **1805**, 096 (2018) doi:10.1007/JHEP05(2018)096 [arXiv:1711.09102 [hep-th]].

[89] R. Britto, F. Cachazo, B. Feng and E. Witten, Phys. Rev. Lett. **94**, 181602 (2005) doi:10.1103/PhysRevLett.94.181602 [hep-th/0501052].

[90] P. Banerjee, A. Laddha and P. Raman, JHEP **1908**, 067 (2019) doi:10.1007/JHEP08(2019)067 [arXiv:1811.05904 [hep-th]].

[91] T. Manneville and V. Pilaud, Discrete & Computational Geometry 61, 507 (2018) doi:10.1007/s00454-018-0004-2 [arXiv:1703.09953 [math.CO]].

[92] N. Arkani-Hamed, Y. Bai and T. Lam, JHEP **1711**, 039 (2017) doi:10.1007/JHEP11(2017)039 [arXiv:1703.04541 [hep-th]].

[93] P. B. Aneesh, P. Banerjee, M. Jagadale, R. Rajan, A. Laddha and S. Mahato, arXiv:1911.06008 [hep-th].

[94] Y. Baryshnikov, New Developments in Singularity Theory 65 (2001) doi:10.1007/978-94-010-0834-1_3.

[95] F. Chapoton, Discrete Mathematics & Theoretical Computer Science 18(3) (2015) arXiv:1505.05990 [math.RT]

[96] Y. Palu, V. Pilaud and P. Plamondon, arXiv:1707.07574 [math.CO].

[97] S. He and Q. Yang, JHEP **1905**, 040 (2019) doi:10.1007/JHEP05(2019)040 [arXiv:1810.08508 [hep-th]].

[98] G. Salvatori, arXiv:1806.01842 [hep-th].

[99] P. Raman, JHEP **1910**, 271 (2019) doi:10.1007/JHEP10(2019)271 [arXiv:1906.02985 [hep-th]].

[100] M. Jagadale, N. Kalyanapuram and A. Prema Balakrishnan, arXiv:1906.12148 [hep-th].

[101] X. Gao, S. He and Y. Zhang, JHEP **1711**, 144 (2017) doi:10.1007/JHEP11(2017)144 [arXiv:1708.08701 [hep-th]].

[102] N. Arkani-Hamed, S. He, G. Salvatori and H. Thomas, to appear

[103] P. Orlik and H. Terao, Arrangements of hyperplanes, Springer.

[104] I. Prlina, ”Landau Singularities in Planar Massless Theories.” PhD Diss, Brown University, 2019